DOCTOR OF PHILOSOPHY

Proton Exchange Membrane Fuel Cells (PEMFC) and Energy Storage System (ESS) passive hybridization for electric vehicles

Ren, Jin

Award date:
2021

Awarding institution:
Coventry University

Proton Exchange Membrane Fuel Cells (PEMFC) and Energy Storage System (ESS) Passive Hybridization for Electric Vehicles

By

JIN REN

PhD

June 2020

Proton Exchange Membrane Fuel Cells (PEMFC) and Energy Storage System (ESS) Passive Hybridization for Electric Vehicles

A thesis submitted in partial fulfilment of the University's requirements for the Degree of Doctor of Philosophy

June 2020

Coventry University

Content removed on data protection grounds

Certificate of Ethical Approval

Applicant:

Jin Ren

Project Title:

Proton Exchange Membrane Fuel Cells (PEMFC) and Energy Storage System (ESS) Passive Hybridisation

This is to certify that the above named applicant has completed the Coventry University Ethical Approval process and their project has been confirmed and approved as Low Risk

Date of approval:

25 April 2019

Project Reference Number:

P90207

Content removed on data protection grounds

Acknowledgements

I had never experienced such a long and lonely life of research. This journey could not be completed without helps from people around me.

First of all, I would like to thank all my supervisors: Dr Olivier Haas for his expert advice and continuous guidance of both academic and university's works throughout the PhD process. As the director of the study, he has always asked my novelties to remind me to find more questions. Dr Jinlei Shang, for his great faith which leads me on the research path. His technical expertise in fuel cell hybrid vehicle provided me with the opportunity to achieve the goal. Dr Asim Mumtaz was also my master course's teacher who I've worked with him about five years now. He was always willing to help me.

I have had the pleasure of working with all my colleagues and friends in the research Institute for future transport and cities. Thanks for their friendship and support in both life and study. I would also like to Coventry University and the staffs of Doctoral College (Lisa Millard and Katy Morrison) who have helped me.

Last, I would like to thank my parents and family. Thanks to my parents that I could study in the UK, and I have no way to repay them. And thanks to my uncle and auntie give me all support.

Abstract

This thesis addresses the need to move to cleaner economic growth based and focuses on fuel cell electric vehicles (FCEVs) to help realised the move to zero carbon emissions by 2050. The review of the state of the art in Zero Emission Vehicle (ZEV), Energy Storage Source (ESS), fuel cell, hydrogen technologies and economy has confirmed the potential of FCEV. The review has also identified the need to reduce cost and improve efficiency to enable widespread market adoption.

This thesis demonstrated the suitability of passive hybrid systems, where fuel cell and battery are directly connected without a DC-DC converter, to reduce the cost and increase the efficiency of FCEVs.

An original passive hybrid powertrain model was developed and validated using experimental data to provide a realistic dynamic behaviour for the FCEV. An original fuzzy logic controller was designed using rules exploiting State of Charge(SoC) and fuel cell load power to determine the most appropriate fuel cell pressure to satisfy the load of the FCEV whist reducing the number of fuel cell start-stop times and extending the vehicle range.

The system model was used to carry out simulation studies to demonstrate the advantages of passive hybrid systems compare to active hybrid systems in terms of reduced cost, complexity, weight, resulting in increased vehicle range. The simulation has highlighted the need to carefully design passive hybrid systems to minimise fuel cell power variation in response to load demand changes. An original set of rules was proposed to size fuel cell and battery and applied for different battery technologies whilst considering well-to-wheel for downsizing passive hybrid powertrain.

Overall, this thesis has demonstrated through the use of surveys, modelling control systems design and component sizing that passive hybridization is a good alternative for Ultra-Low Emission Vehicle (ULEV).

Table of contents

Index of figures

Index of tables

Nomenclature and Abbreviations

The abbreviations and terminology are defined in the following tables:

Abbreviations	Actual
ADVISOR	Advanced Vehicle simulator
BEV	Battery Electric Vehicle
ESS	Energy Storage System
EUDC	Extra-Urban driving cycle
EV	Electric Vehicle
FCEV	Fuel Cell Electric Vehicle
GHG	Green House Gases
ICE	Internal Combustion Engine
SLI	Starting, Lighting and Lgnition
LiFePO4	Lithium ion Phosphate Battery
LCV	Low Carbon Vehicle
NEDC	New European Driving Cycle
Ni-MH	Nickel–metal hydride battery
PEMFC	Proton Exchange Membrane Fuel Cells
SoC	State of Charge
UDC	ECE-15 urban driving cycles
ULEV	Ultra-Low Emission Vehicle
WLTP	Worldwide Harmonized Light Vehicles Test Procedures
ZEV	Zero Emission Vehicle
ZTE	Zero Tailpipe Emission
Modelling	

AccelCmd	Commanded vehicle acceleration, form 0 through 1
AccelPdl	Accelerator Pedal Position
Baro	Barometric, in Pa
BattPwr	Battery power
BattPwrchrgLmt	Battery power charge limit
BattPwrDischrgLmt	Battery power discharge limit
BattSoc	Battery State of Charge
BrakeCmd	Brake command
BrkPrsReq	Brake pedal to total braking pressure request
DecelCmd	Commanded vehicle deceleration, from 0 through 1
DecelPdl	Decelerator Pedal Position
Grade	Road grade angle, θ, in deg
lam_mux	Friction scaling factor
MotSpd	Motor speed
MotTrqCmd	Motor torque command
MotTrqCmdTrac	Commanded motor torque for tractive force
OpCamds	Optional command
PCM	Powertrain control module
PtCtrl	Powertrain control output
Temp	Temperature, in K
TrqCmd	Commanded torque
VehPlnt	Vehicle Plant
VehSpdFdbk	Vehicle speed feedback
VRef	Reference velocity, in m/s

VFdbk	Longitudinal vehicle velocity, in m/s
Wind XYZ	Wind speed along earth-fixed X-, Y-, and Z-axes. In m/s
Xdot	Vehicle centre of gravity velocity along earth-fixed X-axis
Equations	
R_0	outer radius of brake pad
R_i	Inner radius of brake pad
R_m	Radius of brake pad force application on brake rotor
B_a	Brake actuator bore diameter
N_{pads}	Number of brake pads
G	Gibbs free energy
V_m	Molar volume of gas
R	ideal gas constant
T	Thermodynamic temperature
F	Faraday Constant
E_r	Reversible output voltage
H	Standard enthalpy of formation
S	Entropy
i	Current density
i_0	Exchange current density
α	Charge transfer coefficient
R_{ion}	Ion resistance
R_{elec}	Electronic resistance
σ	Specific conductance
δ	Thick of electrolyte layer
A	Activation area of fuel cell

i_{max}	Maximum current density
V_{cell}	Actual voltage of single fuel cell
$O_2\%$	Percentage of oxygen in the oxidant
$H_2\%$	Percentage of hydrogen in the fuel
P_{air}	Absolute supply pressure of air
P_{fuel}	Absolute supply pressure of fuel
$V_{lpm(air)}$	Air flow rate
$V_{lpm(fuel)}$	Fuel flow rate
V%	Percentage of water vapor in the oxidant
Q_{max}	Maximum battery capacity
A	Exponential voltage
B	Exponential capacity
K	Polarization constant
i_c	Available capacity
$Exp(s)$	Exponential zone dynamics
F_x	Longitudinal force
F_{wf}	Longitudinal force on front axle along vehicle-fixed x-axis
F_{wr}	Longitudinal force on rear axle along vehicle-fixed x-axis
$F_{d,x}$	longitudinal and drag force on vehicle centre of gravity
$F_{sx,f}$	Longitudinal suspension force on front axle
$F_{sx,r}$	Longitudinal suspension force on rear axle

$F_{g,x}$	Longitudinal gravitational force on vehicle along the vehicle-fixed frame
C_d	Frontal air drag coefficient
A_f	Frontal area of vehicle
v	Velocity of vehicle
ρ	Mass density of the fluid (air)
m	Vehicle weight
α	Inclined road angle
ω_w	Wheel angular speed
r_w	Wheel radius
J	Motor inertia

Chapter 1: Introduction

1.1 Motivation for 'The Road to Zero'

Historically, the relationship between economic growth and environment protection was complex (Everett et al. 2010). Many countries have spent natural resources such as coal, oil and gas formed and accumulated over hundreds of millions of years ago to ensure economic prosperity. Overuse of the natural resources in the United Kingdom, and the rest of the world have resulted in significant environmental challenges, such as climate change, air pollutants, shortage of energy and ecological collapse. During the worldwide economic downturn [in 2008], there was a realisation of the opportunity that the natural environment can play a significant role in sustaining economic growth. The UK government has pledged to move to cleaner economic growth to create an economy with new outstanding green industries (UK Government 2017).

Therefore, environmental and legislation demands associated with the reduction of Greenhouse Gases (GHG) is encouraging the automotive industry to move from Internal Combustion Engine (ICE) propulsion to Ultra-Low Emission (ULE) systems. Battery electric and hydrogen fuel cell technologies have been recognized as having the most potential for zero-emission automotive systems including Battery Electric Vehicles (BEVs) and Fuel Cell Electric Vehicles (FCEV) (Automotive Council UK 2017; European Commission 2018; SAE 2016).

1.1.1 Environment protection and sustainable development

- **Climate change**

Climate change has become a severe problem in the world, due to carbon emssions, as a result of the continuing global population increase and the increasing demand (and supply) for new technologies. Figure 1-1 highlights the negative impact that road transport has on the climate change. According to the UK Government, the transport sector has become the largest producer of carbon dioxide (CO_2) emissions from fuel combustion, accounting for 33% in 2019 (Government of the United Kingdom 2019). Globally, the CO_2 emissions for transport contributed with 24.6% of the total emissions in 2016 and has significantly increased its contribution since 1990 (71% increase) (International Energy Agency 2018).

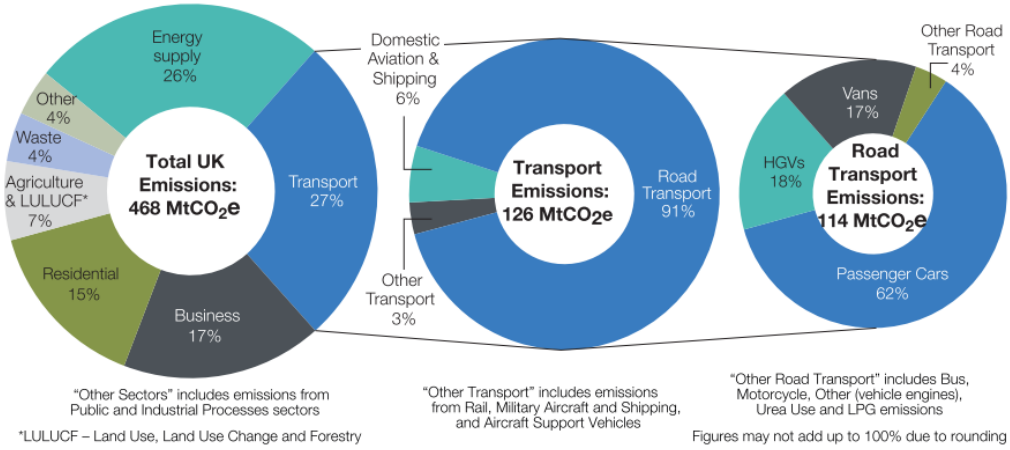

Figure 1-1 Road transport impact on UK GHG (Department of Transport 2018)

- **Ambient air pollution**

In 2016, ambient air pollution caused about 4.2 million deaths in the world (World Health Organization 2018). In densely-populated cities, road transport is usually a significant source that caused air pollution. This pollution is due to combustion engine that use emit CO2, PM 10, and NOx as well as tyre road interaction that produce a range of minor particulate emissions. The Committee on the Medical Effects of Air Pollutants has estimated that 28,000 to 36,000

premature deaths in the UK per year are due to exposure to traffic-related pollutants (Committee on the Medical Effects of Air Pollutants 2018). Perhaps not surprisingly, 81.5% of the permanent resident population of England and Wales live in highly-populated urban areas (ONS 2013), who can be directly impacted by such harmful emissions. In summary, road transport has caused and continues to cause serious health problems because of traffic-related pollutants (Barnes et al. 2019).

- **Energy security**

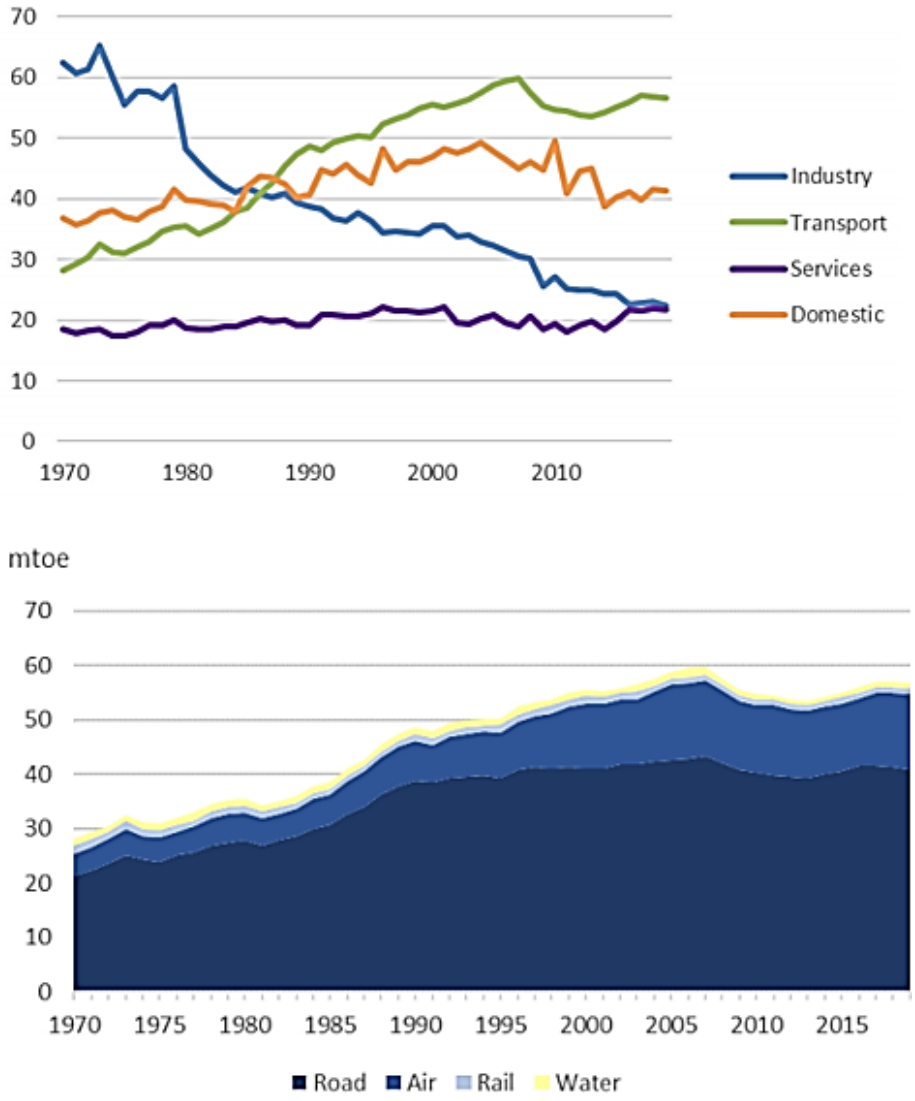

Figure 1-2 Trends in transport consumption from 1970 (National Statistics 2019).

Since 2004, Britain became an importer of energy. In 2017, oil and gas were accounting for approximately 90% of the UK energy import (Bolton 2018). Figure 1-2 shows that transport accounted for the most significant proportion of consumption, and it seems to increase until the recent covid-19 crisis. During COVID-19, the commercial transportation activity was reduced by 32% from 1 March 2020 to 08 June 2020 in the UK (Department for Transport 2020). About 73% of the consumer transport is road transport, and most of the road transport is still relying heavily on imported foreign oil (National Statistics 2019). The dependence on imported energy is linked to a lack of energy security and can cause overpricing or unavailability of energy (International Energy Agency 2019). Therefore, energy security has a significant impact on long-term economic developments, with continued liberalization of fuel prices, increasing diversity and security in energy become a primary target for green economic growth.

1.1.2 Policies analyse

Since 2003, the UK government had set a target to reduce CO2 emissions by 60%, relative to 1990 levels. Moreover, by the suggestion of the Climate Change Committee, the government increased the target to 80% for all GHG emissions. For now, the committee has advised the UK, as a responsible world power to bring fresher air, healthier life and more economic benefits to the citizens (Stark et al. 2019). More concretely, the UK has set an ambitious target to reduce 100% (net-zero) GHG by 2050 (Department for Transport et al. 2019). To achieve this goal, the UK has consistently taken a positive role in the improvement and development of low-carbon technologies. For instance, the promotion of low carbon vehicles, carbon capture and storage (CCS), hydrogen and fuel cell technologies.

Recent policies have focused on the replacement of the internal combustion engine (ICE) with less polluting forms of technology, including battery electric and fuel cell electric powertrains. The UK Department for Transport states they will end the sale of new petrol and diesel cars/vans by 2040 and funded nearly £1.5 billion for Zero Emission Vehicles (ZEV) development to reach net-zero by 2050 (Department for Transport et al. 2019).

In conclusion, road transport is a key sector for the proposal of strategies to fight climate change, ambient air pollution and energy security. The policies have shown clear direction: ZEV is the future. The uncertainty is the scale and pace of ZEV market growth.

1.2 Research question

The aim of this PhD was to investigate the suitability of passive hybrid FCEV powertrain for the Coventry University Microcab H2EV (Hydrogen Electric Vehicle).

To accomplish this aim, the project was divided into following objectives:

1. Develop a passive hybrid FCEV powertrain model for the Microcab vehicle
2. Use experimental data to validate the novel passive hybrid powertrain model.
3. Investigate the potential efficiency gains associated with the proposed passive hybrid powertrain compared to the existing active powertrain.
4. Investigate PEMFC and different ESS passive hybridization combinations for FCEV.
5. Define the suitable size and type of fuel cell and ESS for the Microcab H2EV.

1.3 Contributions

The contributions of this work are as follows:

1. An original passive hybrid powertrain model was developed in MATLAB™ and Simulink® and validated using experimental data to provide a realistic dynamic behaviour for the FCEV.
2. This work has demonstrated that the most significant control variables were the fuel cell pressure and the fuel flow rate for the passive hybrid system controller.
3. An original fuzzy logic controller was designed using rules exploiting SoC and fuel cell load power to determine the most appropriate fuel cell pressure to satisfy the load of the FCEV while reducing the number of fuel cell start-stop times and extending the overall vehicle range.
4. A set of passive hybrid system component sizing rules were proposed to select components for optimal passive hybrid system. The resulting optimal passive hybrid powertrain produces lower GHG emission than many commercial vehicles.

1.4 Thesis overview

Having introduced the research theme, aims, objectives and the methodology, this section presents the remainder of the thesis structure.

Chapter 2 outlines the current state of ZEV and related ESS, fuel cell and hydrogen technologies. Chapter 2 is adapted from the author's published paper "Intelligent Hydrogen Fuel Cell Range Extender for Battery Electric Vehicles". Based on this review, ZEVs has shown that FCEVs have the most potential to achieve the goal of 'The Road to Zero'. A gap was identified between the current and future BEVs and FCEVs.

Chapter 3 details an original FCEV powertrain model based on the Coventry University Microcab H2EV. The model is adapted to simulate both active and

passive hybrid FCEV.

Chapter 4 presents the experimental works for validating the passive hybrid FCEV model developed in chapter 3. The simulation results are shown to be in good agreement with measurements. This provided the confidence continue to analyse and develop the passive hybrid fuel cell powertrain model as described in chapters 5 to 8.

Chapter 5 investigated the benefits of direct passive system effect on FCEV performance and range extension for initial conditions, e.g. different battery SoC level.

Chapter 6 presents an original fuzzy logic controller, which is designed for passive hybrid system to control the power flow between fuel cells and ESS by modulating the hydrogen pressure. The results showed that the passive system can satisfy the load of FCEV while reducing the number of fuel cell start-stop times and extending the overall range. The application of the developed fuzzy controller further improves on the performance of the passive hybrid system without fuel cell power output fuzzy control. This chapter is based on the author's submitted paper "Evaluation of a hybrid FCEV based on a passive fuel cell/battery architecture FCEV".

Chapter 7 presents the impact of Lithium-ion, lead-acid and NiMh battery technologies on passive hybridization system. Despite the advances in the other technologies, it is shown that lead-acid battery is the most appropriate for micro FCEV due to low system cost and the ability to prevent deep discharge due to the fuel cell. Ni-MH battery based passive hybrid system has a relatively lower efficiency than lithium battery but can provide a longer cycle life. Its good

performance when the load is constant makes it more suitable for large vehicle operating mostly on motorways. The current Lithium battery used in the Microcab H2EV vehicle is the best in terms of minimising fuel cell load variation when subject to varying load demand typical of urban driving.

Chapter 8 provides a guideline for selecting fuel cell and batteries size in the passive hybrid system. The demonstrations validated the rules of the guideline. Moreover, it justifies the importance of sizing for a passive hybrid system.
Also presented is the analysis of different drive cycles in order to clarify the scope of use for passive hybrid FCEV. Also, a Well to wheel analysis of different powertrains provides a big picture of environmental impacts on GHG emission.

Chapter 9 provides a summary, conclusions and suggests areas of future work. The overall structure of this thesis is summarised in Figure 1-3.

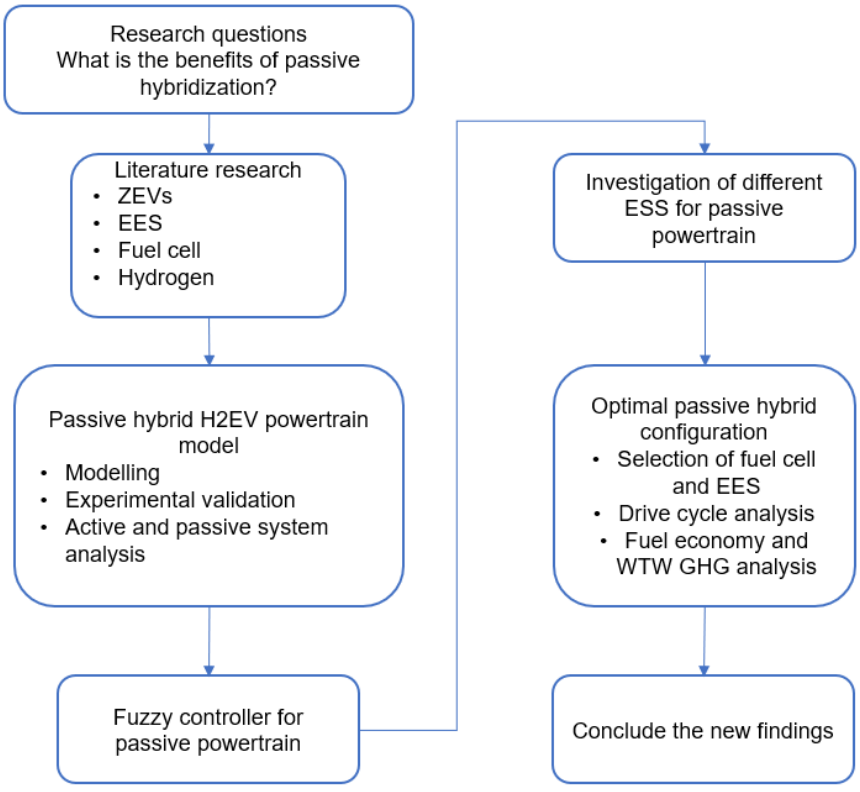

Figure 1-3 Overview of structure of thesis

Chapter 2: Literature Review of ZEV technologies

Road transport is recognized as having a negative impact on the environment. Policies have focused on the replacement of the internal combustion engine (ICE) with less polluting forms of technology, including battery electric and fuel cell electric powertrains. However, progress is slow, and both battery and fuel cell-based vehicles face considerable commercialization challenges.

To understand these challenges, this chapter starts with a review of the state of the art in the academic literature for ZEVs. It then outlines the technologies relating to ZEVs such as batteries, fuel cells and hydrogen. The current gaps in ZEV technologies highlighted and motivation for the research given.

2.1 Overview of zero-emission vehicles

Electric vehicle (EV) technology is developing fast. The population rise and familiarisation with EVs has resulted in governments committing resources to reduce emissions caused by traditional EVs. Ultra-Low Emission Vehicle (ULEV) is a new concept to describe a vehicle that uses low carbon technologies and emits less than 75g/km of CO_2 (SMMT 2016). ULEVs include three types of EVs, Plug-in Hybrid Electric Vehicles (PHEVs), BEVs and FCEVs. ZEV having been identified as the means to deliver ‘The Road to Zero’ strategy is the focus of this work and is reviewed in the following sections.

2.1.1 Current status of battery electric vehicles

BEVs are recognized as a potential Zero Tailpipe Emission (ZTE) automotive solution in the future, which exhibits high powertrain energy efficiency and low running costs compared to other Low Carbon Vehicle (LCV) technologies such

as hydrogen fuel cell and petrol hybrid vehicles (Pollet et al. 2012). However, current BEV limitations include range, cost/efficiency with consideration of the vehicle sizing, as well as the dependency on the charging infrastructure. The following subsections review the current status of BEVs to justify their advantages and limitations in terms of technical and associated business perspectives.

2.1.1.1 BEV Range

The most significant challenge of current BEVs is their limited range compared to ICEV (Internal Combustion Engine Vehicle) average levels, as shown in Table 2-1 based on the New European Driving Cycle (NEDC) and real-world range.

The driving range of BEVs should consider the average driving distance, household vehicle ownership and the percentage of household vehicles used for long-distance journeys. The average daily driving distance in European countries is from 25 miles (UK) to 50 miles (Poland) (EUROPA 2012). In addition, only 19% of vehicles are used frequently to take long-distance trips, but as many as 81% of cars are used for long distance trips. This means that most of the cars will do long distance trips but infrequently (Segard 2015). This is supported by current travel mode behaviours where more than 60% of people prefer to travel by road vehicles for long-distance journeys (over 250 miles). The survey also indicates that only 35% of the families have more than one car to meet the demands of all ranges of their trips (Department for Transport 2019). The conflict between travel demands and daily use cannot be settled with the same electric vehicle (EV). As a result, the range demanded from BEVs cannot be ignored. Since the battery pack is the only energy storage system (ESS) of a BEV, the method used to increase the range is to increase the battery size and improve battery performance. Designing large battery packs to fulfil BEVs' long distances trip requirements will lead to a higher than necessary use of

resources and associated cost for most journeys. It is not efficient to oversize all BEVs to provide equivalent ranges to ICEVs.

Table 2-1 The performance and price of popular BEV models (RENAULT 2019, Volkswagen 2019, BMW 2019, Nissian 2019, TESLA 2019)

Vehicles	Official NEDC range	Real-world range	Retail price	Home charging time (7kW)	Fast charging
NISSAN Leaf 30 kWh	168 miles	124 miles	£26,190	7.5 hours	1 h (50 kW)
Volkswagen e-Golf	186 miles	144 miles	£29,230	5 hours	35–40 min (50 kW)
BMW i3 120Ah	223 miles	160 miles	£36,935	4.5 hours	35 min (50 kW)
Renault Zoe Z.E. 40	250 miles	186 miles	£29,270	7+ hours	1 h (43 kW)
Tesla Model S 75D	304 miles	243 miles	£69,954	11 hours	40 min+ (120 kW)

2.1.1.2 BEV battery Characteristics

Battery performance is one of the most significant features of the BEV; Table 2-2 presents five alternative battery technologies. Lead acid batteries, nickel batteries and lithium batteries are the current commercial solutions. Metal-air batteries and sodium-sulphur batteries are potential candidates for use in future EVs (Tie et al. 2013; Westbrook 2001; Jaguemont et al. 2016; Ren et al. 2015; Das et al. 2017).

Table 2-2 The comparison of energy storage specifications for BEVs

Characteristics	Lead–Acid	Nickel–metal hydride (Ni–MH)	Lithium-ion (Li-ion)	Sodium–Sulphur	Lithium-air
Specific energy (Wh/kg)	35	70–95	118–250	150–240	3463
Energy density (Wh/L)	100	180–220	200–400	-	-
Specific power (W/kg)	180	200–300	200–430	150–230	-
Life cycle	1000	<3000	2000	800+	-
Energy efficiency (%)	>80	70	>95	80	>95
Production cost (£/kWh)	48	160–200	120	200–360	150

The main factors to evaluate battery performance include specific energy (Wh/kg), energy density (Wh/L) and specific power (W/kg). In the automotive industry, consideration of ESS the also includes the life cycle, energy efficiency and production cost. The Ni-MH and Li-ion batteries are widely used in electric vehicles (including BEVs and hybrid vehicles) due to their higher performance compared to other types. Ni-MH batteries are mostly used in hybrid electric vehicles (HEVs) such as the Toyota Prius HEV. Li-ion batteries are widely used as the primary ESS in pure BEVs, such as the Nissan Leaf and VW e-Golf (Pollet et al. 2012). Li-ion batteries are currently offering the best compromise in terms of energy density, lifecycle and cost. This has led to a widespread adoption which has driven its cost down, strengthening its market dominance for the present and the short-term future. However, compared to ICE and FC propulsion, the performance of Li-ion batteries is limited.

The battery performance and BEV range are affected by temperature. The range of Renault ZOE BEV was found to decreases by 56 miles (32%) when temperature decreased from 15 °C to −15 °C, see Table 2-3.

Table 2-3 Range variation against temperature for the Renault ZOE Battery Z.E.40 equipped with 16” wheels and driving at 50 mph (RENAULT 2019)

Temperature	Distance range
−15 °C	120 miles
−5 °C	140 miles
5 °C	169 miles
15 °C	176 miles

According to a report by the Global EV Outlook 2018, the top ten BEV sales (in thousands) by countries in 2017 are China (579), USA (198), Norway (62), Germany (54), Japan (54), UK (47), France (34), Sweden (20), Canada (16) and Netherlands (11) (International Energy Agency 2018). Most of these countries are in the mid-high latitudes of the Northern Hemisphere, and the temperature usually drops under 0 °C in the winter, which means the BEV range in winter is a significant issue.

In summary, increasing battery sizes and associated stored energy in BEVs will lead to an increase in vehicle size and weight without solving the negative impact of temperature on BEV range.

2.1.1.3 Battery Raw Material Limitation

The mass market demand for BEVs with an extended range capable to replace current ICEVs, will lead to a significant growth in raw material usage. The materials involved in battery manufacture includes manganese, nickel, lithium and cobalt. Manganese and nickel have large scale reserves, mature supply chains and only 0.4% of the global nickel demand is for battery use (King and Boxall 2019). They are therefore not expected to be strongly impacted by growing demand for batteries. Lithium and cobalt, which are used in lithium batteries, have a significantly greater influence on the global EV market, with batteries representing about 6% of the total demand for cobalt and 9% of the total demand for lithium in 2017 (King and Boxall 2019).

It is predicted that lithium-ion batteries will remain the market leader for the next twenty years (International Energy Agency 2018). Therefore, even if Li-Air or sulphur batteries overtake the lithium-ion battery in the future, raw materials such as lithium and cobalt will be essential. The availability of resources for the manufacturing of lithium-ion cells is an important topic for the continuing development of electric vehicles. Two key elements of material availability are the material market distribution and the industrial structure (Grosjean et al. 2012). According to McKinsey (Figure 2-1), the battery market for lithium has almost trebled between 2010 and 2017 (Azevedo and Hoffman 2018). It is expected to represent more than three-quarters of overall production by 2025. There is a potential discrepancy between the demand and resource for the amounts of lithium required to feed the expansion of EVs. The latter is envisaged to require 1Mt/year after 2026, whilst current resources are estimated to be between 19.2 Mt and 71.3 Mt (Oliveira et al. 2015).

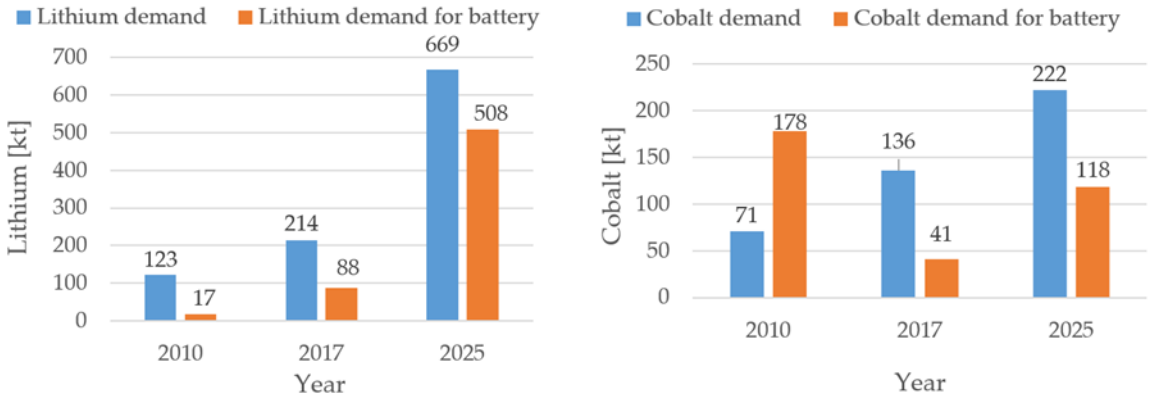

Figure 2-1 Lithium and cobalt demand the evolution of the whole market. Reproduced from McKinsey data (Azevedo and Hoffman 2018)

Despite this gap between supply and demand, some authors believe that the increased demand for Lithium should not become an obstacle in the future due to the presence of untapped reserves. However, commercially viable means to exploit oceanic lithium are yet to be developed and terrestrial stocks have limited extraction capacity. Further, restricted geographic resource distribution has geostrategic implications (King and Boxall 2019). In particular, the lithium supply relies on a minority of countries and companies. China, Chile and Australia occupy 85% of the global production market, and only four companies—Talison, Sociedad Química y Minera (SQM) de Chile, Albemarle, and and Livent Corp. (formerly FMC Lithium)—supply the majority of mining exports (Azevedo and Hoffman 2018).

Although lithium is widely used in EV batteries, cobalt availability is believed to be more critical due to its geographical distribution and geostrategical implications. Global Energy Metals Corp has predicted that 75% of all lithium batteries will contain cobalt by 2020 and above half of the cobalt demand will be driven by batteries (Global Energy Metals 2019). The percentage of cobalt production used for battery manufacturing has so far increased at a much slower rate. It is however expected to grow significantly, reaching more than 50% of cobalt production by 2025. The growing demand for rechargeable batteries

and a low volume of cobalt production has caused the cobalt price to quadruple from 2016 to 2018 (InfoMine 2019). Cobalt is mostly a by-product from mining nickel and copper. Therefore, cobalt production is not expected to be able to meet market demand. According to Macquarie Research, a global production shortfall of approximately 6.4% equivalent to 7194 t is expected in 2020 (Bulletin 2017).

A method to alleviate supply issues is to develop lithium-ion battery remanufacturing and recycling to form a cost-effective supply chain for the electric vehicle battery industry (King and Boxall 2019; Mohr et al. 2012; Gu et al. 2018; Li et al. 2019), as well as other modes of electric mobility. Lithium battery recycling is a long-term strategy to mitigate the magnitude of material shortages. However, less than 3% of lithium batteries are currently recycled, and less than 1% of lithium is reused in new products (Vikström et al. 2013; Wang et al. 2014; Swain 2017). This is firstly due to the recycling technologies lagging behind lithium battery technologies (Huang et al. 2018). Secondly, policy and regulations for lithium battery recycling are not adapted. Therefore, the industry is focusing more on cobalt as opposed to lithium due to its high value (King and Boxall 2019; Huang et al. 2018).

Battery manufacturers, raw material producers and the recycling industry are making a strenuous effort to alleviate the expected raw material crisis. The UK is expected to recycle 339,000 tonnes lithium battery packs (Anwar et al. 2020). The expected improvements in design, materials, manufacturing and recycling should decrease the use of raw materials. Battery end users should also consider the battery capacity requirements for most common journeys; therefore, reducing battery size is a possible solution for material saving. Raw material shortages could not threaten the EV market, provided battery size is not increasing continuously in an attempt to replicate ICEV range, when most journeys require significantly smaller ranges. Alternative solutions should be developed to cater for infrequent longer journeys or adapted to specific vehicles

designed for longer journeys.

2.1.1.4 BEV efficiency and cost

BEVs have powertrains with high energy conversion efficiencies compared to ICEVs. However, the current trend of oversizing batteries to increase vehicle range to become equivalent to ICEVs results in battery size and overall vehicle weight increases. This results in higher energy requirements to move the same vehicle and therefore decreases the vehicle's overall Well-to-Wheel (WTW) energy efficiency, see Figure 2-2.

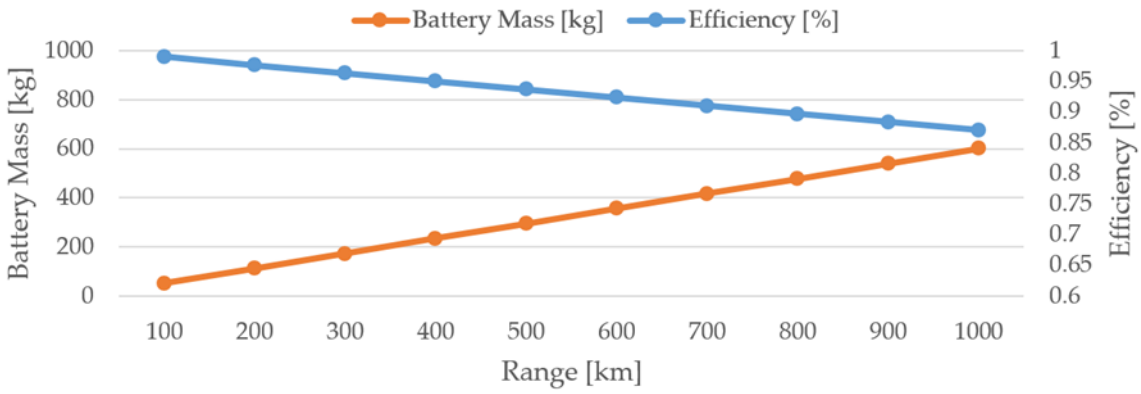

Figure 2-2 Adding battery weight decreases efficiency, which was revealed by an internal analysis based on G4 Vehicles (Golf class). Reproduced from (ERTRAC 2018)

Simultaneous increases in battery size and reductions in overall vehicle WTW energy efficiency and increasing material consumption are increasing both the manufacturing and running costs of BEVs. Brennan and Barder found in 2016 that the average manufacturing cost of a mid-size BEV is £14,000 more than ICE vehicles, with the cost of the battery pack being one of the main costs (Brennan and Barder 2016), see Table 2-1.

Incentives from governments have helped balance the significant price difference between EVs and ICEVs. In addition, changes in customer

behaviours and motivations, and the impact of “diesel-gate” have resulted in increased sales. In particular, registrations of BEVs more than doubled in 2017, whilst they only increased by 7% between 2015 and 2016 (Alawi and Bradley 2013; Noori et al. 2015; Hutchinson et al. 2014; Wu et al. 2015; Palmer et al. 2018; Bundesregierung 2016; Bubeck et al. 2016; Kane 2017). The ICEV cost-effectiveness (high performance-price ratio) is still slightly higher than BEVs (Noori et al. 2015). ICEV’s cost-effectiveness is reliant on the oil price, and uncertainty associated with the latter can potentially make this highly variable. Today, BEV prices are higher than ICEVs for an equivalent model. However, in certain conditions, such as with suitable subsidies, appropriate length of ownership and refuelling costs, the lifetime costs of EVs are competitive when compared to ICEVs (Hagman et al. 2016; Roth 2015). For example, the Toyota Prius is London’s favourite private hire car, with twice as many having been purchased compared to the second-place vehicle – the Ford Galaxy (Ottocar 2018).

According to the 2017 APCUK Roadmap from British Automotive Council, future BEVs need to be ‘tailored for usage’ (Automotive Council UK 2017). This means that the range and size of BEVs should be adapted to demands and applications. This could avoid oversizing the BEV that would otherwise result in increased manufacturing and running costs, and higher purchase prices. Appropriate vehicle and battery sizing will decrease the demand for raw materials that are limited in availability. Based on the National Travel Survey England 2018 by the Department for Transport, the average annual driving range in the UK was 6580 miles in 2017, which equals around 25 miles per day (Department for Transport 2018). Hence, tailored BEVs will mostly be small- or medium-sized vehicles, and they will rely more on charging infrastructure to allow longer ranges.

2.1.1.5 BEV Infrastructure availability

Limited by vehicle efficiency, costs and raw materials, future BEVs require a reduction in battery size, and this will lead to a range decrease. As a result, the charging frequency will increase, and this will make BEVs depend more on charging infrastructure. Table 2-1 presents the charging time using home and fast charging facilities for popular BEVs. Most current BEVs require more than five hours when using home charging, and when using public fast-charging infrastructures, the charging speed is much higher but still over 30 min, which is not comparable to the refuelling speed of ICE vehicles and FCEVs. Thus, to fully commercialize and replace current ICEVs, the demands of BEV charging infrastructure will be much higher than current petrol stations. The growth in the speed of BEV charging infrastructures has been fast in the past few years, due to increasing ownership of BEVs and governmental efforts. Figure 2-3 shows the growth in the total number of charging connectors in the UK from 2011 to 2018.

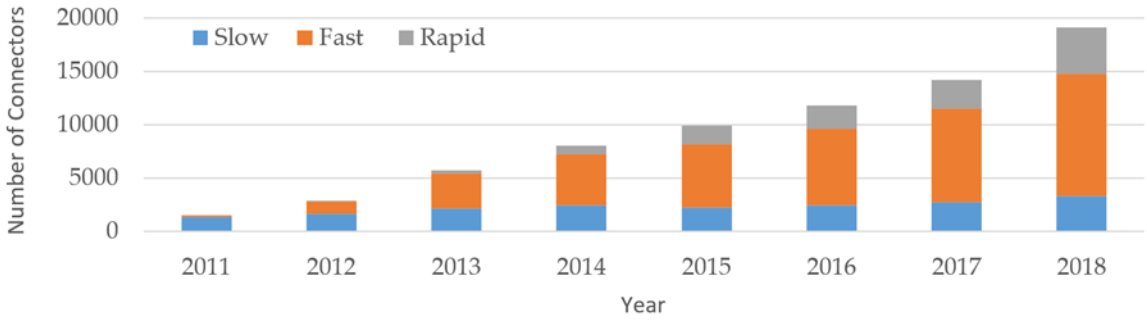

Figure 2-3 Total number of charging connectors in the UK. Reproduced from (ZAP-MAP 2019)

Chargers are divided into three categories: “Slow (7h-8h)” chargers are mostly rated at 3 kW and used in the home. “Fast (2.5h)” chargers have power ratings of more than 7 kW and are found in household and public facilities. “Rapid(45min-1h)” chargers are mostly provided in public facilities with specific vehicle charging points. The latest data from the 2019 UK ZAP-MAP, a UK-wide

map of charging points, indicates that the total number of public points was 1622, the number of rapid charging devices was 2361 and the total number of rapid charging connectors was 5489(ZAP-MAP 2019). It seems that the growth of charging infrastructure is fast, but the total number of public charging points is still very small in comparison to petrol stations. As the Department of Energy and Climate Change claimed in 2012, the distance between each petrol station in the UK is shorter than a 10 min drive (The Department of Energy and Climate Change 2012). Hence, charging infrastructure construction will be a long-term project which will require decades to reach the current level of petrol station infrastructure. The rapid growth of BEV charging infrastructure will also lead to increased demand for electricity, and corresponding actions are required from the National Grid System (National Grid Group 2017).

2.1.1.6 BEV brief summary

BEVs have advantages in energy efficiency and higher environmental performance compared to ICEVs and ICE-based HEVs are recognized as one of the future road vehicle solutions with the most potential. In order to meet the requirements of peoples' vehicle demands and reach the target goals to replace current ICEVs, BEVs will need to increase their range and reduce their cost. However, limited by battery performance and main raw material resources, increasing the battery capacity for drive range extension will decrease vehicle efficiency, and lead to growth in both manufacturing and running costs. Another method to realize future BEVs, "tailored for usage", will not be easy to achieve since more than 65% of families own only one vehicle which is expected to fulfil any length of journey that is demanded. Moreover, the "tailored for usage" BEVs, which are mostly small/medium-sized vehicles, will depend more on infrastructure, but the amount of charging facilities will not reach the level of the current petrol stations in a short period.

Similar to BEVs, another future vehicle solution, FCEVs, have advantages

compared to ICEVs and other competitive vehicles, but also have limitations in both technical and associated business aspects.

2.1.2 Current status of fuel cell electric vehicle

FCEVs use hydrogen as the power source, where the hydrogen fuel cell supplies the appropriate voltage to the battery or the power system. There are some competing energy storage technologies for use in FCEVs. Table 2-5 shows an overview of the latest situation for fuel cell energy storage technologies. The advantages and disadvantages of various fuel cell technologies, such as electro-chemical, chemical and electric, are examined for different kinds of fuel cell vehicles.

2.1.2.1 Performance and pricing of current FCEV fleet

Table 2-4 The performance and price of popular FCEV models

Fuel cell Vehicles	Real-world range	Retail price	Annual fuel cost	Battery
2019 Honda Clarity	360 miles	£295/Month for 36-Month lease	£ 1000	346 V Lithium Ion
2019 Hyundai Nexo	354 miles	£51,200	£ 1200	240 V Lithium Ion
2019 Toyota Mirai	312 miles	£66,000	£ 1000	245 V NiMH

In 2018, there were only 8000 FCEVs in stock in the world, and 4500 of them were in the US (International Energy Agency 2018). In terms of vehicle range (see Table 2-4), the FCEV has a longer a range than the BEV and a similar range in comparison to conventional vehicles. However, the development of fuel cell technology and the high energy density of hydrogen, make it relatively

easy to increase the range without significantly oversizing the ESS. For example, Toyota have targeted a 620-mile driving range with a fuel cell concept car which can offer more than a 50% increase in driving range over the current Toyota Mirai™ FCEV (BLOOMBERG 2017). For example, from Figure 2-2 a 300kg battery pack is need for 312 miles journey for BEV, and for same journey the FCEV only need total 109kg weight for the hybrid system(47kg battery pack with 57kg fuel cell stack and 5kg hydrogen tank) (Green Car Congress 2020). Unlike BEVs, it can be seen in Figure 2-4 above certain point of battery capacity, the fuel cell stack size has limited effect on fuel consumption which means overall efficiency is decreased slightly when battery size and fuel cell size increase (Fletcher 2020). Generally, when the optimal size of hybrid system is selected, FCEV can easily add more fuel to hydrogen tank without increase the battery pack and fuel cell stack size.

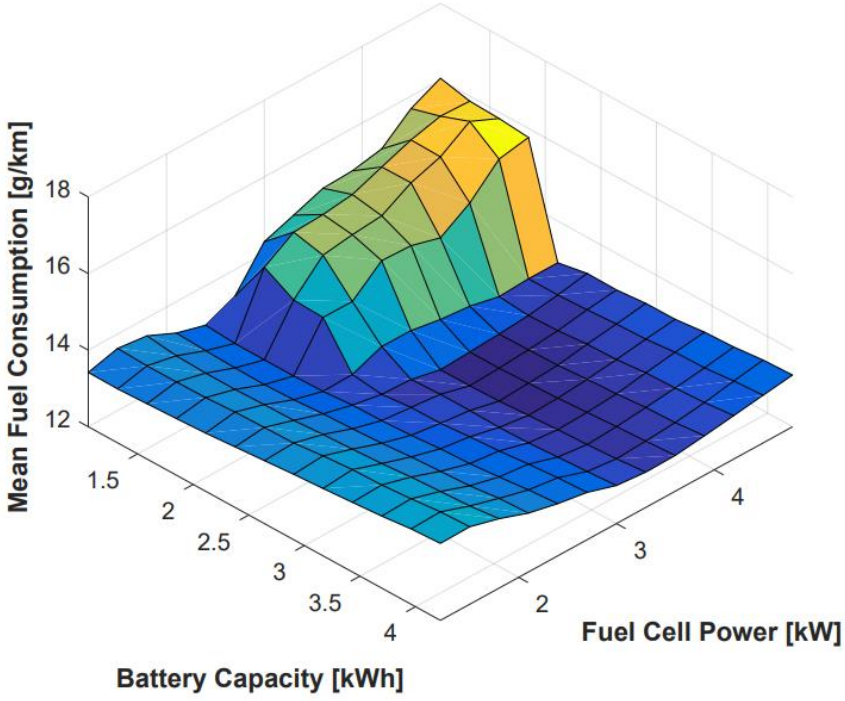

Figure 2-4 Battery and fuel cell size effect on fuel consumption (Fletcher 2020)

From the point-of-view of customers, the purchase price of FCEVs is much higher than for other vehicles. FCEVs is about 4 times more expensive than the ICEVs and 2 times more expensive than the BEVs. This is mainly related to the

production/sales volume, since the current number of FCEVs is incomparable with other types of vehicles. The running costs of FCEVs and BEVs are currently much lower than ICEVs as taxes are not added to the hydrogen fuel and electricity for charging. However, FCEVs' operating costs are still expected to remain lower than ICEVs, even if taxes were to be added for fuel and electricity charging.

2.1.2.2 FCEV Infrastructure availability

The refuelling speed of FCEVs is similar to ICEVs which only takes about a few minutes. The most significant problem for fuel cell vehicles is a lack of hydrogen refuelling stations. In 2018, there were 330 stations around the world and only 15 fuelling stations in the UK (International Energy Agency 2018). In 2017, John Hayes, the UK Transport Minister, acknowledged that the main obstacle to hydrogen fuel cell electric vehicles was the refuelling infrastructure, and a new £23 million fund was announced by the government to boost the development of hydrogen vehicles and the required infrastructure (Department for Transport et al. 2017). This move was part of the ambition of the UK government to achieve zero-emissions for every new car by 2040. Following this help from government, Burgh stated that this incentive program would attract more investment and encourage further development of hydrogen-powered vehicles and infrastructure (Department for Transport et al. 2017).

The increase in hydrogen refuelling stations is significantly increasing the demand for hydrogen. The latter requires a significant growth of hydrogen production and a vast distribution network. Section 2.3 on the hydrogen economy addresses both of these issues.

2.1.2.3 FCEV summary

FCEV advantages include range (compared with BEVs), overall efficiency,

running costs and zero tailpipe emissions (compared to other ICEVs and HEVs). FCEV limitations include the limited hydrogen infrastructure and distribution network, as well as a high purchase cost. FCEVs can meet the requirements of daily use and longer travel demands in the future. FCEVs are currently dependent on the hydrogen economy and could supplement it or be restricted by this relation. The high cost of fuel cell systems, the shortage of infrastructure and the immaturity of the hydrogen economy all limit the development of FCEVs. Hence, a transition solution is required to bridge the gap between today's and future BEVs and FCEVs. Passive hybridization FCEVs might fulfil this gap. The following sub-section will introduce the ESS (in Appendices), fuel cell and hydrogen technologies that can be used in a passive hybrid powertrain.

2.2 Review of different fuel cell technologies

The most popular fuel cell technologies are Direct Methanol Fuel Cells (DMFC), Proton Exchange Membrane Fuel Cells (PEMFC), Alkaline electrolyte Fuel Cells (AFC), Phosphoric Acid Fuel Cells (PAFC), Molten Carbonate Fuel Cell (MCFC) and Solid Oxide Fuel Cells (SOFC). The PEMFCs, AFCs and direct methanol have advantages such as portability and miniaturization. PAFCs and SOFCs are suitable for medium and large power generation, as well as combined heat and power. MCFCs are suitable for large scale energy generation (Das et al. 2017). The technology with ideal characteristics for road vehicle applications is PEMFC. It has high overall efficiency, quick start-up, low-temperature operation, zero-emission, a long lifetime, simple design, small volume, less weight and non-corrosive features (Gencoglu et al. 2009; Bromaghim et al. 2010). However, the costs of the proton exchange membrane and the platinum catalyst are prohibitively high. Researchers and automotive manufacturers are continuing to optimize fuel cells. For example, the Toyota Mirai™ fuel stack not only reduced volume by 43% and weight by 48%, but also improved power delivery by 26% compared with the 2008 model of fuel stacks

(Hunt 2018). Due to the developmental potential of fuel cell for portable applications, transportation applications and stationary applications, the fuel cell could become an environmentally friendly, economically-competitive energy storage device for the future market (Sharaf et al. 2014).

Table 2-5 Summary of fuel cell characteristics (Tie et al. 2013; Mekhilef et al. 2012; Elmer et al. 2015; Sharaf et al. 2014)

Energy storage source type	Alkaline electrolyte fuel cells (AFC)	Phosphoric acid fuel cells (PAFC)	Solid oxide fuel cells (SOFC)	Molten carbonate fuel cell (MCFC)	Proton exchange membrane fuel cells (PEMFC)	Direct methanol fuel cells (DMFC)
Anode catalysts	Nickel	Platinum supported on carbon	Nickel–YSZ composite	Nickel Chromium	Platinum–Ruthenium supported on carbon	Platinum–Ruthenium supported on carbon
cathode catalysts	Silver supported on carbon	Platinum supported on carbon	Strontium-doped lanthanum manganite	Lithiated nickel oxide	Platinum–Ruthenium supported on carbon	Platinum–Ruthenium supported on carbon
interconnect material	Metallic wires	Graphite	Ceramics	Stainless steel	Graphite	Graphite
electrolyte	An aqueous solution of potassium hydroxide	Liquid phosphoric acid	Yttria-stabilized zirconia	A liquid solution of lithium, sodium, and/or potassium carbonates,	Solid polymeric membrane	Solid polymer membrane
Fuel	Pure H2	Pure H2	H2, CO, CH4, other	H2, CO, CH4, other	Pure H2	CH3OH
Cell voltage	1.0	1.1	0.8-1.0	0.7-1.0	1.1	0.2–0.4
Operating temperature (◦C)	70-100	150-220	600-1000	600-700	50-100	60–200
System output (kW)	10-100	50-1000	1-3000	1-1000	1–250	0.001–100
Electrical efficiency (%)	60-70	36-45	35-65	45-65	43-58	40

2.3 Hydrogen economics

Due to the first oil crisis, an attractive proposal, the Hydrogen economy, was presented in the first World Hydrogen Conference by Australian chemist John Bockris. However, the development of hydrogen technology was slow before the twenty-first century, but the concept attracted recent attention due to the awareness of global warming (Moliner, 2016). Hydrogen is widely used for fuel cell and FCEV applications; therefore, the hydrogen economy is directly relevant to the development of FCEVs. In this section, the current situation of hydrogen production, delivery, storage and utilisation will be analysed

2.3.1 Hydrogen policies in different countries

Table 2-6 shows the hydrogen development situation across different countries. Japan being a resource-poor country, the development of hydrogen has been a priority. As a result, Japan is leading in fuel-cell technology. However, other countries are gradually realising the importance of hydrogen and redoubling their efforts to catch up with Japan.

Table 2-6 Hydrogen situation of different countries (Suzanna and Alex 2020, Jason 2019, Fuel Cell & Hydrogen Energy 2020)

Country	Key programs and policy
United States	Creating £101.12 billion per year in revenue and 0.7 million jobs by 2030 for the hydrogen program.
UK	£90 million package funding for hydrogen technology.
Germany	The German government, in conjunction with 300 companies, plan to build over 400 refuelling stations by 2023. The project will cost around £306 million to provide hydrogen infrastructure.
China	Targeting for 1 million FCEVs by 2030.
Japan	A long-term plan for hydrogen energy development from 2014 to 2050.

2.3.2 Hydrogen production

Although hydrogen is abundant on earth, it cannot be obtained directly, unlike oil and gas. There are many ways to produce hydrogen. Natural gas reforming is the most common process used to create hydrogen. Steam reforming and partial oxidation methods can produce hydrogen from methane. Low-cost natural gas reforming can provide hydrogen for FCEVs and other applications such as electric power grids (ENERGY EFFICIENCY & RENEWABLE ENERGY 2019). Usually, industries use the natural gas reforming method to produce hydrogen and CO_2. Due to the unwanted release of CO_2 into the air, the hydrogen resulting from this production method is called “grey hydrogen” (GasTerra 2019). In the long-term, the usage of oil and gas is expected be replaced by solar power and wind power to generate hydrogen. This type of hydrogen is often called “green hydrogen”. A technology called Carbon Capture and Storage can capture almost 90% of the CO_2 by-product during the industrial process, preventing most of the CO_2 from entering the atmosphere (Carbon Capture& Storage Association 2019). This type of hydrogen is called “blue hydrogen”. New techniques to produce hydrogen will be implemented, such as photocatalytic water splitting and high-temperature water electrolysis by nuclear technology. Once these methods become reliable and efficient, the whole production chain will exclude the use of carbon-based energy. Table 2-7 and Table 2-8 show a summary of the different hydrogen production technologies.

Table 2-7 Summary of hydrogen production technologies (ENERGY EFFICIENCY & RENEWABLE ENERGY 2017; Lee and Appleggate 2004; Nikoo et al. 2015; Pandu 2012; Das et al. 2001; Bridgewater 2001; Calzavara et al. 2005; Wang et al. 2007; Meier et al. 2014)

Hydrogen production technology	Hydrogen production methods	Advantages	Disadvantages
Thermo-chemical technologies	Coal gasification	Mature industry technique, low cost of material, By-products are useful	CO2 emission, low-quality hydrogen, high operation temperature, high cost of equipment
	Coal pyrolysis	Mature industry technique, by-products are useful	CO2 emission, high operation temperature 800-820 °C, high energy cost
	Steam reforming	Mature industry technique, highest efficiency of all traditional approaches.	CO2 emission, high cost of equipment, short service life of adsorbent and catalyst
	Partial oxidation	low energy consumption, mature industry technique, low cost of equipment	CO2 emission, high cost of oxygen, stability of catalyst, operating safety
	Auto-thermal reforming	Mature industry technique, lower energy cost than steam reforming	CO2 emission
	sulphur–iodine cycle	Zero emission, clean and renewable energy source	High cost, low efficiency. Highest cost of electro-chemical technologies.
Electro-chemical technologies	Electrolysis of water	Clean emission, clean and renewable energy source	The high cost of construction, low efficiency.
	Microbial electrolysis	Clean emission, solves waste-disposal problems, high conversion efficiency of the material, high economic value.	Low efficiency, electrode corrosion problem, high operation temperature
	Plasma thermal reforming and gasification	Clean emission	High cost, low efficiency, the deferred reaction of photocatalyst
	Photocatalytic water splitting	Zero-emission, clean and renewable energy source	High cost, low efficiency. Highest cost-effective of electro-chemical technologies.

Table 2-8 Summary of hydrogen production technologies (ENERGY EFFICIENCY & RENEWABLE ENERGY 2017; Lee and Appleggate 2004; Nikoo et al. 2015; Pandu 2012; Das et al. 2001; Bridgewater 2001; Calzavara et al. 2005; Wang et al. 2007; Meier et al. 2014)

Hydrogen production technology	Hydrogen production methods	Advantages	Disadvantages
Bio-hydrogen technologies	Fast pyrolysis	Material from gaseous and liquid recycled products.	A high-temperature operation such as 800 °C, carbon deposition will reduce performance of the catalyst
	Steam gasification	Higher purity and quality H2.	High energy cost, temperature and water vapour levels could influence hydrogen production
	Solar gasification	higher efficiency than traditional gasification, low CO2 emission	The high cost of solar panel, slow technology improvement
	Supercritical water gasification	Enhances the solubility of reactants and reaction products, high yield of production	High cost, small scale, conversion yield and the plugging problem caused by the chars, corrosion of materials
	Direct bio-photolysis	Low energy consumption, environmentally friendly.	Safety problem, low efficiency, lack of an available enzyme.
	Indirect bio-photolysis		
	Photo-fermentation	Environmental friendly, waste-water treatment, unremitting hydrogen production ability	Hydrogen production influenced by pH, high cost, lack of an available enzyme.
	Dark fermentation		
	Sequential dark-photo fermentation		
	Plasma gasification/pyrolysis	Less pollutant, Mature industry technique	Very high energy cost, high maintenance cost

2.3.3 Hydrogen storage and distribution

The high-pressure gaseous hydrogen storage method is the most widely used in the world. This method is suitable for vehicles because of its lightweight and low cost. Liquid hydrogen storage results in evaporation of 2–3% of hydrogen

every day (Satyapal et al. 2007). Materials-based storage methods need a reduction in cost and improvements in the capacity to meet future demands. Hence, for vehicular applications, compressed gas storage has two ways it can be improved to meet ongoing demand. One way is to change the composition and structure of the hydrogen that is stored in the tank, such as a combination of liquid hydrogen and cryogenic hydrogen. The other way is to improve the structure inside the tank (Satyapal et al. 2007).

Hydrogen delivery problems are closely linked to hydrogen storage technology. Currently, hydrogen gas is usually stored in a high-pressure tank and delivered by trucks, gaseous tube trailers and by railway. Liquid hydrogen is bulk-stored in low-temperature adiabatic tanks and delivered by planes, trucks, ships and by railway. It is straightforward to deliver solid hydrogen; however, the efficiency of transportation is less than 1% due to the heavy weight (Jia et al. 2011).

2.4 Motivation for passive hybridization of passenger vehicle

The previous reviews have presented the current state of the art in the academic literature of ZEVs, and latest technologies of batteries, fuel cells and hydrogen that impact FCEV development and commercialisation. Based on these reviews, BEV and hydrogen FCEV have been recognized as having the most potential to realise zero-emissions. However, the current challenges to realizing this goal include the race towards larger battery packs, potential shortages of resources and raw materials, battery technology limitations, and limited infrastructure to support a large fleet of BEVs. Commercially available FCEVs typically demonstrate more extended drive range (greater than 300 miles), with the Honda Clarity achieving 360 miles. FCEVs also have faster refuelling times (5 minutes) as compared to BEVs, making them a convenient alternative for zero-emission vehicles.

Since the hydrogen economy is still in the early stages of development, the

main drawback of FCEVs is that they are significantly more expensive than BEVs.

Therefore, it is time to devise the means to reduce the cost and increase the efficiency of FCEVs. A new, highly efficient and low-cost passive hybrid powertrain is a possible solution for FCEVs.

Some research works have previously analysed passive hybrid system. Zhang et al. (2018) used a passive hybrid system for an unmanned aerial vehicle (UAV) to reduce the system weight. It was shown that direct passive hybridization required more hydrogen fuel compared to use of fuzzy energy management with a DC-DC converter. González et al. (2019) investigated the flexibility of a passive hybrid system used in an Unmanned Ground Vehicle (UGV). The researchers presented a 35% operational duration increase (from 5 hours to 7.6 hours) for a passive hybrid system as compared to an active system. Wu et al. (2014) demonstrated the increased system efficiency of a fuel cell super-capacitor passive hybrid system. Bernard (2011) developed a Proportional plus Integral (PI) controller adjusting fuel cell power based on bus voltage of an FCEV passive hybrid powertrain.

Analysis of passive hybrid technologies have been mainly focused on UAVs and UGVs, with only a few studies focused on FCEVs. The following list summarizes academic work relating to passive hybridization:

1. No studies have analysed the relationship between passive hybrid system performance under different battery SoC for passenger FCEV.
2. The fuel cell stack power curve is a critical point that is overlooked. Therefore, there is lack of control method developed to extend the fuel cell and battery lifespan for passive hybrid passenger FCEVs.
3. Studies of passive hybrid passenger FCEV configurations based on an

experimentally validated powertrain model has rarely realised.

4. Studies have investigated passive hybrid systems, but only using lithium batteries as the ESS.

5. Many passive hybridization analysis works use a specific combination of fuel cell and battery. Selection guidelines for different batteries and fuel cells have generally been ignored.

Therefore, this PhD work aims to fill these gaps in current passive hybridization passenger FCEVs.

2.5 Conclusions

Critical analysis of the literature regarding ZEVs has shown that FCEVs have the most potential to achieve the goal of 'The Road to Zero'. Furthermore, the reviews of energy sources, fuel cell and the hydrogen economy have highlighted the existing challenges for FCEVs. Passive hybridization has been found to be a promising solution for FCEVs and is the main focus of this work. The next chapter describes the original model developed that is the basis for the control system development and evaluation of the benefits of passive hybrid passenger FCEV powertrain.

Chapter 3: FCEV powertrain modelling

3.1 Introduction

This chapter describes the modelling work relating to the development of active and passive hybrid Coventry University Microcab H2EV. The original model developed is key to the work carried out in the subsequent chapters of this thesis.

The remainder of this chapter is organised as follows. Section 3.2 describe the features of the Microcab H2V that is used as the target to this research. Section 3.3 describe the active and passive alternatives for hybrid FCEV. Section 3.4 review the modelling tools and justify the use of the MathWorks environment. Section 3.5 describe the main components of the FCEV powertrain model.

3.2 Coventry University Microcab H2EV

The FCEV modelled in this thesis was designed and built by the Coventry University spin-out company Microcab, which is part of the Institute for Future Transport and Cities, Coventry, UK. Microcab participated in two major projects: LREV (Hydrogen for Long Range Electric Vehicle) and SWARM (Demonstration of Small 4-Wheel fuel cell passenger vehicle Applications in Regional and Municipal transport). Figure 3-1 shows the Coventry University Microcab H2EV platform and Computer Aided Design (CAD) model.

Figure 3-1 Coventry University Microcab H2EV platform and CAD model (Apicella 2017)

The H2EV is a four-seat lightweight passenger vehicle which is primarily used in the urban area. The main vehicle specification is summarized in Table 3-1. The standard powertrain is illustrated in Figure 3-2. The hydrogen tank supplies hydrogen to the fuel cell, and the electric power from the fuel cell goes through the DC/DC converter to provide the appropriate voltage to charge the battery. It is an active hybrid power train where the power sources combine a customised Ballard 1020ACS proton exchange membrane and a 72V 4.3kWh Li–FePO4 battery. The fuel cell stack is supplied by a 350 bar 74-litre hydrogen tank (1.8kg hydrogen). It uses a DC-DC converter to adjust the power output to charge the battery to a set SoC level. The fuel cell operation is then stopped until the SoC falls to a set level at which point it is required to re-start battery charging. This active hybrid system management strategy is used as a benchmark against which to evaluate the alternative passive hybrid systems.

Table 3-1 H2EV vehicle characteristics

Weight: 700 kg	Weight including driver: 775 kg
Length: 3.5m	Height: 1.7m
Width: 1.6m	Coefficient of drag: 0.3
Frontal area: 2.5 m^2	Maximum speed: 55 mph 90km/h

3.3 FCEV powertrain introduction

There are two main fuel cell and battery hybrid system architectures: active and passive hybrid (Bernard et al. 2011). In an active hybrid powertrain, see Figure 3-2, fuel cells normally operate with a DC-DC converter to control the voltage differences between each device and provide the appropriate voltage for the battery. The advantages of this traditional strategy are better voltage stability and more flexibile sizing of fuel cell and battery. However, according to Microcab's previous studies (Staffell 2011, Shang et al. 2016), the DC-DC converter can only reach about 80% efficiency at full load and pulls the system efficiency down during real urban driving cycles which include many stops/start and low load situations. In passive hybrid powertrains, fuel cell and battery are directly connected without a DC-DC converter, see Figure 3-3. Such an architecture can overcome the shortcomings of active architecture and results in reduced energy losses from converters, reduced weight and volume of the system as well as reduce cost. However, the fuel cell and battery size as well as the control method need to be carefully considered for the passive hybrid architecture.

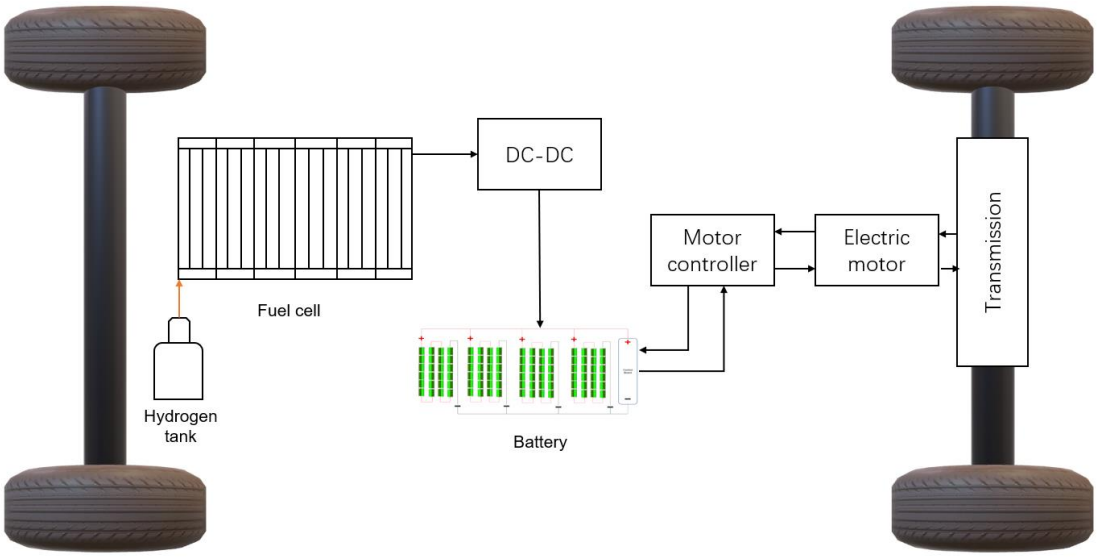

Figure 3-2 Active hybrid FCEV Powertrain with DC-DC converter

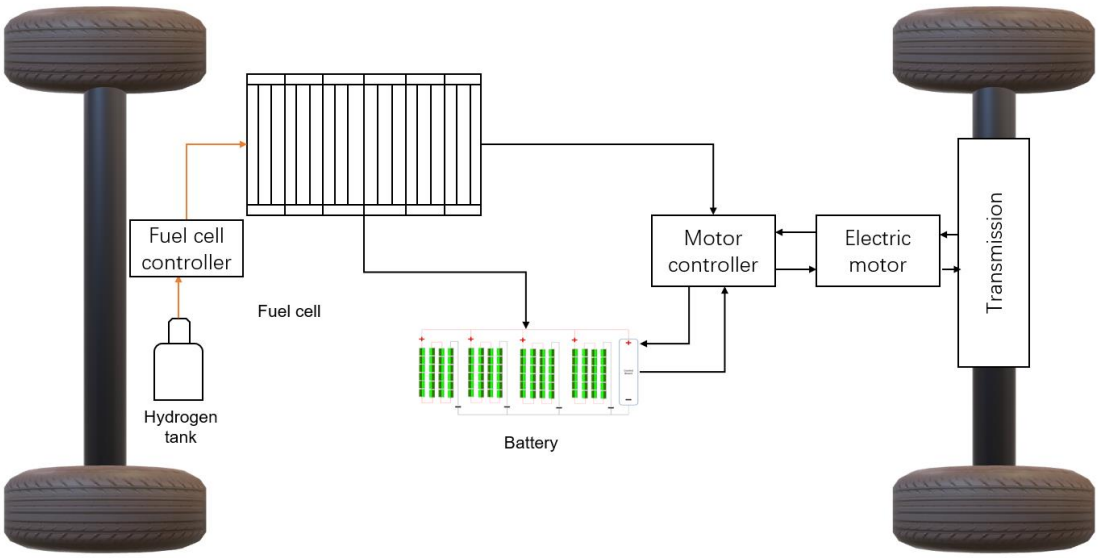

Figure 3-3 Passive hybrid FCEV powertrain without DC-DC converter

3.4 Simulation tool selection

3.4.1 Advanced Vehicle simulator

An advanced vehicle simulator called ADVISOR was developed by National Renewable Energy Laboratory to guide the hybrid vehicle propulsion system in 1994 (Wipke and cuddy 1996). Since then, more than 4500 users have used the ADVISOR including DaimlerChrysler, Ford Motor Company, General Motors Corp, Delphi Automotive Systems, Visteon, and others. However, ADVISOR was initially developed as an analysis tool for classic conventional, electric, and hybrid vehicles (Brooker, et al. 2013). Therefore, programming this software for design and analysis of a novel passive hybrid FCEV is challenging.

3.4.2 AVL CRUISE

AVL CRUISE is a mature simulation package for system-level vehicle powertrain analysis, and it is widely used for industry. The simulation tool is mainly focused on powertrain concepts, and engine development for testbed plant models (AVL 2019). The drawback of the tool is that it requires a large

amount of test data for creating a new component (Apicella 2017). This makes it a time-consuming process to modify hybrid system architectures without sufficient test data.

3.4.3 MATLAB®/Simulink®

MATLAB®/Simulink® is a flexible simulation tool supporting multiple applications. It allows researchers to customise blocks from its library, and adapt the model parameters used by the blocks to the system being modelled. The software combines various toolbox features with a vehicle model to allow design and analysis of FCEV powertrains. Although Simulink cannot provide readily available components like ADVISOR and AVL CRUISE, it gives users the most flexible conditions to develop a novel powertrain, including the most flexibility in terms of the system model and controller development and has therefore been adopted in this work.

3.5 FCEV powertrain modelling

There are two typical modelling method for FCEVs. One is forward modelling, and the other one is backward modelling (see Figure 3-4). For backward modelling, the vehicle transmission direction is the opposite of reality. This modelling method ignores the intention of the driver, in order to reduce the complexity of the integration calculations. However, it is assumed that the FCEV can meet the demands for duty cycle, which is not possible in all scenarios. Unlike backward modelling, the forward modelling structure is similar to the real system. The driver model could use the throttle to adjust the acceleration of the vehicle and the brake pedal to decelerate the FCEV. The controller follows the driver’s command to send the signal to the corresponding parts. The forward modelling is able to simulate a real system, but due to the calculation complexity, the simulation speed is not as fast as forward modelling (Zhou 2017). In order

to build a more accurate model, forward modelling is used in this study.

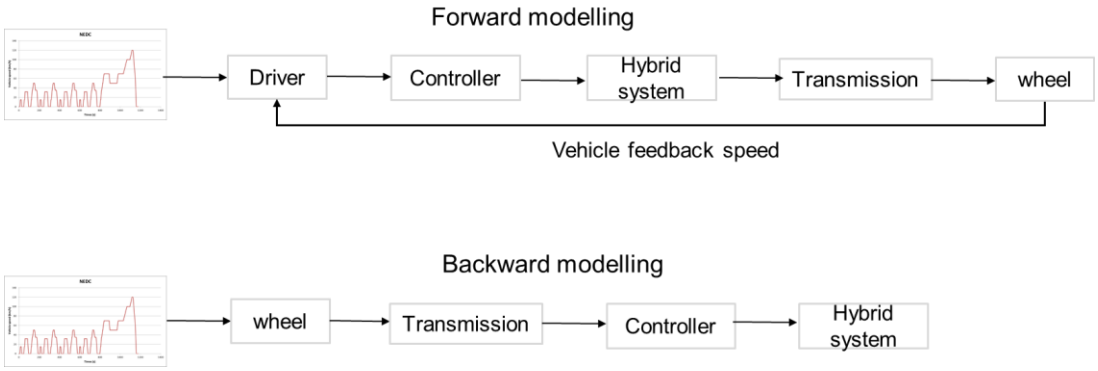

Figure 3-4 Forward and backward modelling

A hybrid FCEV powertrain MATLAB®/Simulink® model was built to evaluate the powertrain efficiency and drive range based on different powertrain configurations. The powertrain blocks were chosen from the MATLAB®/Simulink® toolboxes and libraries (MathWorks 2019). The overview of the hybrid system model is presented in Figure 3-5 and Figure 3-6.

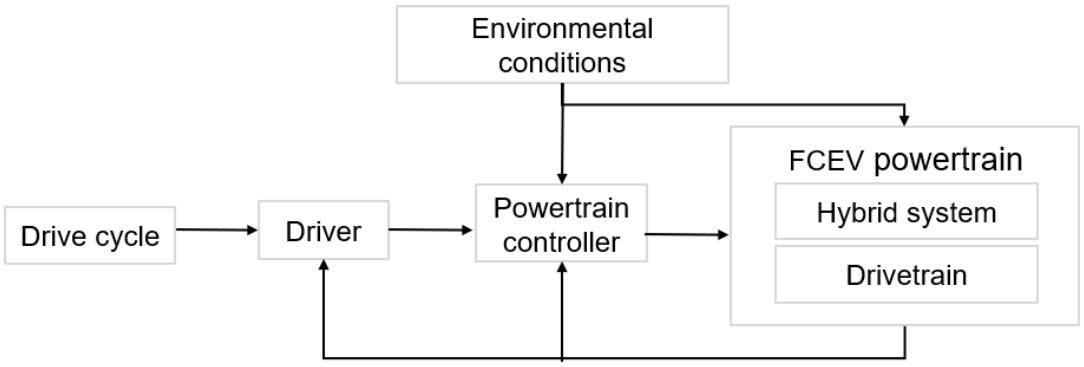

Figure 3-5 Overview of FCEV hybrid powertrain model structure

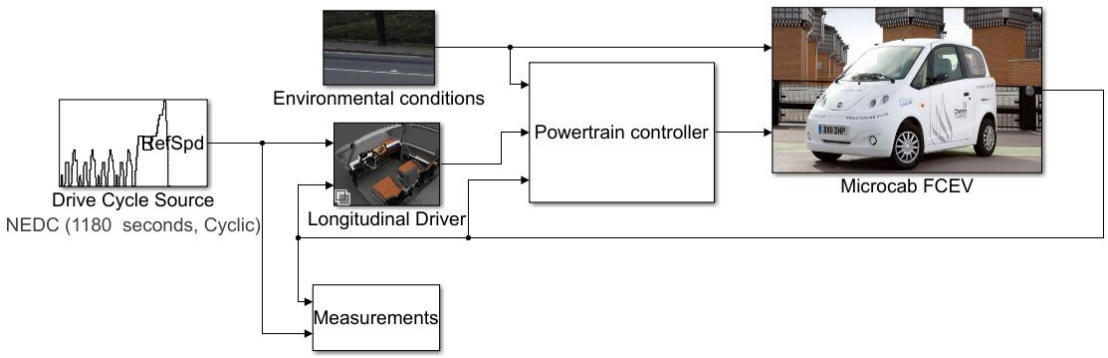

Figure 3-6 Simulink model of Microcab H2EV

The H2EV is a lightweight passenger vehicle which is primarily used in the urban area. Different drive cycles can be selected from the drive cycle source model. The driver model supplies the acceleration and braking commands for the FCEV. It allows the vehicle to follow the required drive cycles or driver request. The environmental conditions model creates the ambient variables, including air temperature and pressure, wind velocity and ground grade.

The powertrain controller module consists of a battery management system, a regenerative braking system and an electric motor management system. The regenerative braking module converts throttle and brake pedal position to traction wheel torque demand and regulates the use of regenerative charge power to prevent the overcharge of the battery. Keeping the battery SoC below 80% enable the FCEV to always be able to use maximum regenerative energy to charge the battery. The electric motor management system provides electric power demand based on required motor torque and speed. The efficiency of the motor is modelled using a lookup table that represents the efficiency map. The electric plant includes a fuel cell and a battery system to supply power to the FCEV.

The drivetrain module can configure the parameters of the vehicle. In this work, the Microcab FCEV is using the front-wheel drive and is equipped with disc brake systems. This subsystem uses the required motor torque to calculate the

motor speed and feeds back the resulting vehicle speed to the powertrain controller. The latter generate normalized acceleration and braking commands to reduce the error between the driver requested speed and the current vehicle speed. This model can simulate different FCEV architectures with different control methods under various environmental conditions. Modelling of each component is described in the following sub-clauses.

3.5.1 Drive cycle and driver model

A drive cycle is a configured schedule for vehicle test which allows the developer to simulate and test the FCEV under a reproducible situation. There are more than 200 standardised drive cycles (Barlow et al. 2009). Therefore, multiple drive cycles could be simulated for the robustness of the proposed FCEV powertrain. For the FCEV powertrain model, the drive cycle is generated by the drive cycle source block, which is able to generate a stylised cycle, a realistic cycle or a user-defined drive cycle. The examples of the first two drive cycles are shown in Figure 3-7 and Figure 3-8.

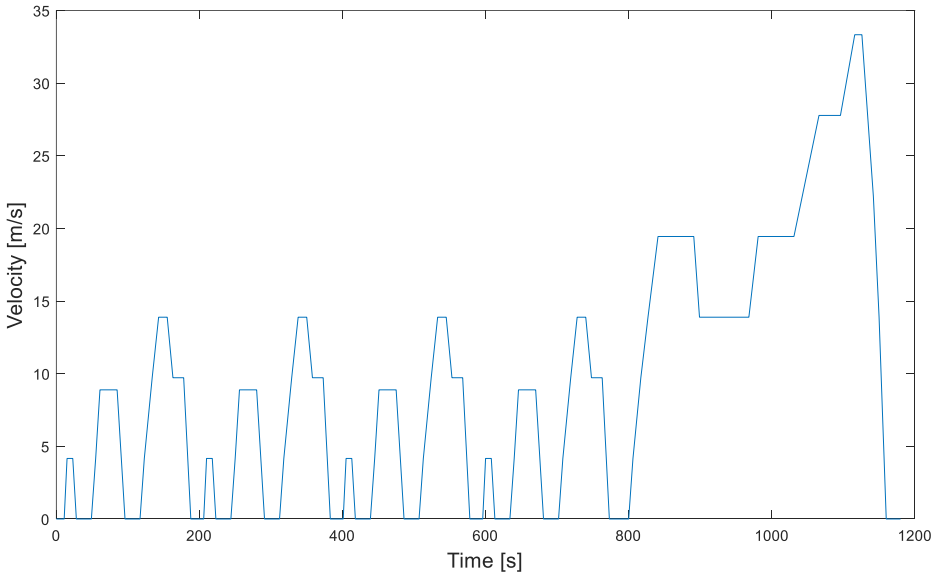

Figure 3-7 Stylized drive cycle: New European Driving Cycle (NEDC)

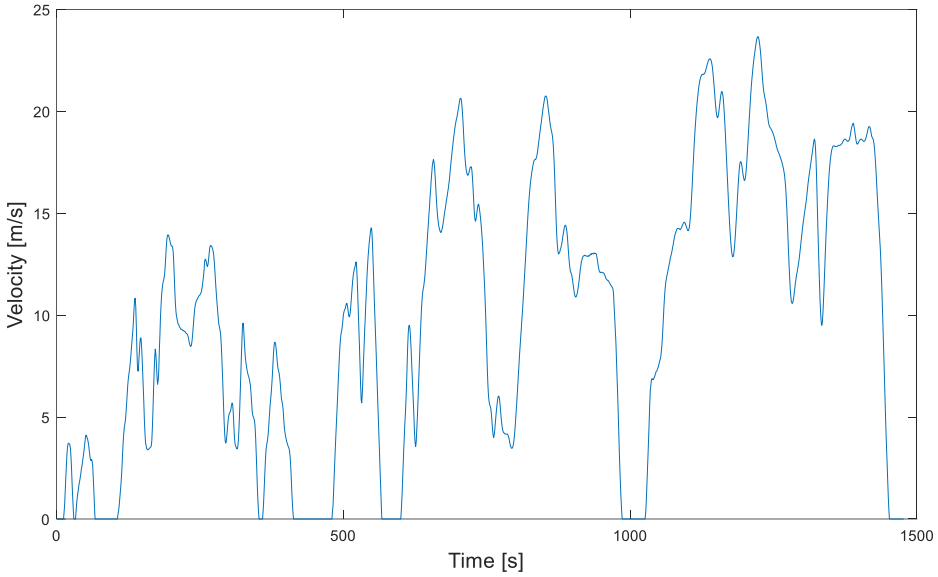

Figure 3-8 Realistic drive cycle: Worldwide Harmonized Light Vehicles Test Procedures (WLTP)

The longitudinal driver model uses an optimal single-point preview control model to simulate the FCEV driver's behaviour (MacAdam 1980). The duty cycle model provides the vehicle reference speed, and the driver receives the vehicle feedback speed to generate acceleration and deceleration commands to achieve the target. The driver model is shown in Figure 3-9.

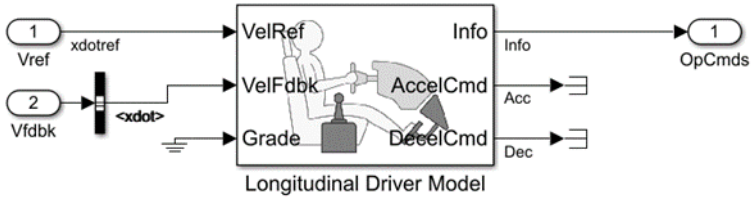

Figure 3-9 Longitudinal driver model

3.5.2 Environment conditions model

The environment model is used for creating environmental conditions including air temperature and pressure, wind velocity and ground grade. In this thesis, the FCEV is considered as longitudinal movement without the effect of ground grade or wind from lateral or vertical directions. The conditions are transferred

to the vehicle drivetrain subsystem to provide accurate road information to the vehicle body model. Figure 3-10 shows the Environment conditions model.

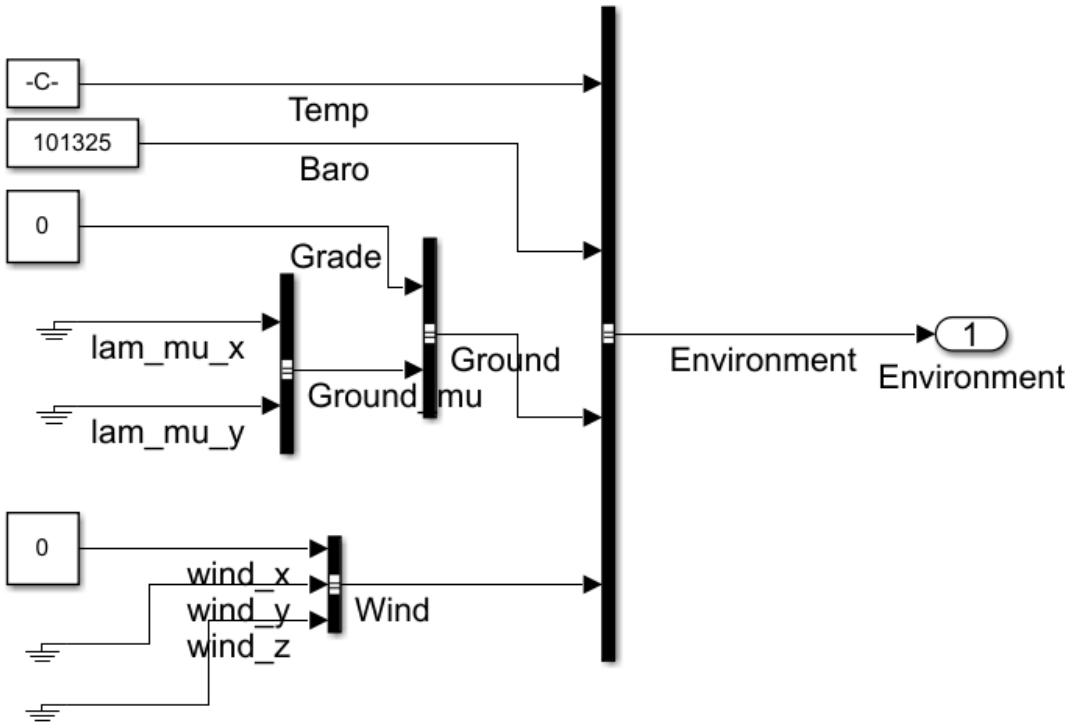

Figure 3-10 Environment conditions model

3.5.3 Powertrain control module

The powertrain control module includes the FCEV regenerative braking system, the motor torque arbitration, and the power management module. The motor torque arbitration and power management module has the following functions:

1. Converts the acceleration and deceleration signal to a torque request or a brake pressure command.
2. Calculates the regenerative braking torque for the motor, and friction brake torque for the FCEV.
3. Ensures that the battery will not be overcharged by regenerative energy or discharged when it is empty.

Figure 17 shows the top level of the powertrain control module with the sub

models will described in the following sub sections.

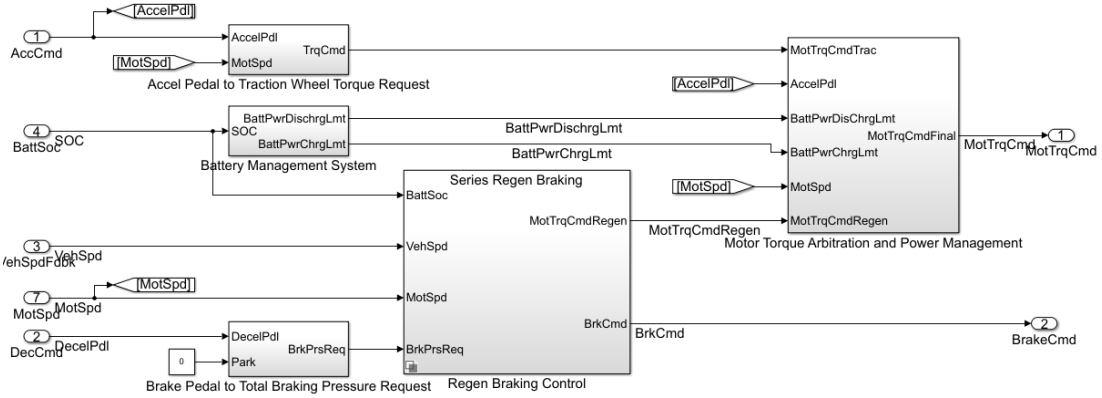

Figure 3-11 Overview of the powertrain control module

3.5.3.1 Torque command submodel

This sub-model receives input signals including motor speed and accelerator pedal position with the output signal being the engine torque command. This sub-model (see Figure 3-12) converts the accelerator pedal position to a torque command using the motor torque-speed curve. The motor speed N in revolutions per minute, is obtained by converting the angular velocity ω using equation 1. This is then applied to the motor torque-speed curve map to obtain the maximum torque which the engine is capable of producing at the current speed. The output torque command is then determined by multiplying by the accelerator pedal position. This is shown in equation 2. The motor torque speed curve map is presented in Appendix 1.

$$\mathrm{N(rpm)} = \frac{60}{2\pi}\omega \quad (1)$$

$$\mathrm{T}_{cmd} = \mathrm{TrqVsSpeed(N)} * P_{acc} \quad (2)$$

ω is the motor speed in rad s^{-1}

T_{cmd} is the motor output torque command (N·m)

$\mathrm{TrqVsSpeed}()$ is the motor torque-speed curve map

P_{acc} is the accelerator pedal position (%)

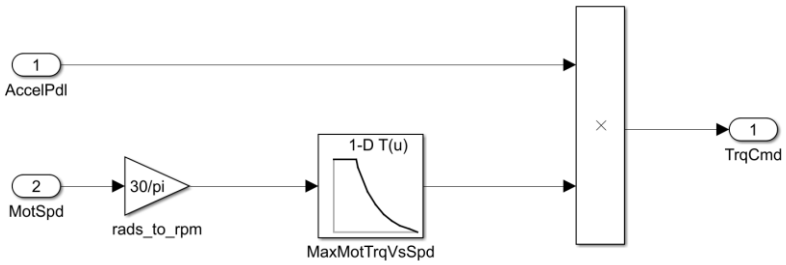

Figure 3-12 Torque command sub model

3.5.3.2 Brake pressure request sub model

This sub-model converts the brake pedal position signal from the drive model to a brake pressure request, see Figure 3-13

$$\mathrm{P}_{req} = \mathrm{P}_{brk} * P_{decel} (3)$$

P_{req} is the brake pressure request (Pa)

P_{brk} is the maximum brake pressure (Pa)

P_{decel} is the brake pedal position (%)

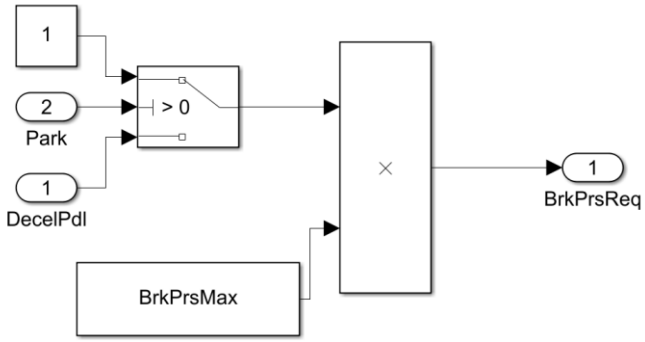

Figure 3-13 Brake pressure request sub model

3.5.3.3 Regen braking control sub model

The regen braking subsystem is shown in Figure 3-14 The inputs of this subsystem are brake pressure request, motor speed, vehicle speed and battery SoC. Furthermore, the outputs are required motor regen torque and command

friction brake torque.

The total brake torque includes regenerative brake torque and friction brake torque. This sub-model is designed to use as much maximum regenerative motor braking torque as possible. When maximum wheel torque is larger than braking torque, the min block selects brake torque multiplied by a regenerative factor to calculate the regenerative torque. When maximum wheel torque is smaller than the brake torque, the regenerative brake torque cannot be provided by the electric motor, so the friction brakes are used to provide the remaining brake force for the FCEV. The regenerative factor varies with the real-time vehicle speed and the battery SoC level: less regenerative power will be supplied to the electric motor when the battery SoC is high or the vehicle speed is low. The regenerative factor maps are shown in Appendix 2 and Appendix 3.

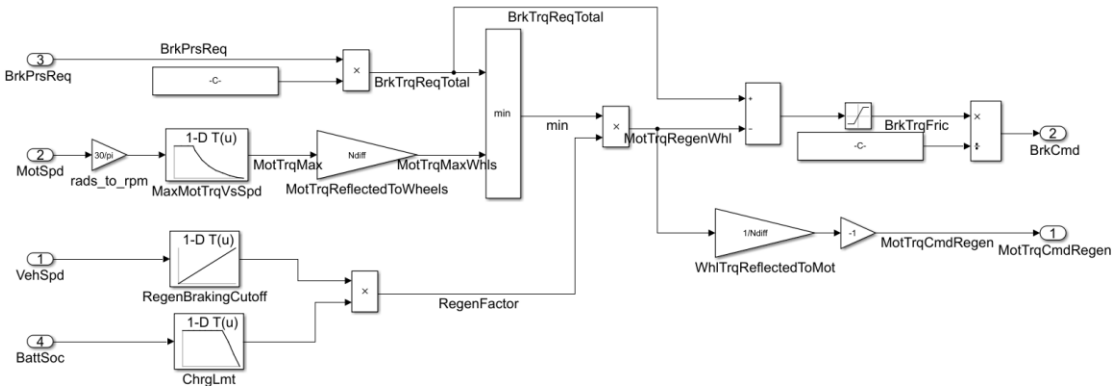

Figure 3-14 Regen braking control sub model

The brake pedal position signal from the drive model is converted to a brake pressure request. Since the FCEV uses four disc-brakes, the total braking torque request is based on brake pressure and a disc brake parameter. Figure 3-15 shows a typical disc brake of the vehicle. Equations 4 and 5 are used to calculate the total brake torque T_{brk}, where R_0 is the outer radius of the brake pad, R_i is the inner radius of the brake pad, R_m is the mean radius of the brake pad force application on the brake rotor, μ is the disc pad-rotor coefficient of

kinetic friction, P is the requested brake pressure, B_a is the brake actuator bore diameter, N_{pads} is the number of brake pads, and N_{diff} is the carrier to drive shaft ratio.

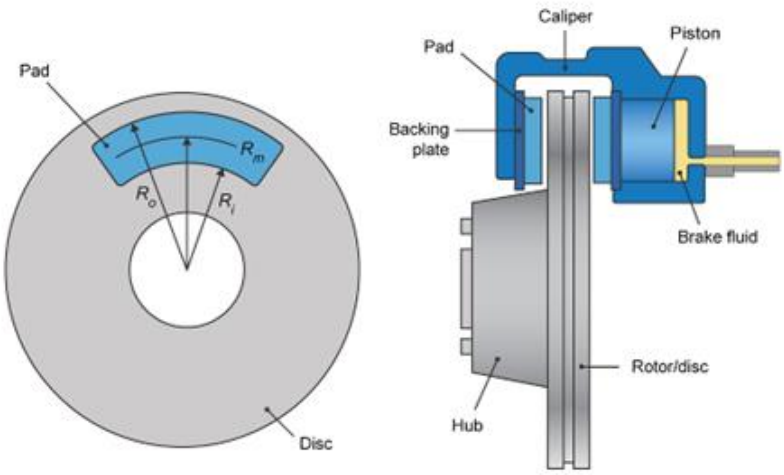

Figure 3-15 Disc brake (MathWorks 2019)

$$R_m = \frac{R_0 + R_i}{2} \quad (4)$$

$$\mathrm{T} = \frac{\mu P \pi B_a^2 R_m N_{pads}}{4} \quad (5)$$

3.5.3.4 Motor torque arbitration and power management submodel

As seen from Figure 3-16, the inputs of the model are battery power discharge and charge limits, motor speed, motor traction torque command and motor regeneration torque command. The switch is used for identifying acceleration mode and braking mode. If the accelerator pedal position is higher than 0, the output torque for the command motor torque is set to the traction torque. Otherwise, it is set to be the regenerative brake torque. The battery power discharge and charge limit is used to limit the battery power based on the SoC.

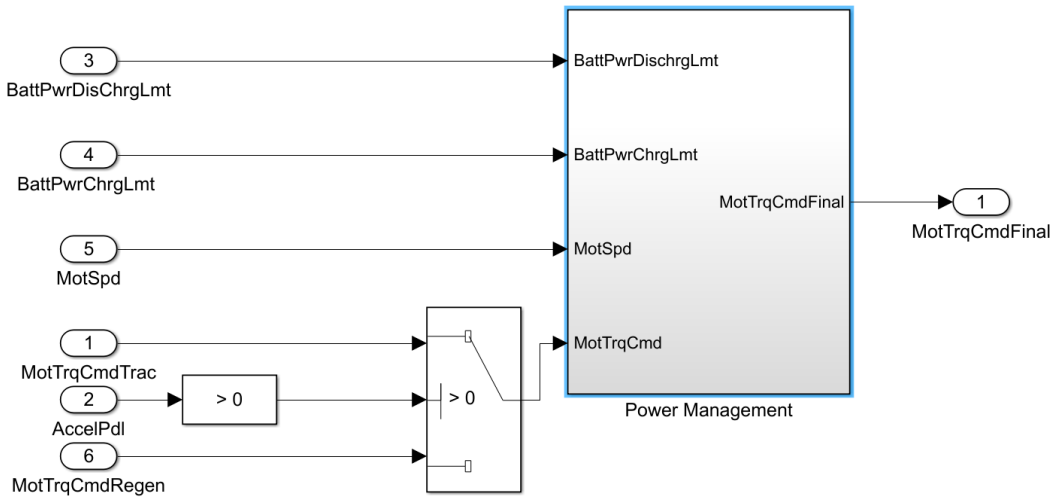

Figure 3-16 Top level of Motor torque arbitration and power management sub model

3.5.3.4.1 Power management subsystem

Figure 3-17 shows the subsystem for the power management model which determines the final motor torque command. The required electrical power is calculated from the motor torque command and the motor speed. The electrical power is limited by the maximum power that can be provided by the energy sources. If the calculated electrical power is within the limits, the output signal is the motor torque command, otherwise the output signal is the torque determined from the maximum power that can be delivered by the energy sources and the current motor speed.

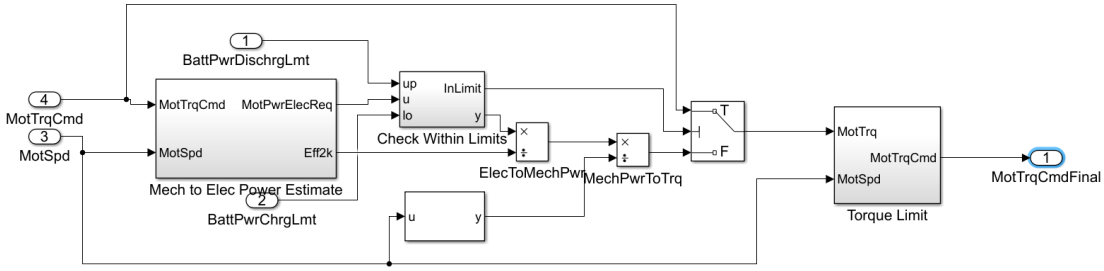

Figure 3-17 Power management subsystem

Figure 3-18 presents the electric power estimation subsystem. The electric power is calculated by the motor efficiency map as a function of electric motor efficiency according to real-time motor torque and speed. A switch is used to

determine if the electric motor is motoring or generating, if the switch output is -1, it means the motor is motoring, otherwise the motor is generating energy. The output of this subsystem is the electric motor power request and the power efficiency from the mechanical power to electric power. These signals are used in the power management subsystem. The motor efficiency map is presented in Appendix 4.

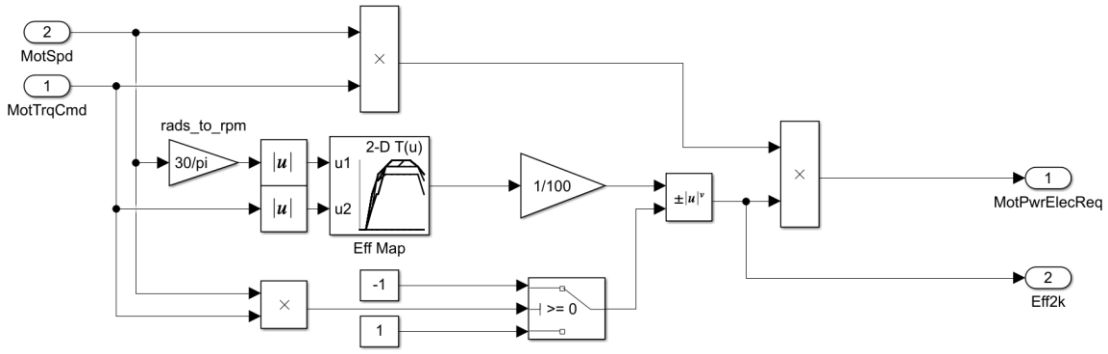

Figure 3-18 Electric power estimation subsystem

3.5.4 Fuel cell model

A PEMFC consists of an anode plate, a cathode plate and a proton exchange membrane, see Figure 3-19. Hydrogen travels through a pipe to arrive at the anode. Positively charged hydrogen ions (protons) and negatively charged electrons are produced by molecular hydrogen dissociation facilitated by the anode catalyst.

Hydrogen ions travel through the proton exchange membrane and arrive at the cathode. In the meantime, electrons travel through the external circuit to the cathode. At the other side of the battery, oxygen ions, hydrogen ions and electrons generate chemical reactions to produce water and heat. The aforementioned process is summarised in the following electrochemical equations (Larminie and Dicks 2003):

Anode reaction: $$H_2 \rightarrow 2H^+ + 2e^- \quad (6)$$

Cathode reaction: $\frac{1}{2}O_2 + 2H^+ + 2e^- \rightarrow H_2O + Heat$ (7)

Total reaction: $H_2 + \frac{1}{2}O_2 \rightarrow H_2O + Heat$+Electricty (8)

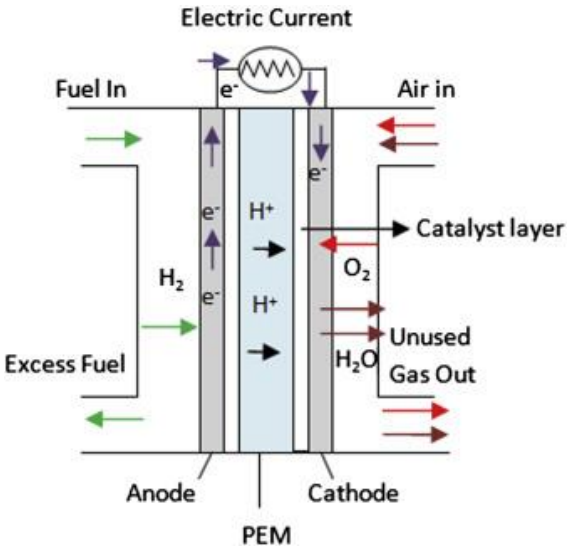

Figure 3-19 Working principle of PEMFC (Dharmalingam et al. 2019)

A single PEMFC consists of an endplate, gasket, current collector plate, field flow plate, gas diffusion layer, catalyst layer and proton exchange membrane (Frano 2005). The membrane electrode assembly, which includes a gas diffusion layer, catalyst layer and proton exchange membrane is the core component between the two current collector plates and the field flow plates. The fuel cell stack is assembled by combining single cells,

A mathematical static fuel cell model is used to generate an ideal fuel cell polarization curve. A MATLAB®/Simulink® generic fuel cell model (Souleman et al. 2009) is used for the hybrid system. The mathematical equations described in the following subsection explain the principle of a typical fuel cell polarization curve (Spiegel 2008).

3.5.4.1 Mathematical fuel cell model

3.5.4.1.1 Fuel cell reversible voltage

In a PEMFC, the electrical energy is converted from chemical energy. The Gibbs free energy equation can represent the energy change between product and reactants. For the hydrogen from the anode and the oxygen from the cathode, the electrochemical reaction is given in equation (9). Therefore, the basic Gibbs free energy change of fuel cell is

$$\Delta G = G_{H2o} - G_{O2} - G_{H2} \quad (9)$$

G is Gibbs free energy

The fuel cell can work at different pressures. Usually, the pressure range is between 1 and 7 bar. For the ideal gas:

$$PV_m = RT(10)$$

P is pressure (Pa)

V_m is molar volume of gas (m^3/mol)

R: ideal gas constant = 8.314 $(m^3 Pa/K\ mol)$

T: thermodynamic temperature = 273 (K)

The relationship between Gibbs free energy, pressure and temperature is given by:

$$dPV_m = dG(11)$$

$$RT\frac{dP}{P} = dG(12)$$

When the pressure and temperature is standard (1atm,25℃), then

$$G = RTln(\frac{P}{P_{stand}}) + G_{stand}(13)$$

The Nernst equation of PEMFC is

$$G = RTln(\frac{P_{H_2}P_{O_2}^{\frac{1}{2}}}{P_{H2O}}) + G_{stand}(14)$$

According to the second law of thermodynamics, the output power of an ideal fuel cell depends on the temperature, so the maximum reversible output is

$$E_{max} = \Delta G = -nFE_r = -2FE_r (15)$$

$$E_r = -\frac{\Delta G}{2F} = \frac{\Delta H - T\Delta S}{2F} (16)$$

n is the number of electrons transmitted

F is the Faraday Constant 96 485.3329 (A s/ mol)

E_r is the reversible output voltage (V)

H is the standard enthalpy of formation (kJ/mol)

S is the entropy

According to the Nernst equation, the reversible output voltage of PEMFC is

$$E_{max} = E_r = \frac{-\Delta G}{2F} = \frac{RTln\left(\frac{P_{H2}P_{O2}^{\frac{1}{2}}}{P_{H2O}}\right) + G_{stand}}{2F} (17)$$

When the fuel cell is in the standard situation, (1atm,25℃), the reversible output is

$$E_r = \frac{-273.3KJ/mol}{2mol \times 96485C/mol} = 1.229V (18)$$

However, the PEMFC reaction is not reversible, and the real output voltage depends on the temperature, so the equation is

$$E = -\frac{\Delta G}{2F} = \frac{\Delta H - T\Delta S}{2F} = 1.229 + \frac{(T - T_{stand})(\Delta S)}{2F} (19)$$

When T is the standard state temperature, and ∆S is the standard state entropy change.

$$E = 1.229 - 8.5 \times 10^{-4}(T - 298.15) + 4.3085 \times 10^{-5}T(\ln (PH_2)(PO_2)^{\frac{1}{2}} (20)$$

In theory, if the fuel cell can convert all thermal energy to electrical energy, the theoretical voltage should be 1.48V/cell. According to the previous results, the reversible theoretical voltage is 1.229V. Because of the irreversibility of the electrochemical reaction, to calculate the actual voltage, three factors need to

be considered: the activation losses, the ohmic losses and the concentration losses.

3.5.4.1.2 Activation loss

The activation loss is caused by the electrochemical reaction on the active catalyst's surface. When the current density is low, more available energy will be lost in the chemical reaction. An activation voltage is required because some energy is needed to start a chemical reaction. The overall activation voltage is typically between 0.1V and 0.2V and depends on the current density. Thus, the equation for activation voltage is

$$\Delta V_{act} = E_r - E_{open} \quad (21)$$

$$\Delta V_{act} = \frac{RT}{\alpha F} \ln\left(\frac{i}{i_0}\right) \quad (22)$$

i is the current density

i_0 is the exchange current density

α is the charge transfer coefficient

The equation of activation loss is

$$\Delta V_{act} = \frac{RT}{\alpha F} \ln\left(\frac{i}{i_0}\right) = V_{anode} + V_{cathode} = \frac{RT}{n\alpha F} \ln\left(\frac{i}{i_0}\right)_{anode} + \frac{RT}{n\alpha F} \ln\left(\frac{i}{i_0}\right)_{cathode} \quad (23)$$

n is the number of protons transmitted per mole

According to the equation 23, the activation loss will increase with an increase in temperature.

3.5.4.1.3 Ohmic Loss

The different components of the fuel cell stack (electrolyte, catalyst layer, Gas Diffuse Layer, bipolar plate) have natural electrical impedance. The ohmic loss is caused by the overall electrical resistance of these components and the ion resistance. The ion resistance is the main factor in determining ohmic loss because ions are more difficult to transmit than electrons. The ohmic loss will reduce the FC voltage according to equation (24-26):

The current density i is

$$i = \frac{I}{A} \tag{24}$$

I is the fuel cell current (A)

A is the activation area of the fuel cell

Therefore, the ohmic loss can be calculated by the current density.

$$V_{ohmic} = i(\mathrm{A} \times R_{ohmic}) \tag{25}$$

$$V_{ohmic} = i(\mathrm{A} \times R_{ohmic}) = i\mathrm{A}\left(\frac{\delta}{\sigma A}\right) = i\frac{\delta}{\sigma} \tag{26}$$

δ is the thickness of the electrolyte layer

A is the activation area of the fuel cell

R_{ohmic} is the ohmic resistance

Therefore, the most effective way to reduce the ohmic loss is to use a thinner electrolyte layer and a better ionic conductor.

3.5.4.1.4 Concentration loss

Concentration loss, also called mass transport loss, occurs when the hydrogen and oxygen concentrations are reduced by production. Therefore, the partial pressures of the reactants are decreased because the other inactive gases fill the catalyst surface by diffusion. According to equation 20, the decrease of hydrogen and oxygen partial pressures will cause a voltage decrease.

The concentration loss can be calculated by the following equations:

$$V_{conc} = \frac{RT}{nF}\ln\left(\frac{i_{max}}{i_{max}-i}\right) \tag{27}$$

i_{max} is the maximum current density

The resultant voltage is the reversible theoretical voltage minus the voltages

due to activation losses, ohmic losses and concentration losses:

$$V_{cell} = E_r - \Delta V_{act} - V_{ohmic} - V_{conc} (28)$$

V_{cell} is the actual voltage of single fuel cell

The mathematical fuel cell model is shown in Figure 3-20. Stack voltage can be calculated by multiplying single fuel cell voltage by the number of cells. The model allows convenient adjustment of parameters, which can help when building a fuel cell stack in the experimental test. Figure 3-21 shows the single fuel cell polarization curve based on the Ballarld datasheet (Ballarld 2011).

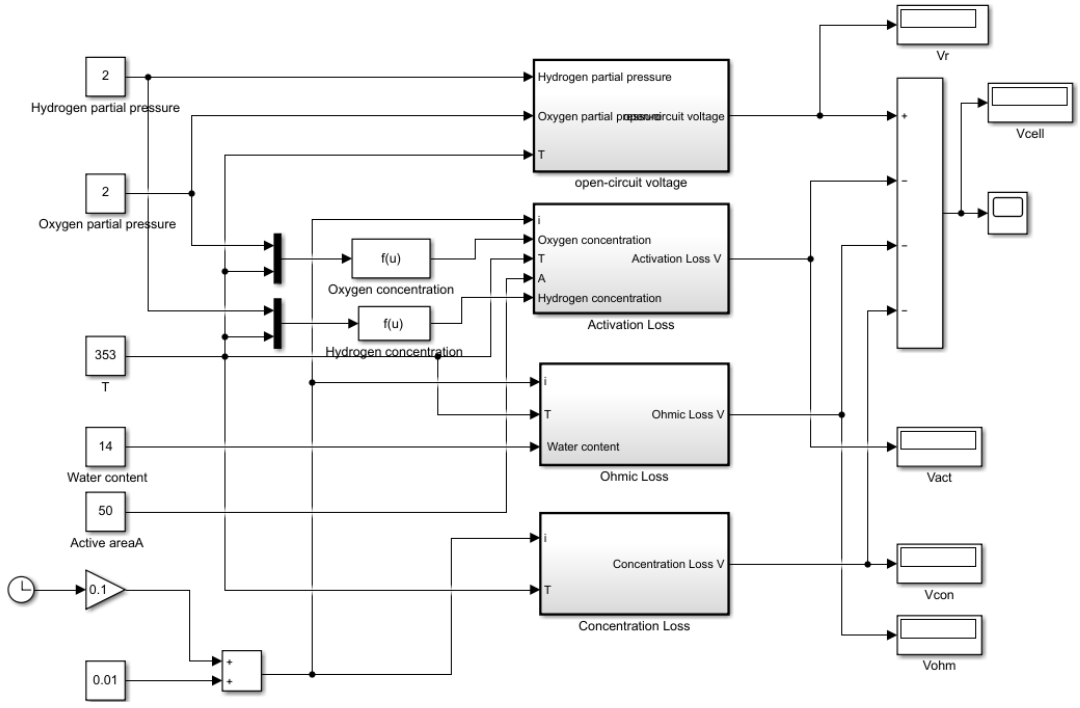

Figure 3-20 Mathematical static fuel cell model

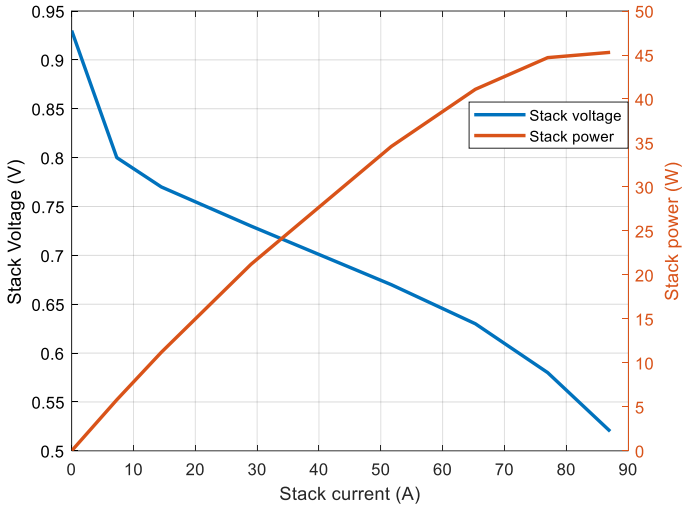

Figure 3-21 Single fuel cell polarization and power curve

3.5.4.2 Generic PEMFC model

The MATLAB®/Simulink® generic fuel cell model is able to measure and adjust hydrogen pressure, hydrogen flow rate, air pressure and air flow rate for real-time optimal control. The modelling error is expected to be less than 1%. The output voltage is calculated by equation 30, and the air and hydrogen pressure and flow rates are determined by equations 31 and 32:

$$V_{fc} = NV_{cell} \quad (29)$$

$$U_{O_2} = \frac{60000RTNi_{fc}}{nFP_{air}V_{lpm(air)O_2\%}} \quad (30)$$

$$U_{H_2} = \frac{60000RTNi_{fc}}{nFP_{fuel}V_{lpm(fuel)H_2\%}} \quad (31)$$

R is the ideal gas constant = 8.314 $(m^3 Pa/K\ mol$

T is the thermodynamic temperature = 273 (K)

F is the Faraday Constant 96 485.3329 (A s/ mol)

$O_2\%$: percentage of oxygen in the oxidant (%)

$H_2\%$: percentage of hydrogen in the fuel (%)

P_{air}: absolute supply pressure of air (atm)

P_{fuel}: absolute supply pressure of fuel (atm)

$V_{lpm(air)}$: air flow rate (l/min)

$V_{lpm(fuel)}$: fuel flow rate (l/min)

n is the number of electrons transmitted

The partial pressures are calculated by equations

$$P_{H_2} = (1 - U_{H_2})H_2\%P_{fuel} \quad (32)$$

$$P_{H_2O} = (V\% - 2O_2\%U_{O_2})P_{air} \quad (33)$$

$$P_{H_2} = (1 - U_{O_2})O_2\%P_{air} \quad (34)$$

V% is the percentage of water vapor in the oxidant (%)

Then, using equations 20,29 and 30, the stack voltage can be calculated.

3.5.5 Battery model

A generic dynamic battery model from MATLAB®/Simulink® has been adopted as it can represent a specialized lead-acid battery, lithium-ion battery or nickel battery (Omar et al. 2014, Saw et al. 2014, Tremblay and Dessaint 2009, Zhu et al. 2013). Although this work is mainly focused on the lithium-ion battery, different energy sources such as lead-acid batteries and nickel batteries will also be used in the hybrid system for further investigation. The maximum error of the model is 5%.

The equivalent circuit of the batteries consist of internal resistances and voltage V. when the low-frequency current dynamics $i^* < 0$, the battery is in charge mode, and when battery $i^* > 0$, battery is in the discharge mode.

For a lead-acid battery, the model uses the following equations 35 to 36

Discharge: $$V_{lead-acid} = V_0 - \frac{KQ_{max}i^*}{Q_{max}} - \frac{KQ_{max}i_c}{Q_{max}-i_c} + Laplace^{-1}(\frac{Exp(s)}{Sel(s)}0) \quad (35)$$

Charge: $$V_{lead-acid} = V_0 - \frac{KQ_{max}i^*}{i_c+0.1Q_{max}} - \frac{KQ_{max}i_c}{Q_{max}-i_c} + Laplace^{-1}(\frac{Exp(s)}{Sel(s)}\frac{1}{s}) \quad (36)$$

For the nickel battery, the model uses the following equations 37 to 38

Discharge: $$V_{nickel} = V_0 - \frac{KQ_{max}i^*}{Q_{max}} - \frac{KQ_{max}i_c}{Q_{max}-i_c} + Laplace^{-1}(\frac{Exp(s)}{Sel(s)}0) \quad (37)$$

$$\text{Charge: } V_{nickel} = V_0 - \frac{KQ_{max}i^*}{|i_c|+0.1Q_{max}} - \frac{KQ_{max}i_c}{Q_{max}-i_c} + Laplace^{-1}(\frac{Exp(s)}{Sel(s)}\frac{1}{s})(38)$$

For the lithium-ion battery, the model uses the following equations 39 to 40

$$\text{Discharge: } V_{lithium} = V_0 - \frac{KQ_{max}i^*}{Q_{max}} - \frac{KQ_{max}i_c}{Q_{max}-i_c} + Aexp(-Bi_c)(39)$$

$$\text{Charge: } V_{lithium} = V_0 - \frac{KQ_{max}i^*}{i_c+0.1Q_{max}} - \frac{KQ_{max}i_c}{Q_{max}-i_c} + Aexp(-Bi_c)(40)$$

Q_{max} is the maximum battery capacity (Ah).

V_0 is the constant voltage (V).

A is the exponential voltage (V)

B is the exponential capacity $(Ah)^{-1}$

K is the polarization constant $(Ah)^{-1}$

$i_c$is the available capacity (Ah)

$Exp(s)$ is the exponential zone dynamics (V)

$Sel(s) = 0$ is battery discharge mode

$Sel(s) = 1$ is battery charge mode

For the SoC, the model use equation 54

$$\text{SoC} = 100(1 - \frac{\int i_c\, dt}{Q_{max}})(41)$$

When the battery is fully charged, the SoC is 100% and when the battery is empty, the SoC is 0.

3.5.6 Vehicle Drivetrain module

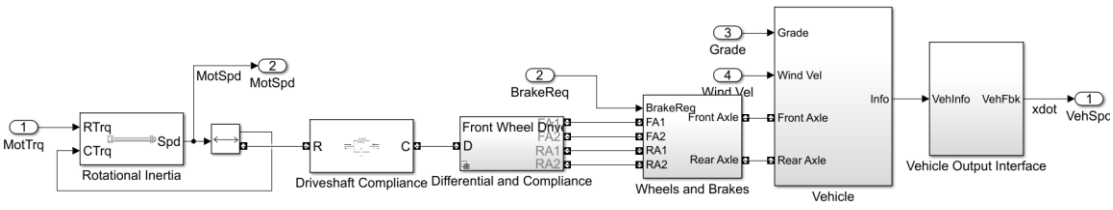

Figure 3-22 Vehicle Drivetrain module

Figure 3-22 shows the vehicle drivetrain module. The input signal of vehicle drivetrain is the electric motor torque, and the output signal is the feedback

speed of the vehicle. The electric power generated from the energy sources flow through the drivetrain and provide the torque to the wheels. The drivetrain module is modelled by a series of mechanical components. The rotational block represents an ideal mechanical rotational inertia for defining the FCEV initial acceleration. This connects to the driveshaft block, and in turn to the differential block, using a coordinate system to model the front-wheel drive coupling torque. The wheels and brakes block can be configured according to the type of brakes and wheels, and provides the total longitudinal force at the front and rear axles. The vehicle block implements the three degrees-of-freedom (3DOF) rigid vehicle body model to calculate rigid-body vehicle motion, suspension system force, and aerodynamic drag force. See equations 43 to 45. Using the wheel angular speed, the vehicle speed can be calculated by equation 46.

$$F_x = F_{wf} + F_{wr} - F_{d,x} - F_{sx,f} - F_{sx,r} - F_{g,x} (42)$$

$$F_{d,x} = \frac{1}{2}\rho C_d A_f v^2 (43)$$

$$F_{g,x} = mgsin\alpha\ (44)$$

$$v = \omega_w r_w (45)$$

The x axis points forward from the vehicle.

F_x is the longitudinal force

F_{wf} is the longitudinal force at the front axle along the vehicle-fixed x-axis

F_{wr} is the longitudinal force at the rear axle along the vehicle-fixed x-axis

$F_{d,x}$ is the longitudinal and drag force at the vehicle centre of gravity

$F_{sx,f}$ is the longitudinal suspension force at the front axle based on default stiffness and damping parameters

$F_{sx,r}$ is the longitudinal suspension force at rear axle based on default stiffness and damping parameters

$F_{g,x}$ is the longitudinal gravitational force on the vehicle along the vehicle-fixed frame

C_d is the frontal air drag coefficient

A_f is the frontal area of vehicle

v is the velocity of vehicle

ρ is the mass density of the fluid

m is the vehicle weight

α is the inclined road angle

ω_w is the wheel angular speed

r_w is the wheel radius

3.5.7 Active hybrid system module

As Figure 3-23 and Figure 3-24 have shown, the active hybrid system module consists of a fuel cell stack model, DC-DC converter model, battery model and electric motor model. The fuel cell stack input is constant to supply stable power to the battery based on the BALLARD fuel cell manual (Ballard 2011). The optimal fuel pressure is set as 0.36 bar, the pressure drops will reduce the performance of the stack. In an active system, the fuel cell stack operates with a DC-DC converter to provide the appropriate power for the battery. At the same time, the battery supplies voltage to the electric motor. The motor model provides the motor output shaft torque signal to the vehicle drivetrain module.

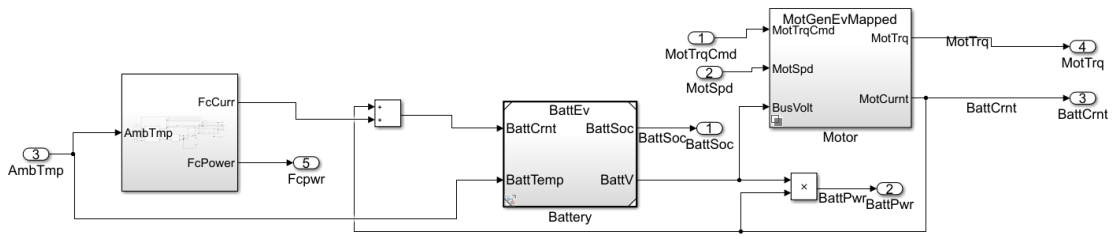

Figure 3-23 Active hybrid system module

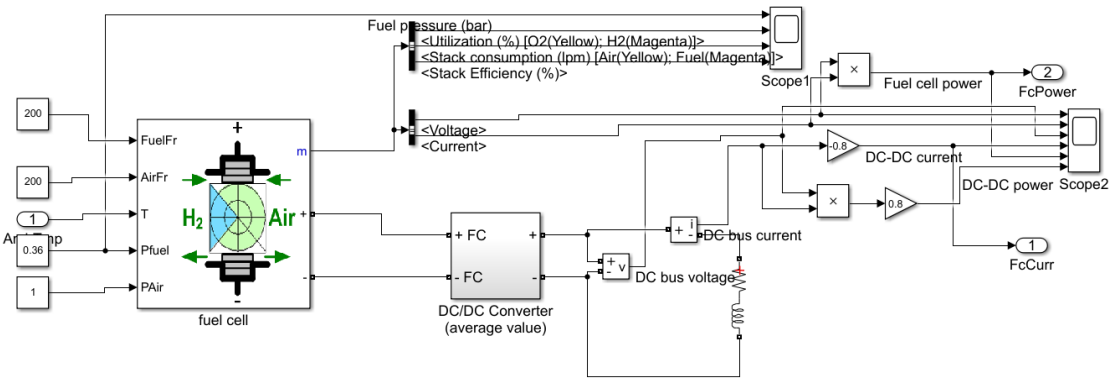

Figure 3-24 Fuel cell hybrid system with a DC-DC converter

According to the motor torque command signal and motor speed signal from the powertrain control module, the mapped motor model outputs the battery current draw or demand signal to the battery model. The equations of the motor are:

Mechanical power calculation:

$$P_{mech} = \omega T (46)$$

Electric Bus power calculation:

$$P_{electic} = P_{mech} + P_{loss} (47)$$

Motor power loss calculation:

$$P_{loss} = -(P_{mech} + P_{loss} - P_{stored}) (48)$$

Motor

$$P_{stored} = \omega \dot{\omega} J (49)$$

T is Motor output shaft torque

ω is Motor shaft speed

J is Motor inertia.

$$\text{The battery discharge/charge current } = \frac{P_{mech} + P_{loss}}{Battery\ voltage} (50)$$

3.5.8 Passive hybrid system module

Figure 3-25 and Figure 3-26 shows show the passive hybrid system module, where the fuel cell and battery are directly connected without a DC-DC

converter. The battery and fuel cell system can both supply power to the electric motor, and the fuel cell system can also charge the battery while the load demand is low, such as during a low-speed vehicle cruise. This module can run in either FCEV mode or EV mode.

In the passive hybrid mode, the bus voltage is based on the impedance and the voltage deviations of the fuel cell system and battery (Bernard et al. 2011). The subsystem is flexible, allowing configuration of the fuel cell size and type, which is a prerequisite to the scientific consideration of matching two energy sources. In direct passive hybrid system, the inputs of stack pressure, stack flow rate are constant, the output is fuel cell stack power. In the fuzzy passive hybrid system, the inputs of stack is controlled by the controller which can affect the output power of stack. Detailed simulations examples are provided in following chapters.

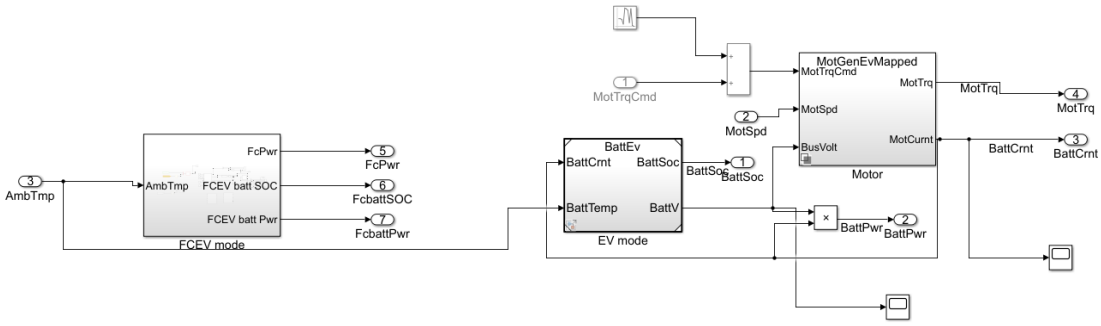

Figure 3-25 Passive hybrid system module

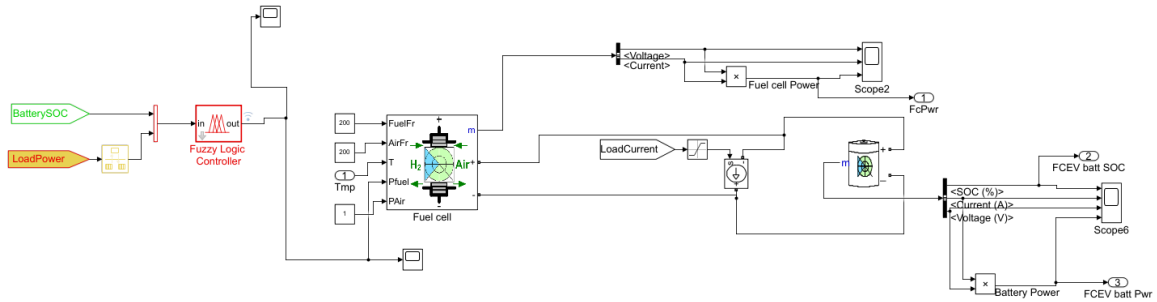

Figure 3-26 Fuel cell and battery passive hybrid subsystem

3.6 Conclusion

This chapter has explained a novel hybrid FCEV model. The model is exploited in subsequent chapters to carry out simulation studies involving different FCEVs under multiple scenarios. Each module of the powertrain can be modified by published industry data or experiment data; allowing the accuracy of the model to be improved for different simulation purposes. In this thesis, the model is validated based on data from bench test as well as from the Microcab H2EV.

The passive hybridization between a fuel cell stack and battery require careful integration to meet the requirements of FCEVs. The proposed simulation model provides an ideal development environment to evaluate alternative solutions thereby reducing the cost and risk to test prototype vehicles. The ability to switch between passive and active energy management strategies is exploited in Chapter 5 to demonstrate some of the advantages associated with passive hybridisation schemes. Chapter 6 exploit the models to develop a fuzzy logic controller. Chapter 7 exploit the capability of the model to simulate different battery technologies to study the impact of battery technology for FCEV. Chapter 8 exploits the model to evaluate the performance of passive hybrid FCEV for different fuel cell and battery pack sizes and for different journey purpose.

Chapter 4: Experimental validation of FCEV powertrain model

4.1 Introduction

Having presented the FCEV powertrain model in chapter 3, this chapter focuses on tuning and experimentally validating the model for subsequent use for the purpose of control that will be presented in chapter five. The experimental results demonstrate the importance of component selection to suit the passive hybrid system. The latter is addressed in more details in Chapter 8 which provide original selection guidelines for the passive hybrid system.

This chapter presents the experimental work relating to the FCEV powertrain and the passive hybrid system. The complete passive hybrid FCEV is still under development; therefore, the FCEV powertrain is validated using the current Microcab H2EV powertrain. FC response to different load conditions is used to validate the fuel cell operation for the passive hybrid system in section 4.3. The passive hybrid system used a smaller battery to match the fuel cell stack. The good agreement between data and simulation justified the subsequent exploitation of this validated model in the remainder of this thesis.

This chapter is organised as follows. Section 4.2 presents the experimental and manufacturers data used to validate the fuel cell stack and the battery pack against the ECE-15 drive cycle. Section 4.3 evaluate the proposed passive hybrid system using bench testing.

4.2 Microcab H2EV model validation

The H2EV is designed to have the flexibility to operate with different types of

hybrid systems. The following sections will introduce the hybrid system used in the experiment and the validation of the powertrain load modelling.

4.2.1 Specification for the customized hybrid system

Fuel cell stack

A customized 3kw Ballard 1020ACS PEMC is used as the energy source of the H2EV, which is operating in active hybrid mode in its current form. The fuel cell controller operates the air-cooling and purge system based on the stack temperature and hydrogen flow. The fuel cell stack has 70 cells, with static performance curves shown in Figure 4-1.

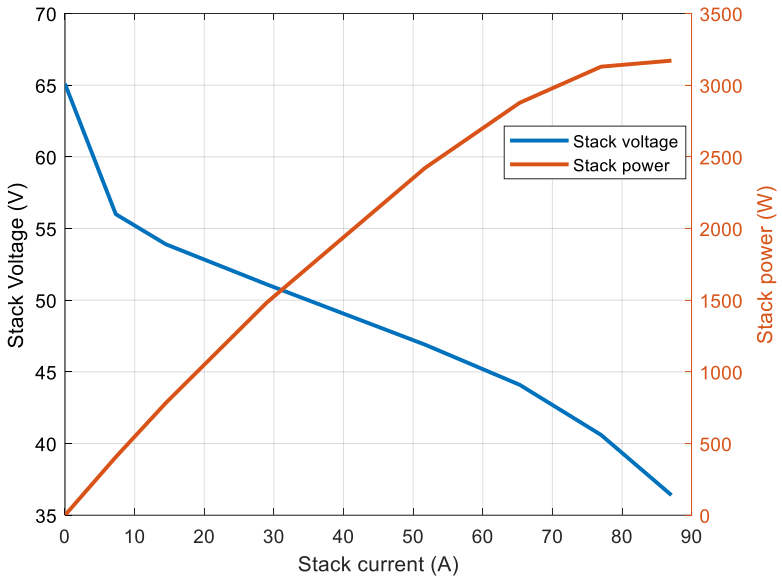

Figure 4-1 Fuel cell stack polarization curves for experimental test

Battery pack

The 72V 4.3kWh lithium-ion battery pack consist of 96 cells of Goodwolfe X2E 15Ah 40166 battery (Goodwolfe 2019). The internal layout of the battery pack is shown in Figure 4-2. The battery cells are arranged as four groups, each group containing 24 cells connected in series and charged with the same

voltage, the groups being connected in parallel to supply power to the load.

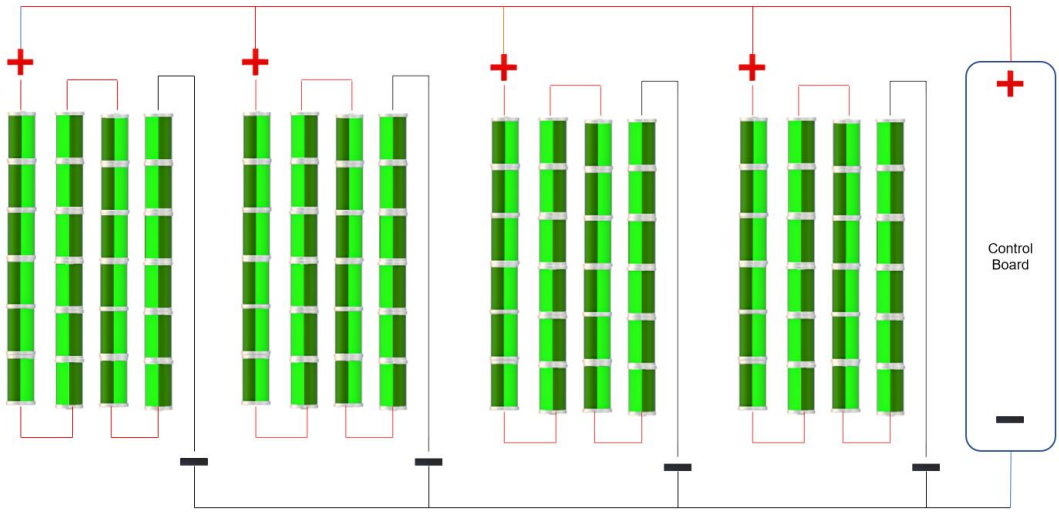

Figure 4-2 Experimental test battery pack layout

The discharge characteristic is shown in Figure 4-3. The figure shows that the lithium-ion battery can provide a stable discharge voltage over the nominal area.

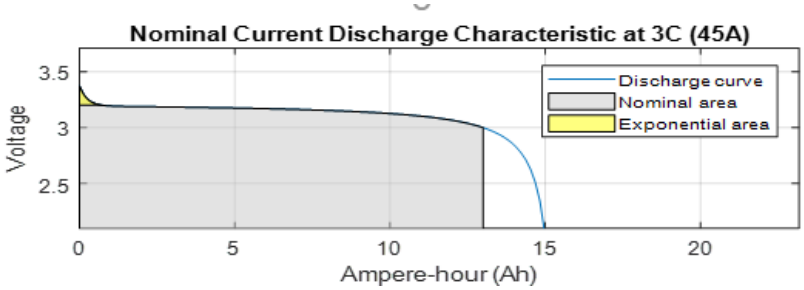

Figure 4-3 Battery cell 3C discharge characteristic

4.2.2 ECE-15 drive cycle test

Accurately modelling the FCEV powertrain load is critical in assessing the performance of the passive hybrid system. The H2EV is a lightweight passenger vehicle which is primarily for use in urban areas. Therefore, the ECE-15 urban driving cycles (UDC average speed 18.4km/h) were selected as a representative performance test for the vehicle. In order to give a precise result, the experimental test consists of eight UDC drive cycles lasting approximately 27 minutes to drive 7.997 km. Figure 4-4 shows the FCEV load

power and vehicle speed over a single drive cycle.

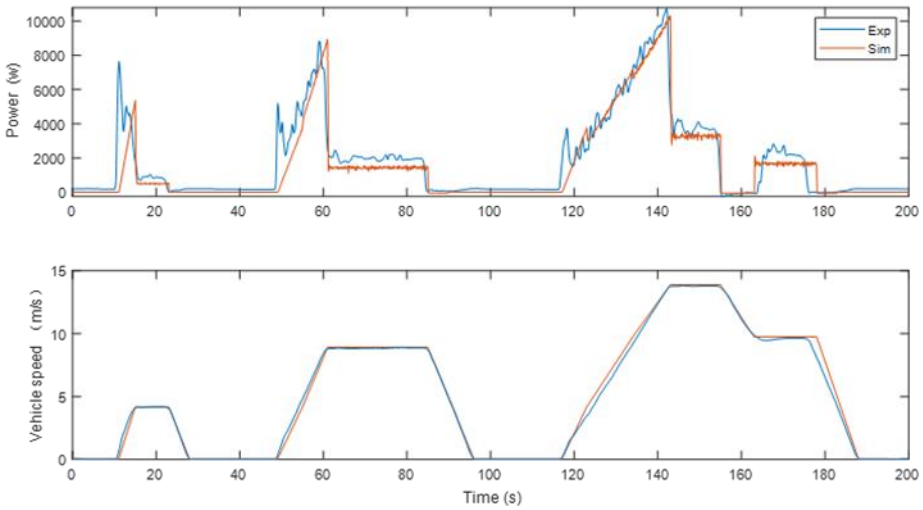

Figure 4-4 Microcab H2EV model validation

The average energy required over one drive cycle is 368.2kJ and 305.8kJ for the experimental measurements and the simulation, respectively. This difference is mainly caused by the following factors:

1. Effects of auxiliary components

The auxiliary system components of the H2EV, such as indicators and lights, need approximately 300W to operate. In a 200s drive cycle, this requires approximately 60kJ energy. The powertrain model does not include the auxiliary system, and once the additional energy consumption of this part is added, the total energy required is calculated as 365.8 kJ, which is close to the experimental test value of 368.2 kJ.

2. Effects of driver behavior

Although the same drive cycle is repeated eight times, the driver behavior has a significant effect on the FCEV performance. Figure 4-5 shows the actual driver's drive cycle for each test. A human driver can not provide exactly the correct and consistent pressure to the throttle and brake for each drive cycle, resulting in small oscillation around the ideal speed trajectory. During natural

driving, it is typical to press the throttle pedal more than required to overcome stiction from a stopped condition. The latter explains the spikes observed for the experimental measurements shown in Figure 4-4.

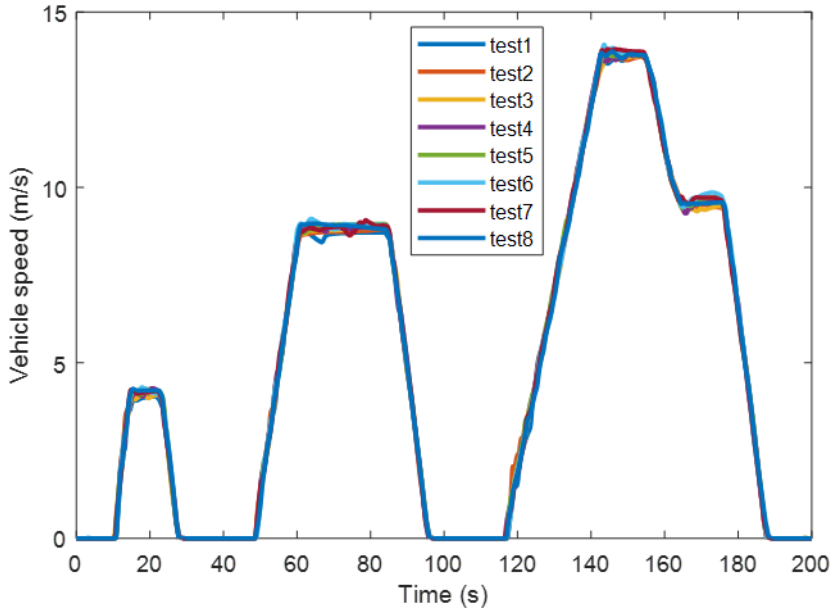

Figure 4-5 Actual drive cycle for eight tests

3. Effects of the battery pack and fuel cell stack

For the fuel cell, the supply pressure sensors measure the hydrogen pressure, the pressure regulator regulates the hydrogen pressure, the supply valve controls the hydrogen flow to the fuel cell stack, and the purge valve controls the hydrogen flow from the stack. Although expensive and accurate sensors are used for the fuel cell stack, errors still exist. Individual battery cells cannot be charged at precisely the same capacity resulting in slightly different initial characteristics. Therefore, in this work, the average cell capacity of the battery is assumed to be at 95% of the nominal capacity.

4. Effects of environmental conditions

The modelling parameters are designed to reproduce the environmental conditions. However, the accuracy of the sensors and other measurements has

not been considered in this work as they are expected to give errors of less than 1%.

Based on the experimental validation it is concluded that the H2EV powertrain model is sufficiently realistic.

4.3 Passive hybrid system module validation

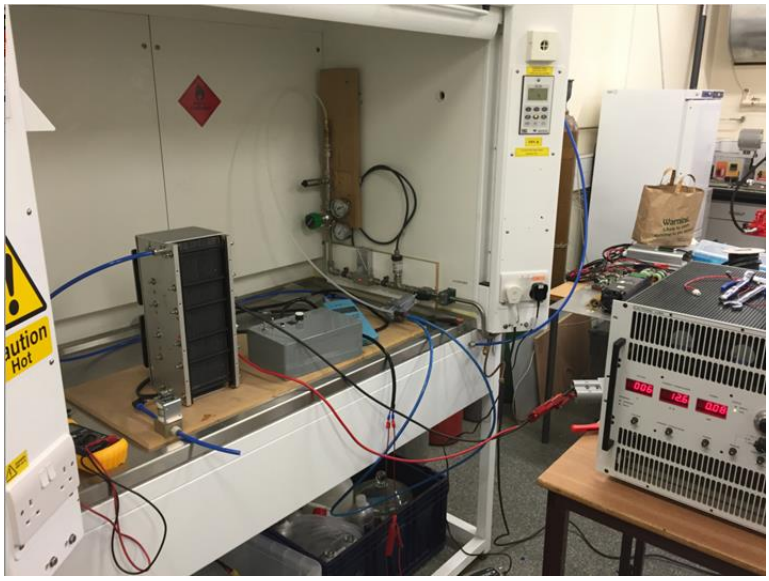

Figure 4-6 Fuel cell system test platform

The passive hybrid system experiment test bench consists of a 3kW self-humidified fuel cell, 45V 180Ah lithium-ion battery with battery management system under different SoC levels and a 3kW electric load (see Figure 4-6). The fuel cell stack is able to charge downsizing battery pack constantly because of higher voltage deviations. The fuel cell and battery are connected in parallel to provide power to the electrical load. The load increases by 50W every 15 seconds while the battery and fuel cell supply power to the load during the experiment. The time resolution for experimental measurement is 15s.

The experimental results show the fuel cell connected in a passive hybrid configuration with a lithium-ion battery. Three representative SoC, namely 20%,

50% and 80%, are selected to evaluate the fuel cell under a range of conditions. During the test with the battery at 20% SoC, the voltage gap between the battery and the fuel cell resulted in the fuel cell generating its maximum power to charge the battery and supply the load at the same time. Increasing the initial battery SoC from 20% to 80% reduces the fuel cell power generated because of the increased battery SoC. The fuel cell was found to be able to provide a relatively stable power output, calculated to operate the fuel cell in its most efficient mode of operation.

The simulation results (shown in Figure 4-7) exhibit similar dynamic characteristic to the Microcab experimental data. Because the dynamic response time in the model is faster than the experimental results, at the low load power (<200W) part of the figure, the fuel cell power increases more rapidly than the experimental results. The fluctuations in experimental data is because of battery SoC charging rapidly when charging by the fuel cell or discharging the electric load. The temperature change and error of measuring instrument can are also affecting the results.

The average fuel cell power is slightly lower than for the experimental data for 20% and 80% SoC than the average experimental power between 400W and 2000W. It is slightly higher in the case of 50% SoC.

The average experimental fuel cell power for 20%, 50% and 80% SoC is 3274W, 3096W and 2972W, respectively. This compares with the average simulated fuel cell power of 3214W, 3154W and 2927W for 20%, 50% and 80% battery SoC respectively. The overall accuracy of the model is around 98.15%. Such bench test provided the confidence that the passive hybrid system can smoothly operate with the H2EV model and that the model is suitable for the purposes of this work.

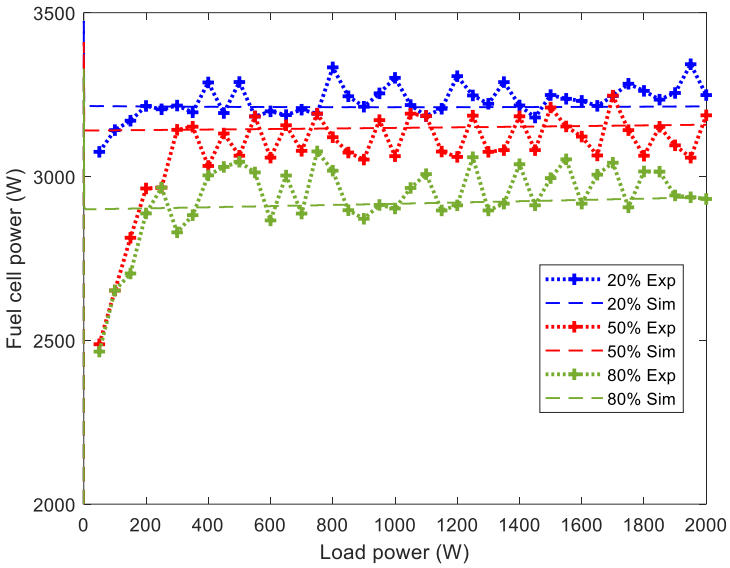

Figure 4-7 Passive hybrid system model validation

The experimental results also show that the fuel cell stack temperature increases rapidly from 20℃ to 50℃ at 20% battery SoC level. When the battery SoC is 50%, the temperature increases from 20℃ to 46℃. When the battery SoC is 80%, the temperature increases from 20℃ to 44℃ respectively. It was found that when the battery SoC is low due to higher voltage deviations of the fuel cell system and the battery, the stack was overloaded under maximum temperature. The higher operating temperature might cause problems such as lower efficiency and performance degradation. Therefore, it is important to control the battery SoC and select a suitable battery pack and fuel cell stack for the passive hybrid system.

4.4 Conclusion

The above experimental validation results prove that the passive hybrid fuel cell powertrain modelling is sufficiently realistic for the FCEV. Moreover, the experimental tests proved the passive hybrid system needs to be carefully designed for FCEVs in order to increase the system efficiency as well as maintain the lifespan of the fuel cell. The results described in this chapter

provide the experimental foundation upon which further system-level evaluations of a hybrid FCEV with a passive fuel cell/battery architecture are presented in the following chapters.

Chapter 5: Comparison of active and passive hybrid powertrain

5.1 Introduction

Having validated the model developed in chapter 3 using experimental data collected in chapter 4, this chapter exploits the validated model to investigate the benefits of passive hybrid FCEVs. The simulation results indicate that passive hybrid Microcab H2EV can successfully increasing battery charging efficiency under same fuel cell stack performance and simplifying the hybrid system by removing DC-DC converter.

The chapter is organised as follows. The first section uses simulation to explain the dynamic behaviour of the direct passive hybrid Microcab H2EV. The second section compares a direct passive hybrid powertrain with an active hybrid powertrain for the H2EV. The aim of such a comparison is to demonstrate the potential benefits of a passive hybrid against conventional active hybrid systems.

5.2 Dynamic behaviour of the direct passive hybrid system

According to previous research from Microcab, fuel cell stacks between 4kW and 5kW are the most appropriate for the H2EV (Ryan et.al. 2014). Therefore, in the passive hybrid system design, a 4.1kW fuel cell stack and 72V 4.3kWh lithium-ion battery are selected for the required missions.

The aim of this simulation study is to evaluate the efficiency of active and passive hybrid systems for the Microcab H2EV. The simulation study makes use of a drive cycle created by combining four repetitions of the UDC drive cycle,

representing an overall drive cycle of 780s (13 min) duration with a distance covered of 3.98km. The SoC of the battery is initially assumed to be 70%. The vehicle parameters are listed in Table 3-1 in chapter 3.

The outcome of the simulation is shown in Figure 5-1. At the beginning of the drive cycle, the fuel cell is operating at its nominal output of 3180W to provide power to both the battery and the load. As the load increases, the battery starts to supply energy to the load. The battery power curves show negative values when charging and positive values when discharging. In a passive hybrid system, the battery charge and discharge threshold points are determined by the voltage deviations between the fuel cell and the battery. Once the power demand from the load exceeds the 3180W threshold, the battery starts supporting the fuel cell to provide power to the load, and therefore stops recharging until the load power drops below the threshold point. The behaviour of the passive hybrid system can be expressed as follows:

If $P_{load} < P_{fc} \quad P_{load} = P_{fc} - |P_{batt}|$ (51)

If $P_{load} > P_{fc} \quad P_{load} = P_{fc} + P_{batt}$ (52)

P_{load} is the load power of FCEV

P_{fc} is the power supplied from the fuel cell stack

P_{batt} is the power supplied from the lithium battery pack

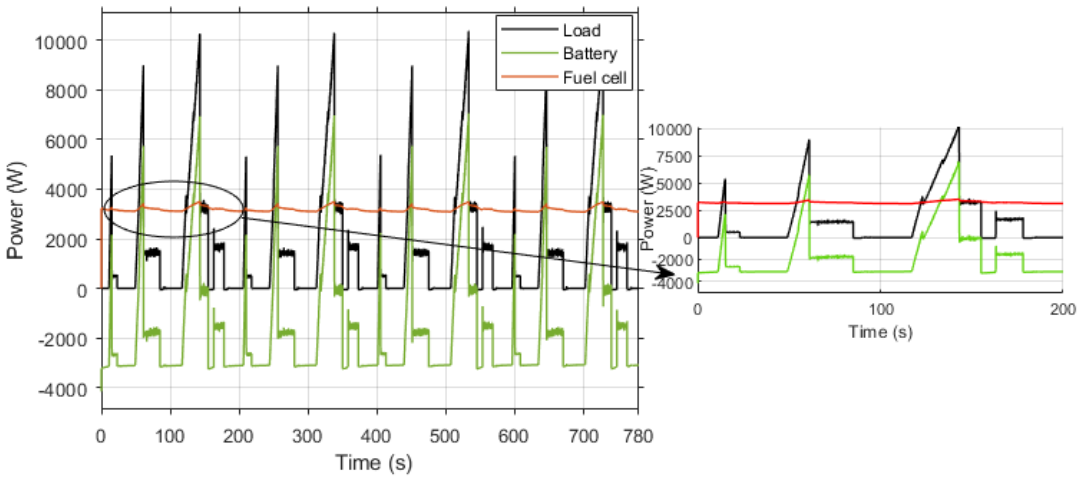

Figure 5-1 Simulation results of direct passive hybrid powertrain

5.3 Comparison of active hybrid and direct passive hybrid strategies

An active hybrid system management strategy is currently used in the Microcab H2EV. It uses a DC-DC converter to adjust the power supplied to charge the battery until 80% SoC level is reached, at which point the operation of the fuel cell is stopped until the SoC falls below 50% level and the fuel cell is re-started to charge the battery. This active hybrid system management strategy is used as a benchmark against which to evaluate the direct passive hybrid systems. To evaluate the relative benefits of a passive hybrid for representative conditions, 70% initial battery SoC levels was selected.

Figure 5-2 shows the comparison between active and direct passive strategies, assuming a battery SoC equal to 70%, with the vehicle following the UDC drive cycle. The active strategy uses a DC-DC converter to supply a constant power to the battery, with the battery supplying power to the motor. After four drive cycles, the battery SoC for the direct passive strategy (77.24%) is higher than for the active strategy (75.66%). This difference is due to the ability of the fuel cell to supply power to both the battery and the load when used a direct passive

strategy is used. Note that, for both strategies, the average power of the fuel cell is at a similar level (3187W). It can be seen that the passive hybrid strategy provides more energy to the battery pack, helping the FCEV to run further before depleting both energy sources. In pure EV mode, a 780s drive cycle will cost a lithium battery about 896.292kJ energy, equivalent to a 5.79% decrease in the SoC. Therefore, the energy saved using a passive hybrid would enable the driving range to be extended by approximately 27.28% (1.08km).

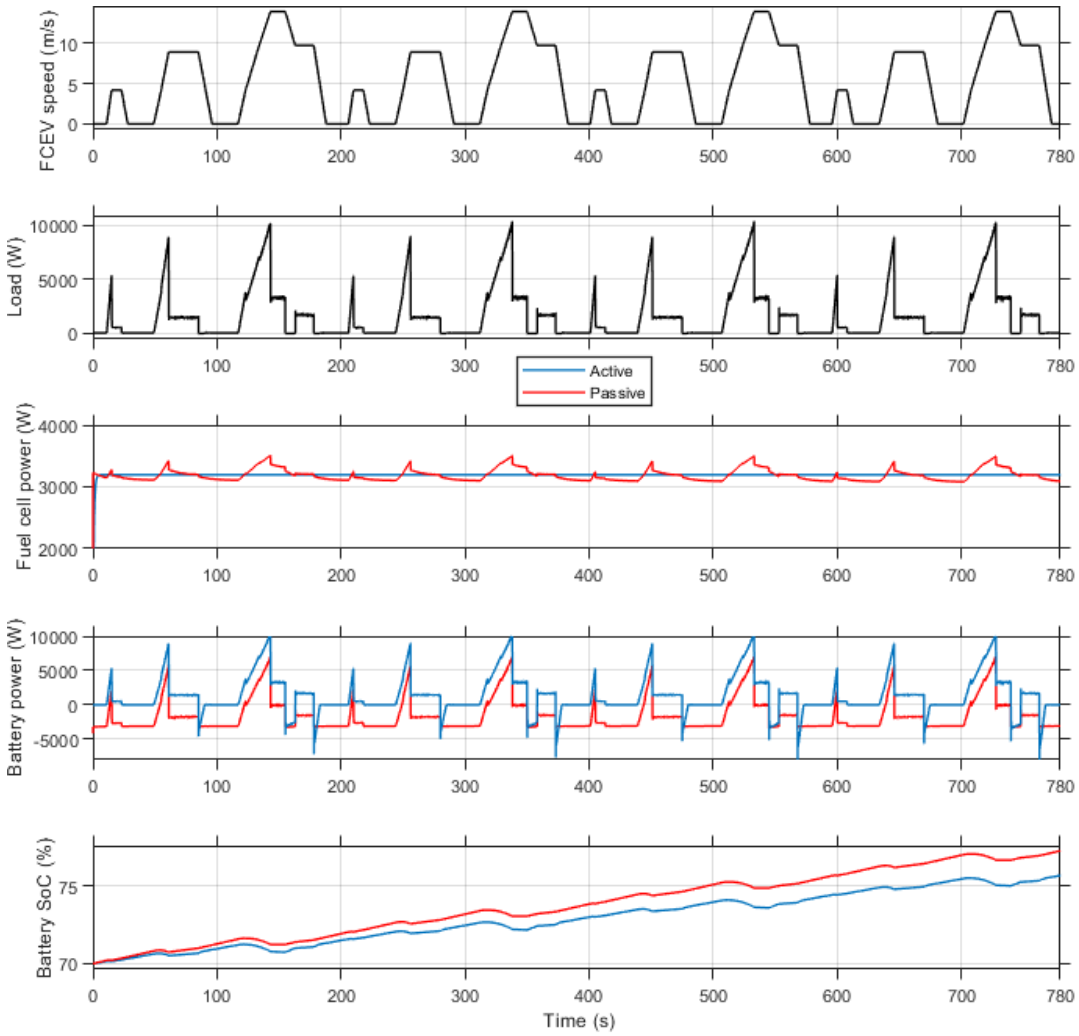

Figure 5-2 Comparison of active hybrid and direct passive hybrid strategy when battery at high SoC level under UDC drive cycle

Table 5-1 shows that the proposed direct passive hybrid powertrain provides more energy to the battery whilst keeping the fuel cell average power at a similar level. It is important to highlight that the passive hybrid powertrain increases the range by an average of 27.28% for FCEV over four UDC drive cycles, compared to the active powertrain. This shows the proposed system has higher efficiency than an active powertrain system, especially at lower battery SoC levels

Generally, fuel cell and lithium battery passive hybrid systems can provide relatively stable output power under different SoC conditions. Note, however, that the FC power fluctuation is higher compared to an active hybrid system where the FC is kept operating at a constant level. Such fluctuation is however detrimental to the life of the FC. Therefore, appropriate sizing of the FC and battery are required to ensure that the change in amplitude of FC power is acceptable

Table 5-1 Performance comparison of active and direct passive strategies

Initial SoC 70%	Active	Passive
Battery SoC after test	75.66%	77.24%
Fuel cell average power	3187W	3187W
Range extension	-	27.28%
Standard deviation of passive fuel cell curve		100.3W

5.4 Conclusion

This chapter has demonstrated that an FCEV direct passive powertrain is able to achieve the requested load under different SoC levels, and results in reduced use of the total energy sources under a UDC drive cycle. When the FCEV load increases, the battery fulfils the additional power demand by providing power when the load exceeds a threshold limit. Consequently, the energy generated in the fuel cell stack is relatively stable.

Having verified the benefits of the passive hybrid strategy for the H2EV in terms of increased efficiency and potential for range extension, the next chapter investigates the application of fuzzy logic control to manage the load demand for a passive hybrid strategy, taking into account the health of the fuel cell and the battery systems.

Chapter 6: Fuzzy logic for passive FCEV powertrain control

6.1 Introduction

Previous chapters have described a set of original, experimentally validated, powertrain models for active and passive FCEV. This chapter exploits these models to present the one of the main novelties of this thesis which is the application of a fuzzy logic control scheme to a passive hybrid system used in a passenger FCEV.

A fuzzy logic management strategy was selected based on their previously successful use in multiple applications and because of their robustness (Hemi et al. 2014). Relevant FCEV management strategies implemented include (Li et al. 2012), where it was applied to a DC-DC converter and ultracapacitor to reduce hydrogen usage. Bernard et al. (2011) developed a Proportional plus Integral (PI) controller based on bus voltage of an FCEV passive hybrid powertrain. The proposed fuzzy controller differs in its approach in terms of the application of fuzzy to passive hybrid and the means selected to control the power from the FC.

The proposed controller modifies the power delivered by the fuel cell to the battery and the powertrain to achieve the desired load demand, taking into account the battery SoC. The proposed passive control strategies are demonstrated under two well-established test cycles; ECE 15, and Extra Urban Driving Cycle (EUDC).

The remainder of this chapter is organised as follows. Section 6.2 presents an

evaluation of the hybrid FCEV power management strategies. Section 6.3 analyses the control parameters for the fuzzy logic controller. Section 6.4 describes the fuzzy logic scheme that controls the hydrogen pressure to adjust the power from the fuel cells. Section 6.5 presents the simulation studies, comparing with the passive and fuzzy controlled passive hybrid FCEV. Section 6.6 concludes the key findings.

6.2 Hybrid system management strategy

Chapter 4 involving the Microcab H2EV have evaluated passive hybrid systems experimentally, where a 3kW fuel cell stack and a 45v 180Ah lithium-ion battery were connected in parallel, to provide power to a 3kW electric load. The system was evaluated under different state of charge (SoC) levels for the lithium-ion battery pack. It was found that the fuel cell could operate at a relatively stable output power when the battery SoC was in the range 20% to 80%. When the SoC level is below 20%, the fuel cell stack might output more energy than its nominal power. When the battery SoC is higher 80%, the fuel cell stack power will decrease. In both situations, performance degradation of battery and fuel cell life cycle will worsen. Therefore, the most efficient and effective operating condition for the fuel cell corresponds to this recommended range for the battery SoC. Operating the fuel cell at a low SoC led to the fuel cell generating maximum power to charge the battery and supplying the load at the same time. This resulted in rapid fuel cell temperature increase which can negatively impact the FC state of health. It is only when the load reduces at a high SoC level that the fuel cell can return to the power output it is designed to deliver. Therefore, the experimental results indicated that once the appropriately sized fuel cell was selected, the SoC condition had the most impact on the passive hybrid system efficiency.

There are two primary objectives to be fulfilled by the management strategy for

automotive fuel cell and battery hybrid systems. The first is to improve the energy efficiency of the system. The second is to extend the battery pack and fuel cell lifetime. The passive hybrid system already meets the first requirement. The designed fuzzy logic controller is aimed to achieve both objectives.

The lifetime of lithium batteries is affected by the depth of discharge for different SoC levels. Therefore, high and low SoC levels should be avoided to extend the battery life (Wikner and Thiringer 2018, Qadrdan et al. 2018). The FCEV fuel cell lifetime is shorter than the lifetime of the stationary fuel cell, and this lifetime degradation is mainly due to frequent start-stop cycles (Pei et al. 2010, Pei et al. 2008, Zhang et al. 2018). Ideally, the fuel cell should keep working at nominal power. However, maintaining the battery SoC and improving fuel cell efficiency are two conflicting objectives faced by current systems. The first objective is to maintain the battery between 20% and 80% SoC and only allow the charging of the battery when the SoC is within these limits. The second objective is to keep the power supplied by the fuel cell stable to prevent performance degradation. Therefore, the best strategy should be to keep the battery between 20% to 80% SoC whilst reducing the number of fuel cell start-stops and occurrence of fuel cell power fluctuations.

Having identified the requirement in terms of power management, the next section identifies the most appropriate variable to control to achieve the desired objectives.

6.3 Sensitivity analysis

A sensitivity analysis was carried out to identify the most critical parameters from the fuel cell stack power control perspective. The proposed passive hybrid powertrain is able to investigate the parameters that affect PEMFC power. Based on the BALLARD fuel cell manual (Ballarld 2011) and previous

experimental test data, the fuel cell parameters investigated are set to constant values. Then, consecutively, one parameter at a time is changed to observe its impact on the fuel cell power variation for the passive hybrid system. The tests are carried out for the UDC drive cycle, which is representative for the use of the Microcab H2EV. The control group parameters for the fuel cell stack are described in Table 6-1.

Table 6-1 Fuel cell stack control group parameters

Fuel cell stack	Control group
Fuel flow (lpm)	200
Air flow (lpm)	200
Fuel pressure (bar)	0.36
Air pressure (bar)	1

6.3.1 Fuel flow rate

Fuel flow rate is an operating parameter that can have a significant effect on fuel cell stack performance. In this study, the fuel flow rate is varied from 125 to 300 Litres per minute (lpm). The fuel cell stack power curves for various battery SoC level is shown in Figure 6-1.

Figure 6-1 shows the fuel flow rate effect on the stack performance for a passive hybrid system with a 70% SoC lithium battery. It can be seen that the stack power increases faster when the fuel flow rate increases from 125 lpm to 200 lpm. A 75 lpm increase in the fuel flow rate results in a 3.9% average increase in the power. The rate of change in power increase is lower in the region from 200 lpm to 300 lpm, where a 100 lpm increase in the fuel flow rate results in only a 1.5% performance increase.

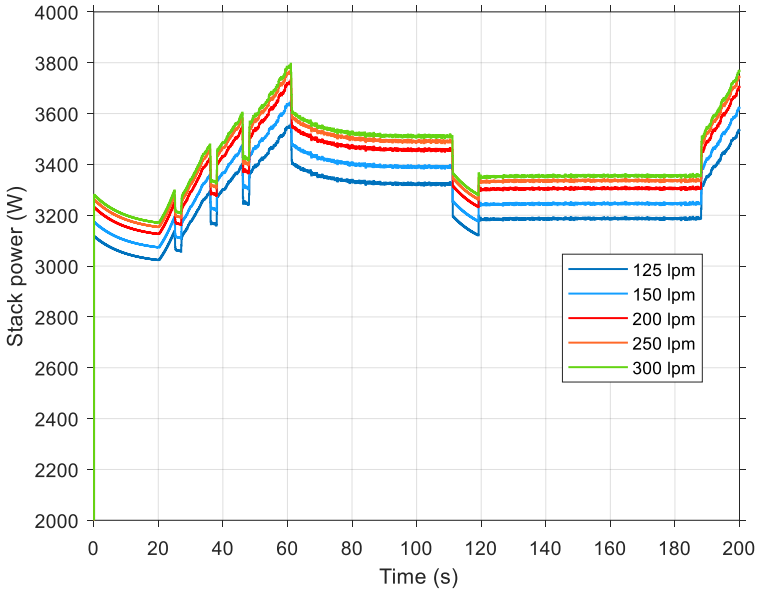

Figure 6-1 Fuel flow rate change on stack power at battery 70% SoC

Lower battery SoC increases the power curve in all regions. Increasing the flow from 125 lpm to 200 lpm results in a 4% average increase in stack power when the battery SoC is 50%. Similar to the case with 70% SoC, a hydrogen flow rate increase from 200 lpm to 300 lpm results in a stack power increase of 1.4%.

As a result of 30% SoC, the average curve for the stack power increases by 109 W compared to the situation with medium SoC level. A 60% fuel flow rate increase, between 125 lpm and 200 lpm, results in a 4.3% average increase in the stack power. Similar to the previous simulations, only an average 56 W increase in the stack power resulted in a 1.5% average increase when the fuel flow rate increased from 200 lpm to 300 lpm.

These simulation studies have shown that the fuel flow rate is an effective means to change the fuel cell performance under different battery SoC level.

6.3.2 Air flow rate

The air flow rate has the lowest effect on the PEMFC power. In the simulation, the air flow rate is changed from 150 lpm to 350 lpm, and the results are illustrated in Figure 6-2. By comparison, increasing the air flow rate by 200 lpm results in only 27W average increase in power, which is less than 1%. This indicates that the air flow rate's influence is not significant for PEMFC.

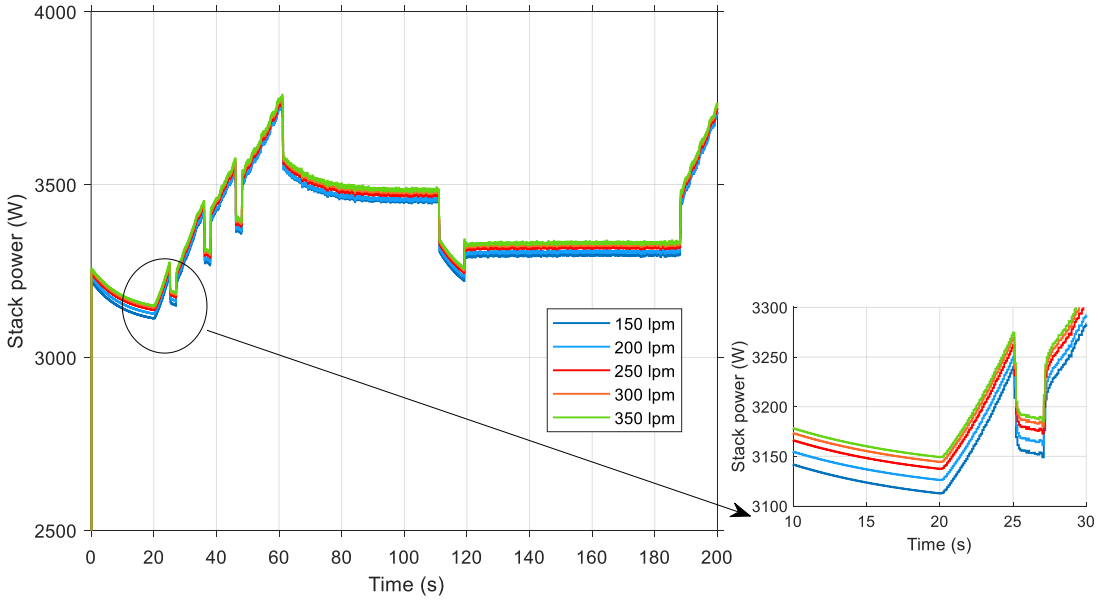

Figure 6-2 Air flow rate change on stack power at battery 70% SoC

6.3.3 Fuel pressure

Fuel pressure is the most important parameter for PEMFC. The results of changing fuel pressure under different battery SoC levels are illustrated in Figure 6-3. The operating fuel pressure range is 0.26 bar to 0.56 bar.

The comparison of the effect of hydrogen fuel pressure at a battery 70% SoC is presented in Figure 6-3. As fuel pressure increases from 0.26 bar to 0.56 bar,

the average power of the fuel cell increases by 285 W. It can be seen that the highest performance gain is in the region of fuel pressure increase from 0.26 bar to 0.36 bar, which results in 4.2% average increase in fuel cell power. When the fuel pressure changes from 0.36 to 0.45, the performance increases by about 2.6%. There is only a 1.8% increase in stack power when the pressures is increased between 0.46 and 0.56 bar.

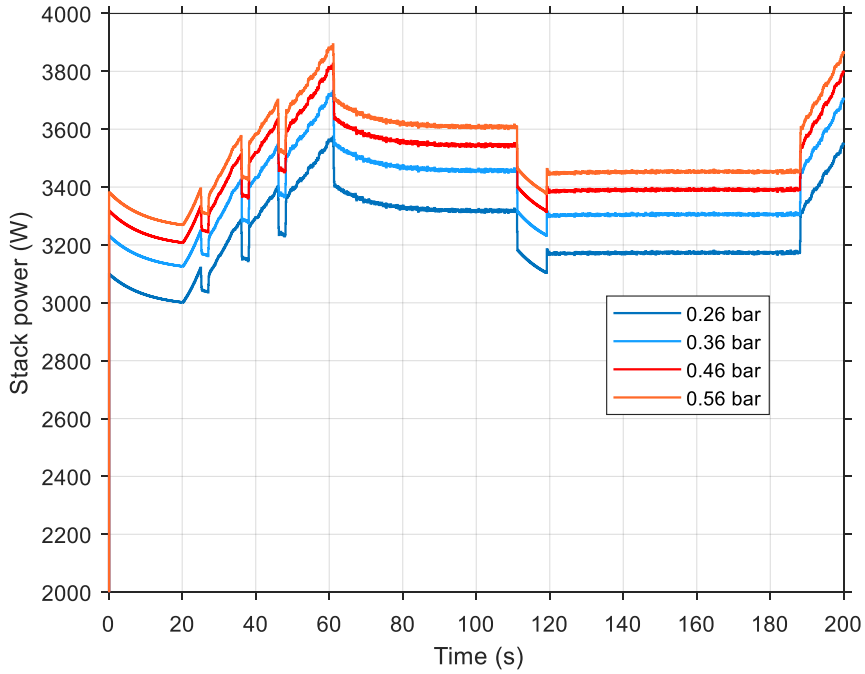

Figure 6-3 Fuel pressure change on stack power at battery 70% SoC

50% battery SoC level slightly shifts the power curve upward by 54.75 W compared to a 70% battery SoC level. From the results, a 0.1 bar rise in fuel pressure results in a 4.2% average increase of fuel cell power in the range 0.26 bar to 0.36 bar. The power increase is lower in the regions from 0.36 bar to 0.46 bar (2.5%) and 0.46 bar to 0.56 bar (1.8%).

It can also be seen that higher average stack power is found at 30% battery SoC level. Similar to the previous two results, changing the fuel pressure has less effect on stack performance at higher fuel pressures. These simulations

have shown that the fuel pressure changes lead to appreciable improvements in the stack performance. Therefore, the fuel pressure is a key control parameter for the PEMFC.

6.3.4 Air pressure

A study to test the sensitivity of the air pressure on stack performance is carried out at a high battery SoC condition. Figure 6-4 shows the effect of three levels of air pressure from 1 bar to 2 bar. Similar to the other variables, a more significant effect is seen when the control variable is changed in the low region. In this case, an increase in air pressure of 0.5 bar (50%) results in an increase in power to 66 W (1.9%). This results in an average improvement in cell performance by 3.3% due to the increase in air pressure. These simulation studies have shown that air pressure does not have a very significant influence on stack power.

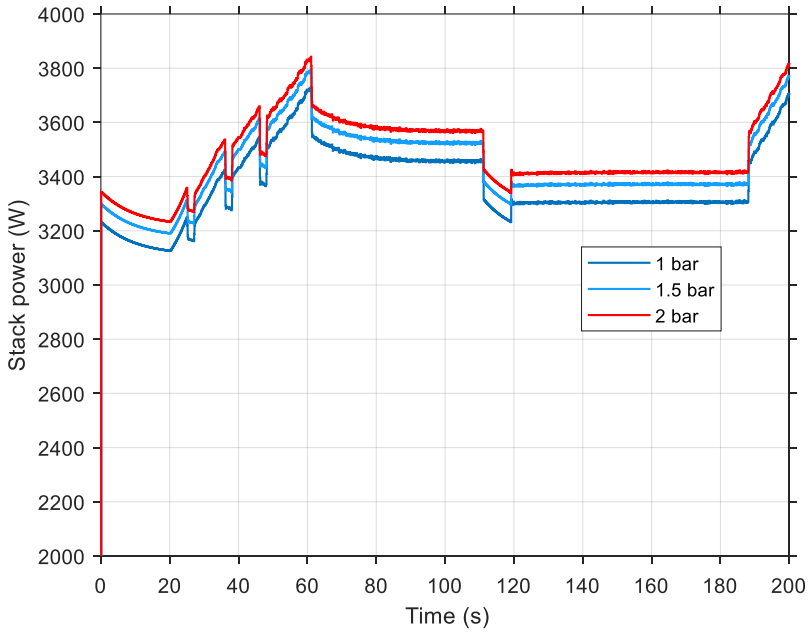

Figure 6-4 Air pressure change on stack power at battery 70% SoC

6.3.5 Sensitivity analysis summary

Table 6-2 summaries the outcomes of the sensitivity analysis. The fuel pressure is a key parameter that can control PEMFC power. Normally, under constant current conditions, the voltage of the fuel cell increases with fuel pressure. When the fuel pressure increases from 0.26 bar to 0.36 bar, the average power increases by 139 W, which accounts for 48.1% of the total power increase. Similar to the fuel pressure, the fuel flow rate in litres per minute (lpm) can affect the fuel cell power. The power gain is higher in the region from 125 lpm to 200 lpm compared with the region from 200 lpm to 300 lpm. the power of the PEMFC can affected by air pressure and air flow rate. However, the impact is much lower than the hydrogen pressure and flow rate. Based on the parameter sensitivity test results, fuel pressure is selected as the most appropriate control variable.

Table 6-2 Sensitivity analysis of process parameters on the PEMFC

Parameters	Change	Effect of fuel cell performance
Fuel flow (lpm)	125-300	5.6%
Air flow (lpm)	150-350	0.98%
Fuel pressure (bar)	0.26-0.56	8.76%
Air pressure (bar)	1-3	3.3%

The following section describes the proposed fuzzy logic management strategy that controls the fuel pressure for the passive hybrid system and evaluate it against the benchmark direct passive strategy.

6.4 Fuzzy logic controller for the passive hybrid system

The objectives of the control algorithm are to satisfy the FCEV load power and manage the fuel cell system while keeping the battery operating in a secure, safe and efficient manner. Figure 6-5 shows a schematic of the fuel stream configuration with a controller. In a fuel stream system, the hydrogen tank stores the hydrogen fuel. The pressure regulator measures and control the pressure of the hydrogen, and the controller regulates the supply pressure. In this work, a fuzzy logic controller is selected. The control algorithm has two input variables: the battery SoC and the FCEV load power. The Mamdani fuzzy logic controller aims to control the pressure regulator to deliver hydrogen fuel to the stack at the appropriate pressure. During the operation, the supply valve controls hydrogen on/off into the stack. The purge valve controls the impurities gas from the anode out of the stack at a specific duration. Therefore, the fuel cell stack is able to use fresh hydrogen from the tank.

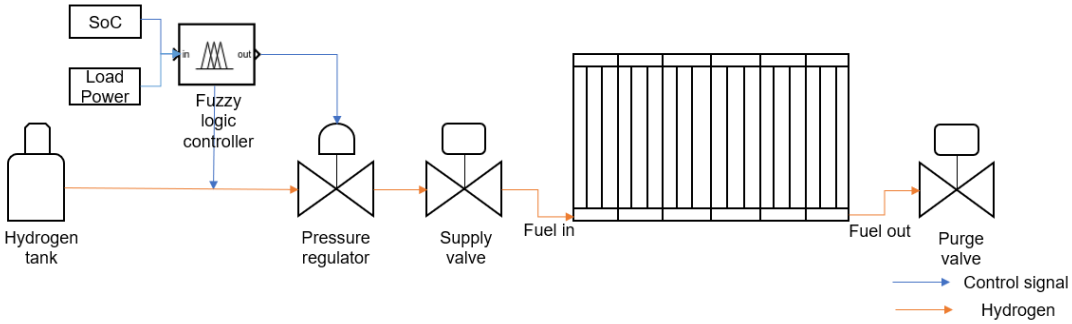

Figure 6-5 Fuzzy logic controller for fuel stream configuration

The membership functions of the inputs and the outputs variables are shown in Figure 6-6, Figure 6-7 and Figure 6-8. The SoC of the battery is between 0% and 100%, which represents an empty to a fully charged battery, respectively. The second input variable membership function represents the range of load power and is selected between the minimum and maximum load power generated by the FCEV. The output variable is chosen for the optimal operating range of the fuel cell stack based on the BALLARD fuel cell manual, that says

the fuel cell pressure upper limits is 0.56 and lower limits is 0.16.

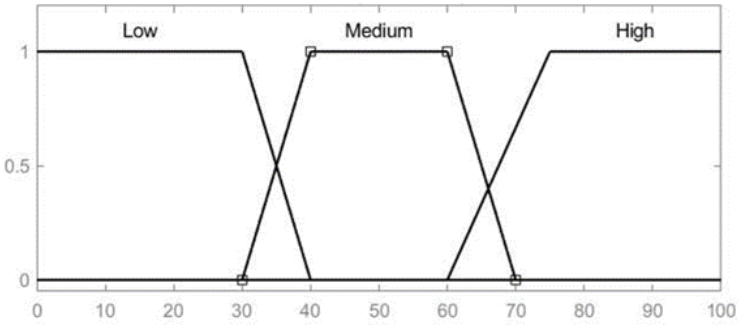

Figure 6-6 Membership function of Input variable SoC

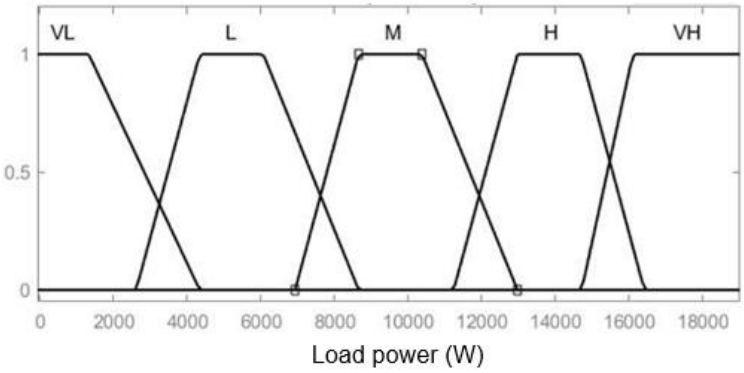

Figure 6-7 Membership function of Input variable FCEV load power

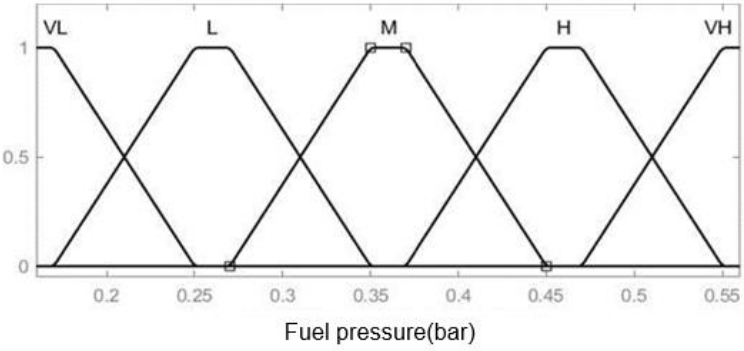

Figure 6-8 Membership function of Output variable hydrogen fuel pressure

The fuzzy logic control algorithm with 15 rules are set up, as shown in Table 6-3. The rules are of the form: "if SoC is X, and FCEV load power is Y, then hydrogen fuel pressure is Z". The rules are based on experimental experience in order to provide better performance for the fuel cell stream system. Because the battery SoC change is relatively small, it is divided into three fuzzy subsets: L (low battery SoC), M (medium battery SoC） and H (high battery SoC). As

presented in Chapter 4, maximum battery power is 13.8 kW and we that FC power is around 4 kW, so the summation is around 18 kW. The FCEV load power is categorised into five states to satisfy different drive cycles: VH (very high power demand), H (high power demand), M (medium power demand), L (low power demand) and VL (very low power demand). The output variable fuel pressure is assigned to five subsets: VH (very high fuel pressure), H (high fuel pressure), M (medium fuel pressure), L (low fuel pressure) and VL (very low fuel pressure). Trial-and-error method is used for determining the 'break points' of membership functions. The Mamdani Inference approach is utilized to carry out the centroid defuzzification.

Table 6-3 Fuzzy controller rules

SoC	FCEV load power	Hydrogen fuel pressure
L	VL	H
	L	H
	M	H
	H	VH
	VH	VH
M	VL	L
	L	M
	M	H
	H	VH
	VH	VH
H	VL	VL
	L	VL
	M	L
	H	M
	VH	H

6.5 Comparison of fuzzy control for the passive hybrid strategy and direct passive hybrid strategy

The UDC (average speed 18.4km/h) and EUDC (average speed (62.6km/h) were selected to evaluate the performance of the model and controller for different architectures, as these cycles are representative of the urban use of the vehicle.

Figure 6-9 shows the comparison results of two passive methods when the battery SoC is high. In the case of the direct passive hybrid strategy, the battery SoC reaches 80% at 400s, at which time the FCEV switches to EV mode and the fuel cell turns off to prevent battery overcharge and overheating. In EV mode, battery will supply energy to the FCEV, until battery SoC drops to 50%. Then the fuel cell stack will turn on. By contrast, the fuzzy passive strategy reduces the power provided to the battery by reducing the fuel pressure, thereby delaying the need to switch off the fuel cell. The reduction of fuel pressure to 0.193 bar reduces the power generated by the fuel cell by 9.57%, resulting in an average power of 2894W. This simulation demonstrates the ability of the proposed controller to regulate the fuel pressure to save hydrogen and prevent the SoC from increasing too fast to a very high level. Thus, the FC can continue to operate 18.25% longer before it has to stop.

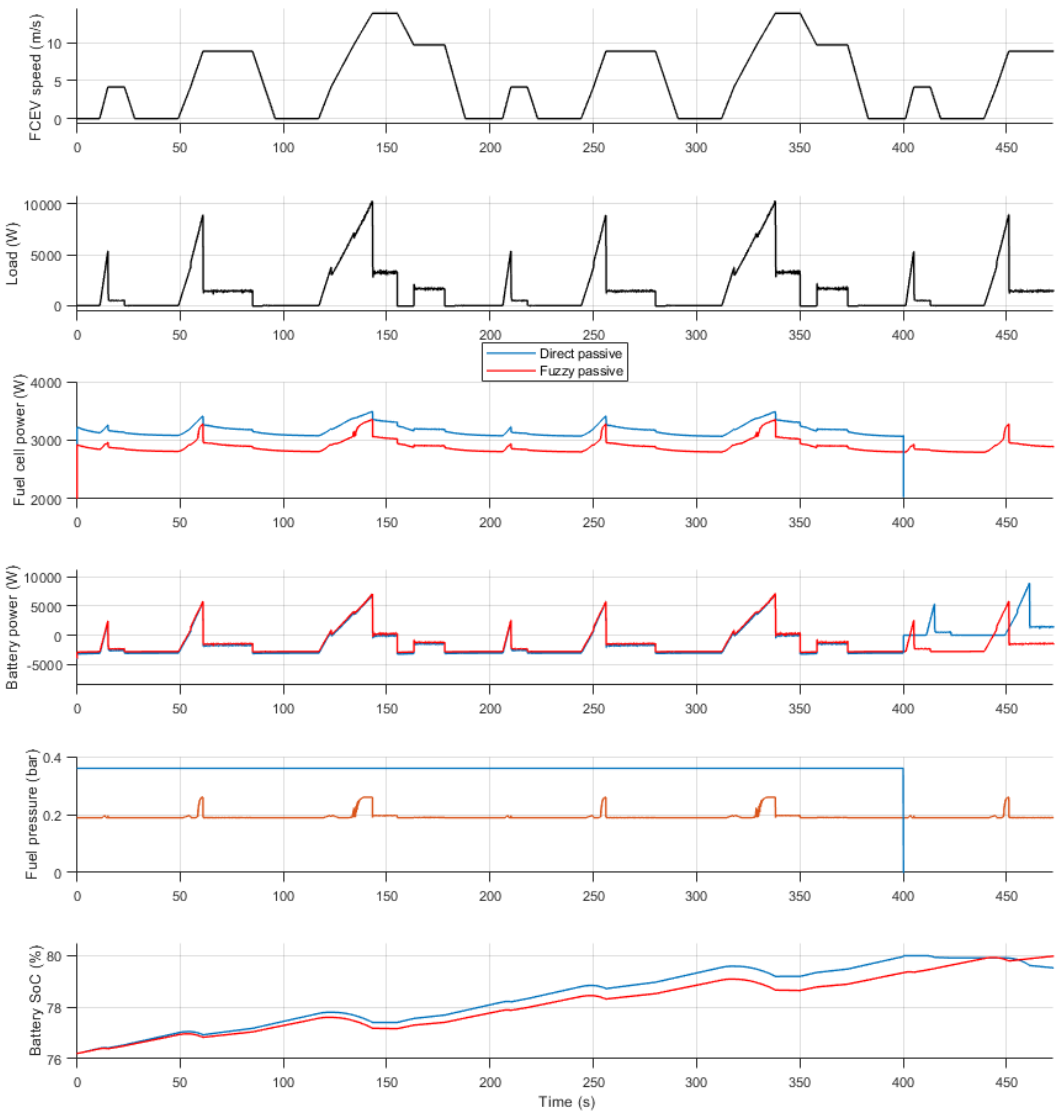

Figure 6-9 Comparison of direct and fuzzy passive strategies with the battery at a high SoC level under a UDC drive cycle

Figure 6-10 then shows the comparison between two passive methods when the battery SoC is medium. By adjusting the battery SoC to a medium level, the average fuel cell power for the direct passive strategy increases from 3171 W to 3248 W. The fuzzy controller reacts to the SoC reduction from high level to medium level and increases the fuel pressure to 0.233 bar to increase the power delivered by the fuel cell. As the SoC drops, the fuel pressure increases, resulting in the fuel cell power gradually increasing to 8.84%. Because the SoC

level and load condition are still acceptable for the passive hybrid system, the controller continues to save hydrogen for future use.

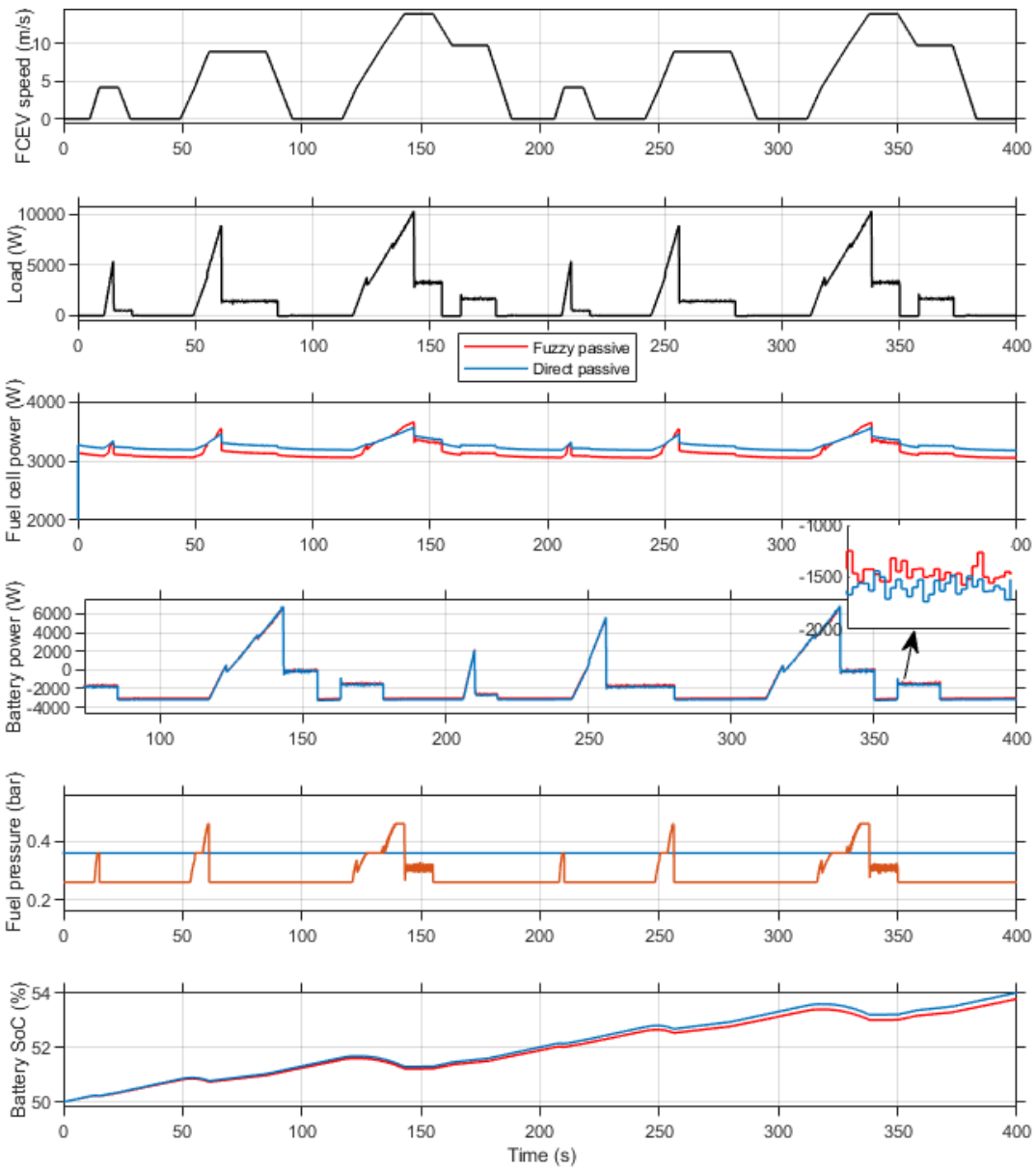

Figure 6-10 Comparison of direct and fuzzy passive strategy with the battery at a medium SoC level under a UDC drive cycle

By reducing the battery SoC to low level, it can be seen that the fuel cell constantly operates at a higher performance to meet the load, as shown in Figure 6-11. In the case of the fuzzy passive hybrid strategy, the increase of fuel pressure to 0.462 bar increases the stack performance by 11.44% compared to a 50% SoC level, resulting in an average power of 3514 W. Therefore, the battery can charge by 4.78% more than the direct passive strategy. By contrast, the FCEV with the fuzzy controller enables the battery SoC to return to high efficiency and a health SoC region more quickly.

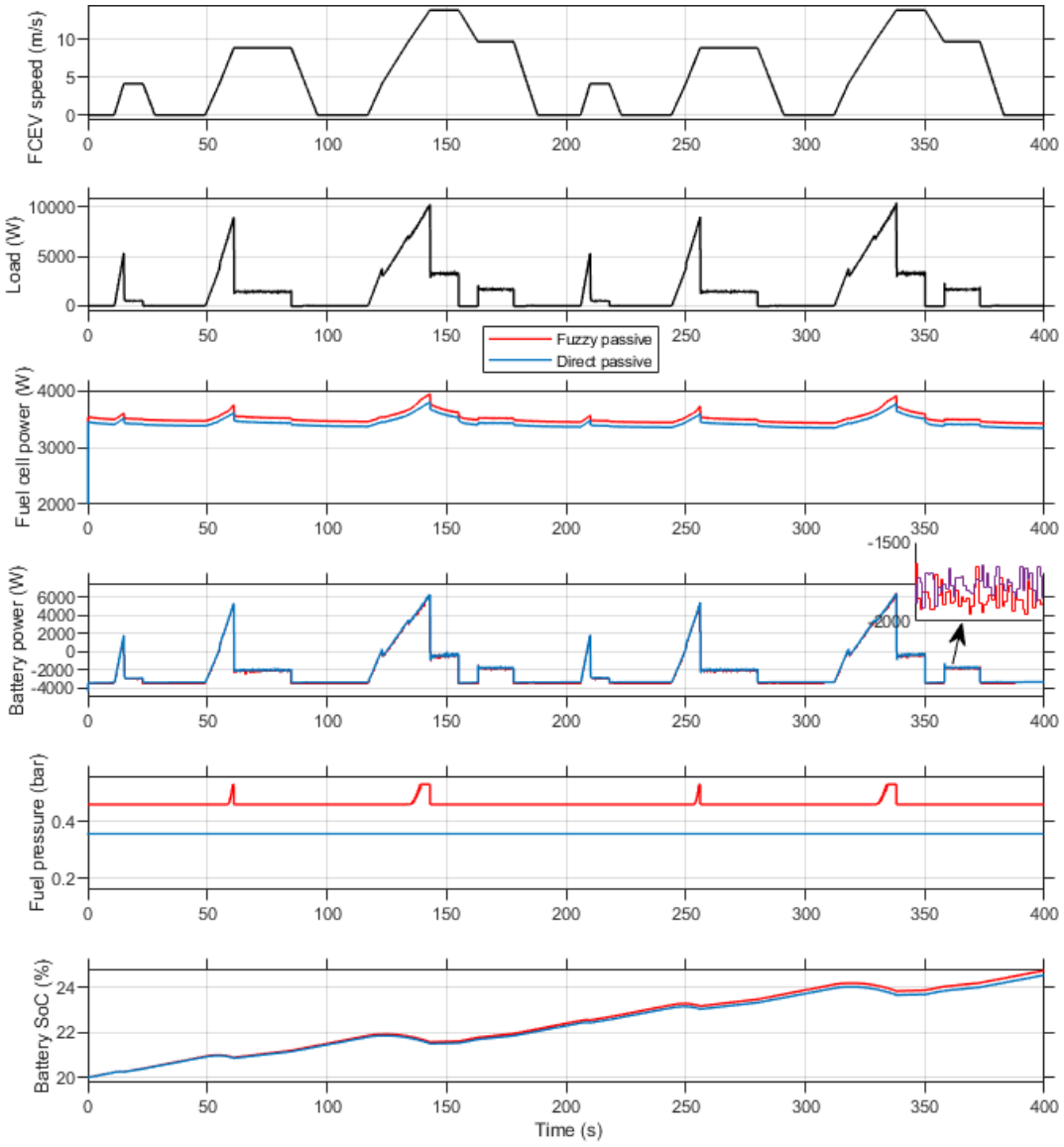

Figure 6-11 Comparison of direct and fuzzy passive strategy with the battery at a low SoC level under a UDC drive cycle

The EUDC drive cycle is used to evaluate the performance of the fuzzy-controlled passive method, when the fuel cells are required to provide additional power to delay the SoC from reaching its minimum value. It is assumed that the initial SoC is below 40%. The demanding drive cycle in terms of load, for the selected fuel cell and battery size, results in the SoC reaching 20% after 900s with the direct passive strategy. By contrast, the FCEV with the fuzzy controller can drive 1.2km (17%) further until the SoC reaches the 20% level. This is achieved by increasing the average fuel pressure by 27.78% compared to the direct passive strategy, resulting in an average fuel cell power increase from 3645W to 3739W for the direct and fuzzy control, respectively. The fuzzy passive strategy outputs more power to satisfy the requested load, resulting in higher hydrogen consumption by 12.41g/km compared to 9.73g/km with the direct passive strategy. This results in an average battery power 76W lower than for the direct passive strategy.

These simulation results indicate that the fuzzy control strategy is applicable to adjust the power of the passive hybrid configuration of FCEV to either extend the range of the FCEV or reduce the number of times the FC is switched on/off. The latter positively impacts on the life of the FCEV. However, in the case where the fuzzy controller is required to increase the fuel cell output, see Figure 6-12, the increase in variation of the FC power output, characterised by its higher standard deviation (see Table 6-4) will have a detrimental effect on the fuel cell stack life. There is therefore a trade-off between improving the battery SoC and its life whilst at the same time delivering the performance required by the driver and managing the life of the FC. Fuzzy logic offers the possibility to achieve the required trade-off dependencies. In this project, the focus was on extending range and reducing the number of FC shutdown cycles.

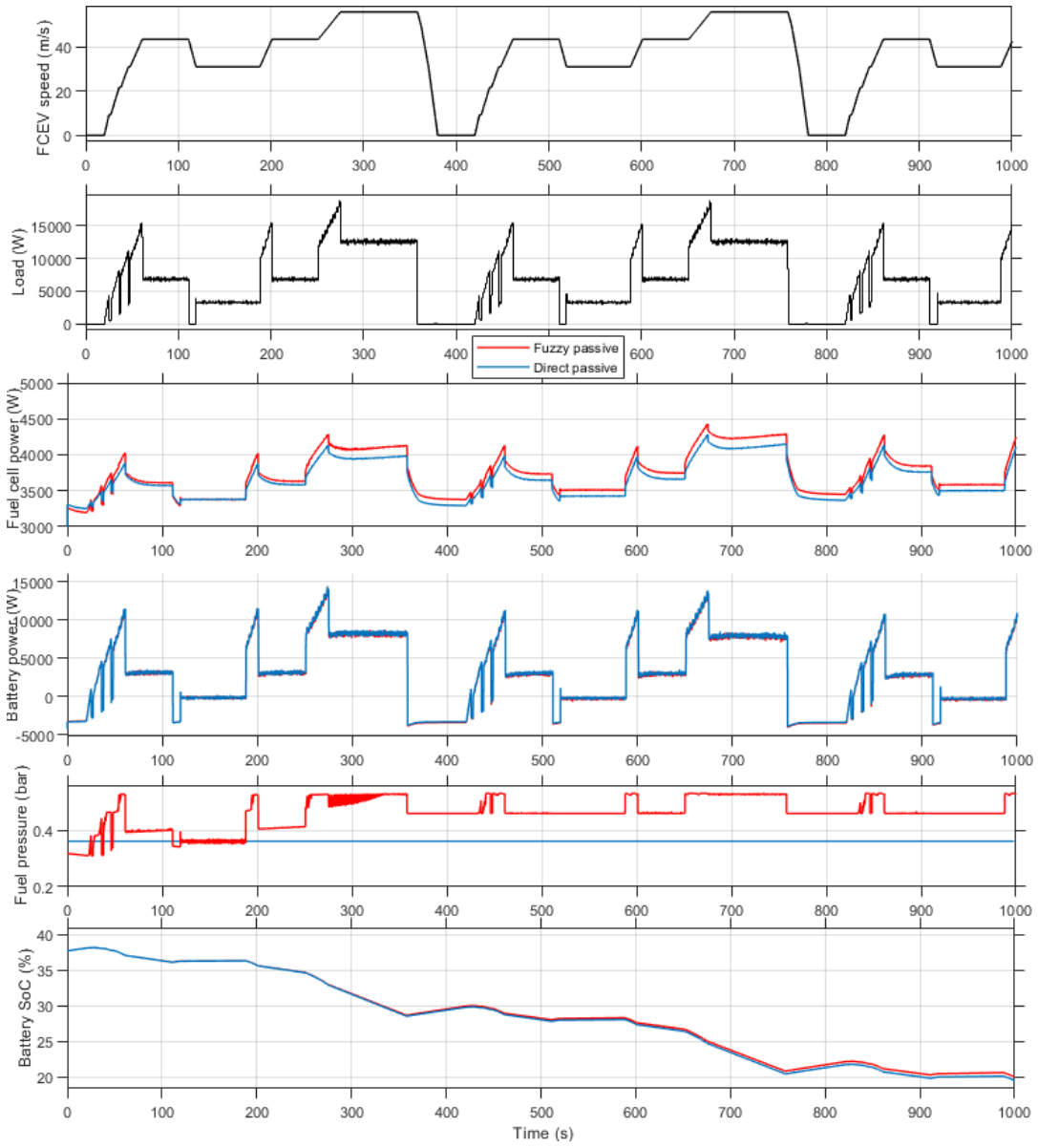

Figure 6-12 Comparison of direct and fuzzy passive strategy with battery at a low SoC under an EUDC drive cycle

Table 6-4 Analysis of the fuel cell and battery power curves for the direct and fuzzy passive hybrid systems

	Fuel cell direct	Fuel cell fuzzy	Battery direct	Battery fuzzy
Mean	3645W	3730W	2830W	2754W
Standard deviation	259	295.2	-	-

6.6 Conclusion

This chapter has proposed a fuzzy logic control strategy to improve the performance of passive hybrid FCEVs by controlling the hydrogen fuel pressure. The prime objective was to meet the driver torque request and associated load. The secondary objective was to maintain the SoC of the Li–FePO4 battery between 20% and 80%. Maintaining the battery at its recommended operating condition enables both prolonging the life of the battery and keeps the fuel cell power relatively stable and near its most efficient operating region. The latter advantage, combined with reducing the number of fuel cell start-stop cycles, helps to meet the third objective, which is to operate the fuel cell safely and to prolong its life. The fourth objective is to improve the efficiency of the FCEV. These objectives were achieved through the Fuzzy logic controller for a fuel stream passive hybrid configuration.

The sensitivity test for the passive hybrid system found that the fuel pressure was the most significant parameter to affect the fuel cell power. Note that the fuel flow was the second most significant parameter and its inclusion in the control strategy has been identified as an area of further work

The UDC and EUDC drive cycles were selected, as they are appropriate for urban use. These were used to evaluate the performance of the model and controller for the different architectures.

Analysis of comparison between direct passive and fuzzy passive strategies demonstrated that the fuzzy passive strategy could reduce the start-stop frequency caused by maintaining the battery SoC level above 80% and prevents large load changes caused by excessively low SoC levels.

The efficiency of the controller is reduced in the EUDC drive cycle due to the important increase in power demand for the FCEV with lower SoC level. The average driving speed in the UK's major cities has fallen by about 20%, with the average speeds at around 3 m/s in 2017, which is far below the UDC drive cycle speed (APH 2018). The Microcab H2EV is designed for low powered drive cycles. Thus, the investigation shows that the passive hybrid system with a fuzzy control strategy exhibits good effectiveness for an FCEV targeting urban driving conditions in the UK and at the same time extends the battery/fuel cell lifespan for an urban-use passenger FCEV.

Further investigation on the fuel cell passive hybridization with different batteries is analysed in the following chapters.

Chapter 7: Impact of battery technology on Passive hybrid systems

7.1 Introduction

Chapter 2 has highlighted the dominance of lithium battery-power in BEVs for automotive transport applications. This is mainly due to their lightweight and high energy density, fast charging time and wide range of operation compared to lead-acid batteries. However, as the first commercially available rechargeable battery, lead-acid batteries are still used in most vehicles as the primary or secondary battery due to their cost-effectiveness. Ni-MH batteries started to infiltrate the market of lead-acid batteries in the nineteen nineties. Ni-MH batteries are mostly used in HEVs and FCEVs, e.g. Toyota Mirai. This chapter will exploit the model developed in chapter 3, to investigate the impact of these three main battery technologies for small lightweight FCEVs used in urban environments. The simulation results of these batteries point out the applicable applications for different passive systems.

This Chapter is organised as follows; Section 7.2 describes the different components of Lead-Acid, NiMH and Lithium Ion batteries. In section 7.3, simulation studies are performed using the same drive cycle and initial conditions as in Chapter 6. Section 7.4 contains a critical analysis of the different battery technologies investigated.

7.2 Battery components

In the lead-acid battery and fuel cell passive hybrid powertrain, the 4.3 kWh lithium battery pack is replaced by a 4.3 kWh lead-acid battery pack. Six 12V 60Ah lead-acid rechargeable batteries are connected in series to provide the same power as the original lithium battery pack. This new design adds 100 kg to the vehicle, which increases the total weight from 775 kg to 875 kg. According to the production cost of batteries in Table 2-2, using lead-acid rechargeable batteries will save £309.60.

The Ni-MH battery based passive hybridization powertrain comprises a 4.3 kWh Ni-MH battery pack in place of the 4.3 kWh lithium battery pack. Six 12V 20Ah Ni-MH rechargeable battery packs are connected in series, and three groups of these are connected in parallel to provide the same power as the original lithium battery. The new design also adds 29 kg weight to the vehicle, which increases the total vehicle weight from 775 kg to 804 kg. Based on the production cost of batteries in Table 2-2, the Ni-MH battery pack will cost £172 more than a lithium battery pack.

In both cases, the weight increase is expected to have a negative impact on the vehicle's load power.

7.3 Simulation studies of different battery technologies on Passive hybrid systems

The lithium battery passive hybrid system is used as a benchmark against which to evaluate the lead-acid and NiMH battery passive hybrid systems. In all cases the UDD drive cycle is used as it is suitable for a low power, small FCEV designed to operate in an urban environment.

The impact of lead acid, NiMH and lithium battery technologies is evaluated for low, medium and high SoC levels. Figure 7-1, Figure 7-2 and Figure 7-3 illustrate the dynamic performance of these three configurations. Table 7-1 summarises the overall performance of lead-acid and NiMH against the reference lithium battery.

It can be observed that at a high SoC, e.g. 70%, the increase in weight by 12.9% and 3.7% leads to a battery pack load increase of 9.08% and 2.5% for the lead-acid battery and the NiMH batteries, respectively.

The fuel cell power provided to the battery is, on average, slightly lower (53W) for lead acid but as much as 260 W lower for NiMH. This lower charge to the lead acid and NiMH batteries results in a range reduction of 20% (0.4km) and 37.4% (0. 74km) for lead acid and NiMH, respectively.

Use of lead acid and NiMH batteries results in a higher variation in the power outputs provided by the fuel cell. Fuel cells combined with lead-acid batteries were by far the most affected. The variations are potentially unwanted as they may affect the fuel cell life. Note that further work is required to evaluate if the impact of a higher fuel cell power variation is similar to fuel cell start-stop cycles that have been shown to have a detrimental impact on the state of health of the

fuel cell.

The NiMH battery exhibits similar behaviour, irrespective of the initial battery SoC. The fuel cell power is consistently lower than the reference battery resulting in a reduction in range of around 30%. The change in amplitude of the fuel cell power is similar, with a standard deviation 60 W higher than the reference battery.

By contrast, the performance of the FCEV with a lead acid battery improves in terms of the SoC level, average fuel cell power and a range extension (by 11.4% or 0.22km) when the initial battery SoC decreases. The change in amplitude of the fuel cell power is slightly reduced, however the standard deviation is still above 290 W. The variation caused by the load demand can be clearly seen on the 'fuel cell power plots' presented in Figure 7-1, Figure 7-2 and Figure 7-3.

Common to all battery types, reducing the battery SoC increases the current drawn by the fuel cell to supply the increased load. The interaction between the batteries and the fuel cell can be explained by the battery packs' discharge curves illustrated in Figure 7-4 and Figure 7-5. Three 72V nominal batteries are compared, corresponding to 77.8V for the lithium battery, 73.3V for the lead-acid battery and 84.81V for the NiMH battery.

The lithium battery pack discharge curve is slightly flatter than NiMH and significantly flatter than the lead-acid battery, especially at nominal voltage range. Small deviations in the voltage of the fuel cell system and battery voltage results in the fuel cell power output being relatively constant, which is believed to be desirable from a fuel cell life expectancy perspective.

In the case of the lead-acid battery pack, the operating point of the fuel cell is

in a more efficient region due to the lower nominal voltage.

The Ni-MH battery pack has the highest nominal discharge voltage curve, followed by the lithium battery and the lead-acid battery. A higher nominal voltage enables a battery pack to provide more power to the load, which is desirable. After the exponential voltage drop, the lithium battery pack discharge curve is more stable than the Ni-MH battery which results in a stable output power from the fuel cell stack.

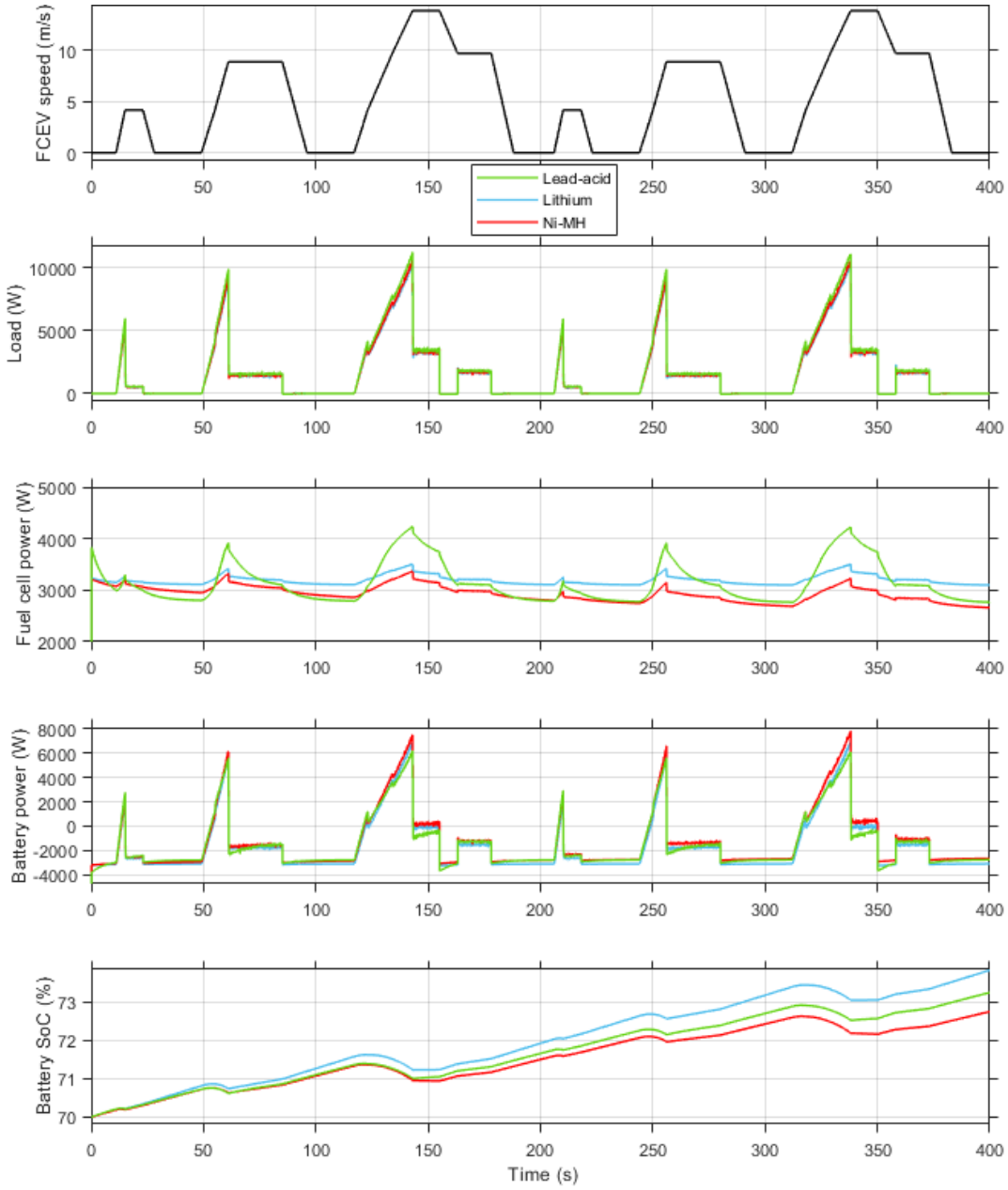

Figure 7-1 Comparison of different batteries passive hybrid system when battery at high SoC under UDC drive cycle

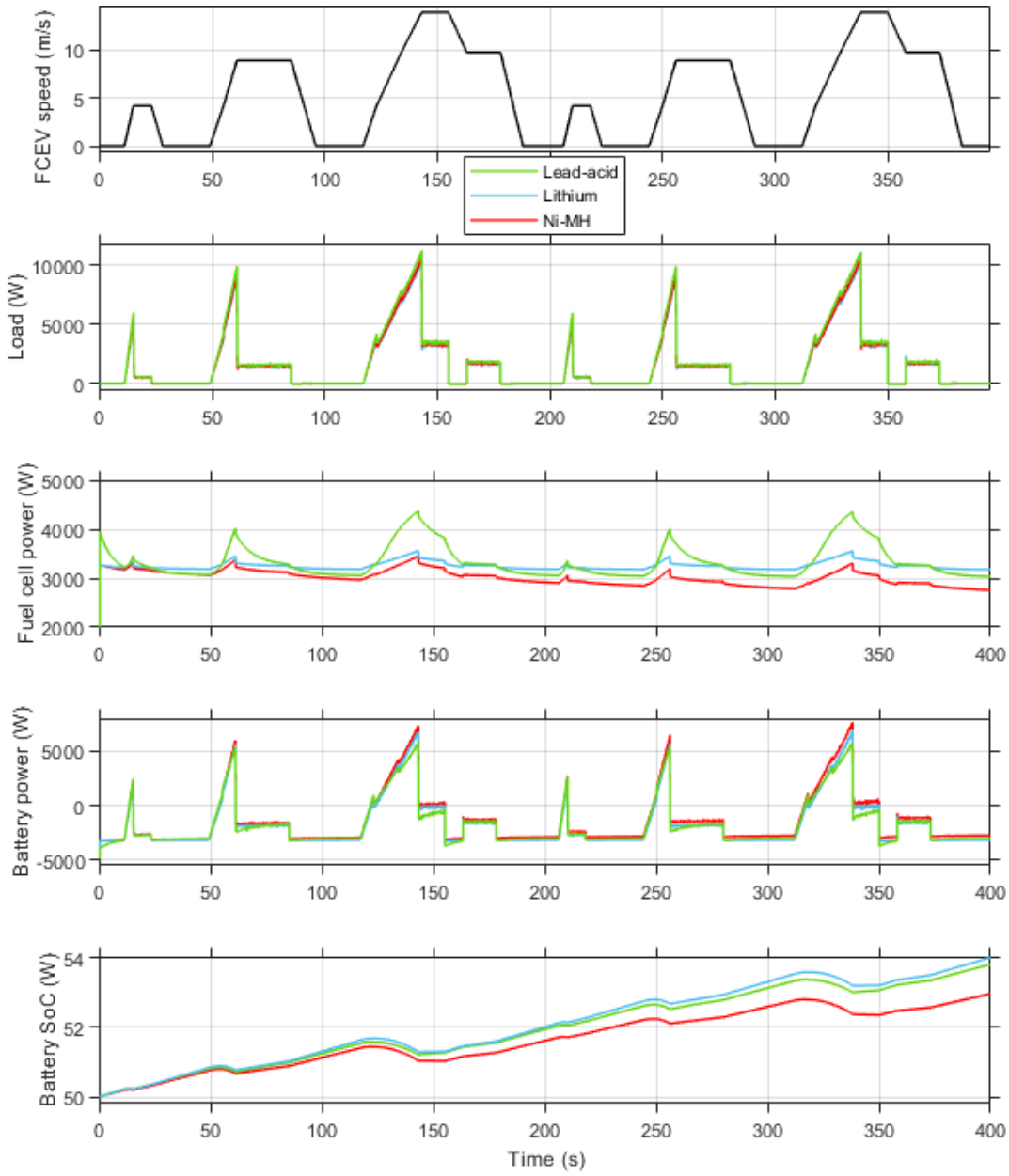

Figure 7-2 Comparison of lead-acid and lithium passive hybrid system when battery at medium SoC under UDC drive cycle

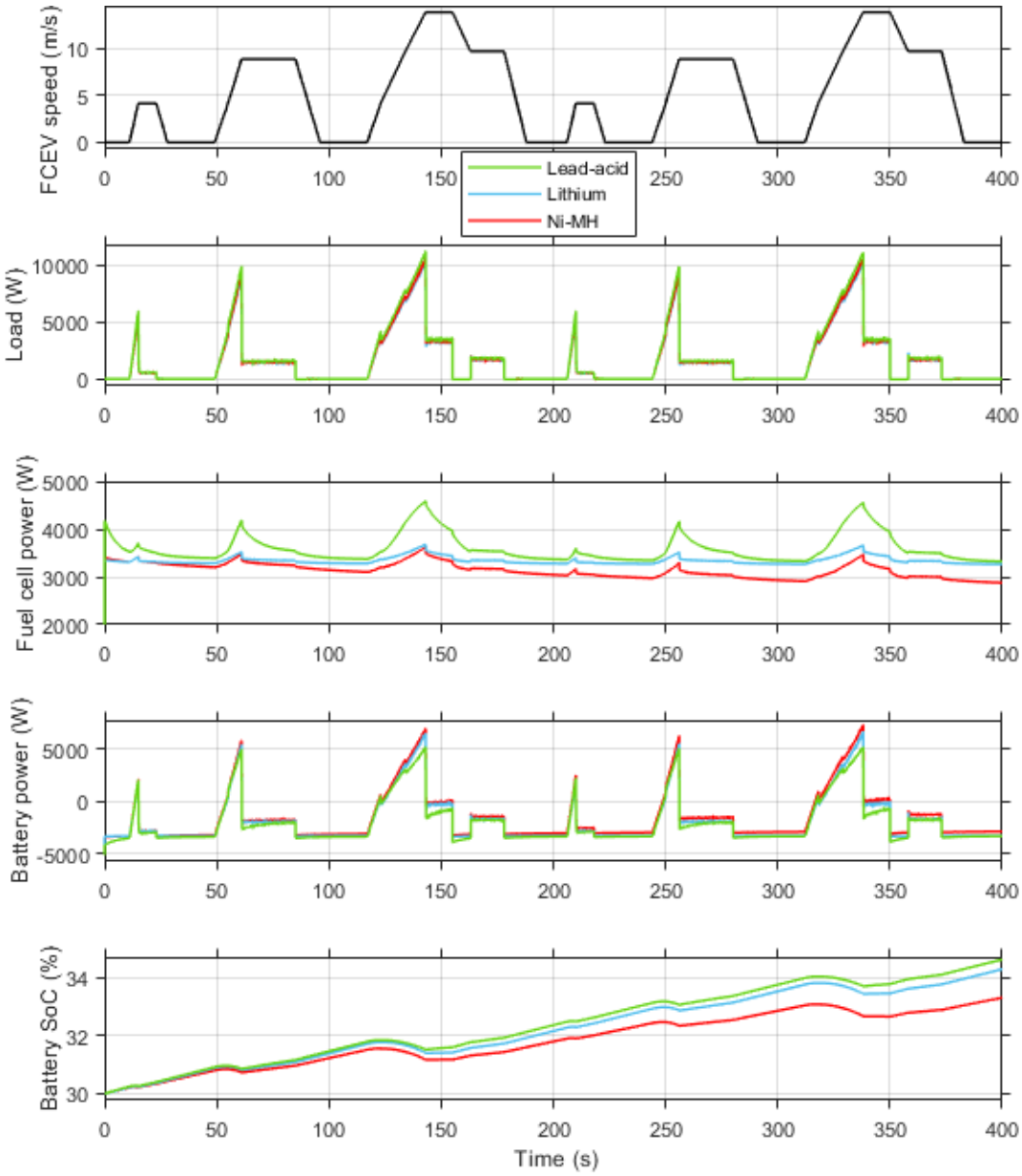

Figure 7-3 Comparison of lead-acid and lithium passive hybrid system when battery at low SoC under UDC drive cycle

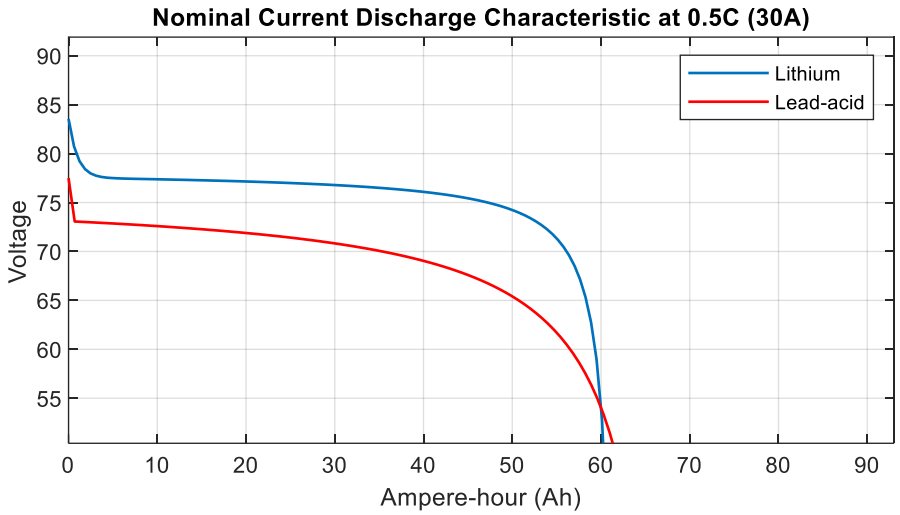

Figure 7-4 Comparison of lithium battery pack and lead-acid battery pack discharge curve

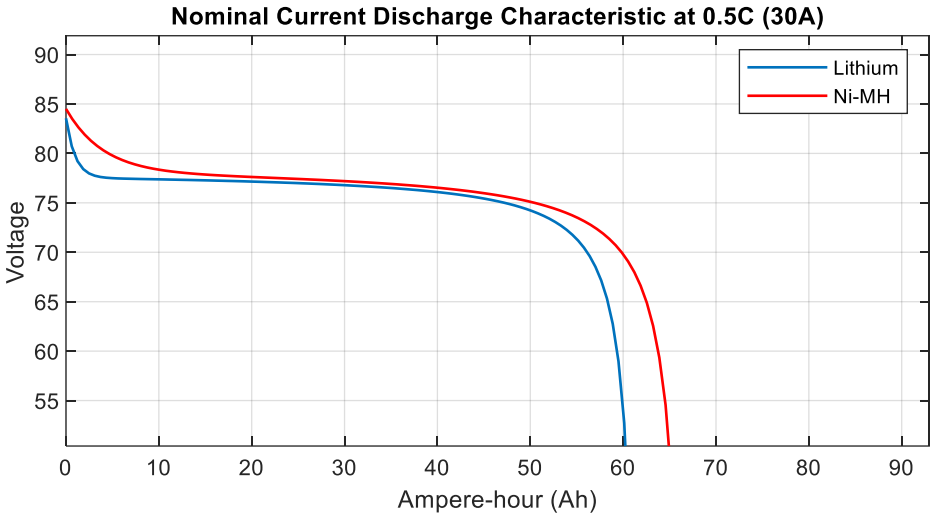

Figure 7-5 Comparison of lithium battery pack and Ni-MH battery pack discharge curve

7.4 Discussion and analysis of different battery passive hybrid systems

Table 7-1 Analysis of fuel cell performance of different battery passive hybrid systems

Initial SoC 70%	Ni-MH passive	Lithium passive	Lead-acid passive
Battery SoC after test	72.75%	73.83%	73.25%
Fuel cell average power	2932W	3192W	3139W
Range change	-37.3%	0	-20%
Standard deviation of power curve	160	103.8	388.1
Initial SoC 50%			
Battery SoC after test	52.97%	54.02%	53.82%
Fuel cell average power	3014W	3252W	3335W
Range change	-36.26%	0	-6.9%
Standard deviation of power curve	154.6	95.41	
Initial SoC 30%			
Battery SoC after test	33.31%	33.85%	34.62%
Fuel cell average power	3135W	3339	3589
Range change	-33.85%	0	11.4%
Standard deviation of power curve	160.5	95.26	293.5

Table 7-1 summarises the outcomes of the fuel cell curve analysis for different batteries. The simulation studies have shown that each battery has different advantages in terms of life expectancy, efficiency, range and power. The aim of this section is to identify application areas where fuel cells could be combined with these battery technologies.

According to a National Travel Survey, 56.46% people who have a disability lasting more than one year, are stated as having mobility difficulties. Although many old people have difficulties in walking as their age increases, the survey also shows that those aged 60+ have the highest interest in going on trips compared to younger people (Department for Transport 2019). Major cities in the UK have problems of congestion. As a result, electric mobility scooters have become more and more popular in the UK. The market study estimates the annual growth in sales of scooters at approximately 5-10%, and the buyers were most interested in the range that could be achieved (Barton et al. 2014). Currently, commercial electric mobility scooters mainly use lead-acid battery packs for the ESS. Because of the limited space in electric mobility scooters, the driving range is much worse than BEVs. Adapting fuel cell and lead-acid battery passive hybrid systems to mobility scooters would solve the range issue and prevent deep battery discharge, whilst keeping the system relatively cheap (for a fuel cell vehicle). It would provide a simple and efficient system.

However, the problems associated with the weight of the lead-acid battery pack and the degradation to the fuel cell stack due to high fuel cell load variability need to be carefully considered for larger FCEVs. Simulation results suggest that the lead-acid battery passive hybrid system is more suitable for applications which have lower and more stable load power and a smaller lead-acid battery pack.

.

NiMH has a longer life cycle than a lithium battery and only slightly worse performance than lithium batteries in terms of fuel cell load variability. NiMH can therefore be a good alternative for large, long-range passive hybrid FCEVs used for motorway driving that require a large power but at a stable output.

Lithium batteries have the best battery performance specification, including specific energy (Wh/kg), energy density (Wh/L) and specific power (W/kg) compared to lead-acid and NiMH batteries. Furthermore, lithium batteries have the flattest discharge curve which is highly suited to passive hybrid systems. This can reduce maintenance cost of the fuel cell stack, for a longer lifetime.

7.5 Conclusion

This chapter has presented simulation studies investigating the relative benefits of three combinations of batteries and fuel cells for passive hybrid systems. The benchmark system with a lithium battery outperformed the lead acid system except at a low SoC level, based on lead-acid battery passive hybridization simulation results that have been presented and analysed in this chapter. It is critical to assess the stability and power output of the fuel cell system when modelling a passive hybrid system. Comparison of two passive hybrid systems showed that lead-acid batteries can provide higher efficiency when the battery SoC level is not high, as well as increasing the driving range of the FCEV.

Hence, a fuel cell and lead-acid battery passive hybrid system can avoid the deep discharge problem, maintaining the health of lead-acid batteries. However, the problems of increased weight of the lead-acid battery pack, and higher degradation of the fuel cell stack need to be carefully considered for FCEVs. Simulation results suggest that the lead-acid battery passive hybrid system is

more suitable for applications which require lower power demand and small lead-acid battery packs.

The work presented in this chapter also covered the investigation of performance for changes in load demand with Ni-MH batteries and fuel cell passive hybrid systems under all SoC conditions. It can be seen that the Ni-MH passive hybrid system has slightly larger fuel cell power output variability than lithium-based battery systems, but much lower fuel cell power output variation than lithium-based passive hybrid systems, and higher variability than lead-acid passive hybrid systems. The weight of the Ni-MH battery pack is also in-between the weights of the equivalent lithium and lead-acid batteries. As the Ni-MH battery has a longer life cycle than a lithium battery, it can be a good alternative choice for long range passive hybrid FCEVs operating on the main road networks.

Overall, the current lithium-based passive FCEV is the most appropriate for urban environments due to the smaller impact of load demand variation on the fuel cell, and the smaller weight of the battery pack.

Chapter 8: Passive hybrid system component sizing

8.1 Introduction

Chapter 6 demonstrated that a passive hybrid FCEV is more sensitive to high-speed drive cycles than active hybrid FCEVs due to the increased variability in fuel cell output power. Chapter 7 has shown the impact of the battery type and fuel cell combination on passive hybrid system performance. It highlighted the need to carefully select the fuel cell and battery size to meet the vehicle's operating requirements.

This chapter proposes a design method for fuel cell and battery selection for passive hybrid FCEVs. The validity of selection rules is then evaluated using simulation studies exploiting the research work carried out in Chapter 2 and the modelling of the Microcab H2EV vehicle done in Chapters 3 and 4.

This chapter is organised as follows; Section 8.2 describes the battery and fuel cell selection guidelines for the passive hybrid system. Section 8.3 to section 8.5 cover the demonstration and validation of the optimal passive hybrid system selection methodology. Section 8.6 comprises of a critical analysis of the passive hybrid system under different drive cycles and the carbon footprint for the passive hybrid H2EV.

8.2 Battery and fuel cell selection methodology

Battery and fuel cell sizing is a crucial step for the design of passive hybrid systems. This section proposes a set of rules to select the most optimum combination of cell sizes and battery sizes. These rules can be adapted to different battery technologies and are demonstrated for lithium, lead-acid and NiMH battery technologies. Having described the rule, the subsequent subsection describes the constraints associated with the vehicle under consideration. The model developed in Chapter 3 is then used to simulate a reference system for different drive cycles. The data gathered in the simulation studies are then exploited, and the voltage current curves, for different battery technologies, are used to select candidate fuel cell battery size combinations. Finally, a simulation study demonstrates the application of these rules for the purpose of optimum sizing to save weight on the vehicle.

The following methodology and rules are proposed

1. Determine the fuel cell stack power and battery power required to meet the power demand for the vehicle and its typical journeys.

a) Determine the vehicle characteristics including passenger load.

b) Use a powertrain model to analyse the target drive cycle and determine the maximum speed and acceleration to calculate the peak power demand, and range based on the Microcab H2EV vehicle.

c) Determine the requirements (weight, volume, downsizing, upsizing) in the vehicle for battery and fuel cell stacks.

2. Make use of the fuel cell and battery combination map in Figure 8-1, Figure 8-6 and Figure 8-8 to:

a) Check that the maximum fuel cell voltage is higher than the battery open-

circuit voltage to identify possible combinations. Fuel cell stack can continually charge battery without DC-DC converter when stack voltage is higher than battery open circuit voltage.

b) Check that the battery voltage curve is always higher than the fuel cell stack voltage at the maximum current point (75A for Ballard.) Fuel cell voltage is lowest at maximum current point, at this moment the battery help fuel cell supply power to load to ensure the safety of fuel cell stack. In passive hybrid system, battery voltage and fuel cell voltage are same when they are in parallel circuit. Therefore, the battery voltage should higher than the lowest fuel cell voltage to prevent accident.

c) Determine the overlap point between the fuel cell and the battery. This is the threshold point which is the turning point of the battery charge/discharge.

d) Make full use of the fuel cell curve before the maximum current point (dashed line) and the overlap point, leading to the maximum performance for the fuel cell stack. At the maximum current point, the battery pack will help fuel cell to supply energy to the load.

3. Simulate, using the reference electrical power train, pertinent drive cycles such as UDC, Artemis-urban, JC08 as well as more demanding drive cycles to investigate the performance of the vehicle for extreme cases based on its expected usage, e.g. FTP-75 and WLTP2.

a) Record the simulated fuel cell peak power, the power at idle and the average power output for different drive cycles.

b) Identify areas of improvement in terms of hydrogen fuel economy and carbon footprint.

As the rules are presented, the following sections will demonstrate how to use these rules to select a downsized passive hybrid system for H2EVs

8.3 Passive hybrid H2EV target drive cycles

An important consideration in BEVs or H2EVs is to increase the range of use for the passive hybrid powertrain. Chapter 6 showed the passive hybrid FCEV is more sensitive to a high speed drive cycle than the active hybrid FCEV. The main characteristics of the H2EV vehicle, designed for urban use, were given in Table 3-1. Therefore, different drive cycles such as Artemis-urban, JC08. FTP-75 and WLTP2 are selected to probe the limits of downsizing the passive system. After selecting the drive cycles of the H2EV, the peak power demand can be measured by the modelling. According to rule 1b, FTP-75, as the most aggressive drive cycle, required a peak load power of 24.27kW. The aim is to determine the most cost-efficient system with the smallest possible battery and fuel cell sizes that still meet the operating demands of the vehicle. In order to provide peak power to the load, the lower limit of cell numbers for three battery packs are: lithium battery - 20 cells for each group, lead-acid battery size is limited to 31 cells for each group and NiMH battery size is limited to 60 cells for each group.

The next section will explain the fuel cell and battery selection based on the hybrid combination maps.

8.4 Fuel cell and battery selection based on hybrid combination map

Having limited the range of power required to be delivered by the fuel cell and the battery based on the vehicle used and the expected journey, this section determines suitable combinations based on voltage-current curves for three different battery technologies.

8.4.1 Rule verification for lithium batteries and fuel cell selection

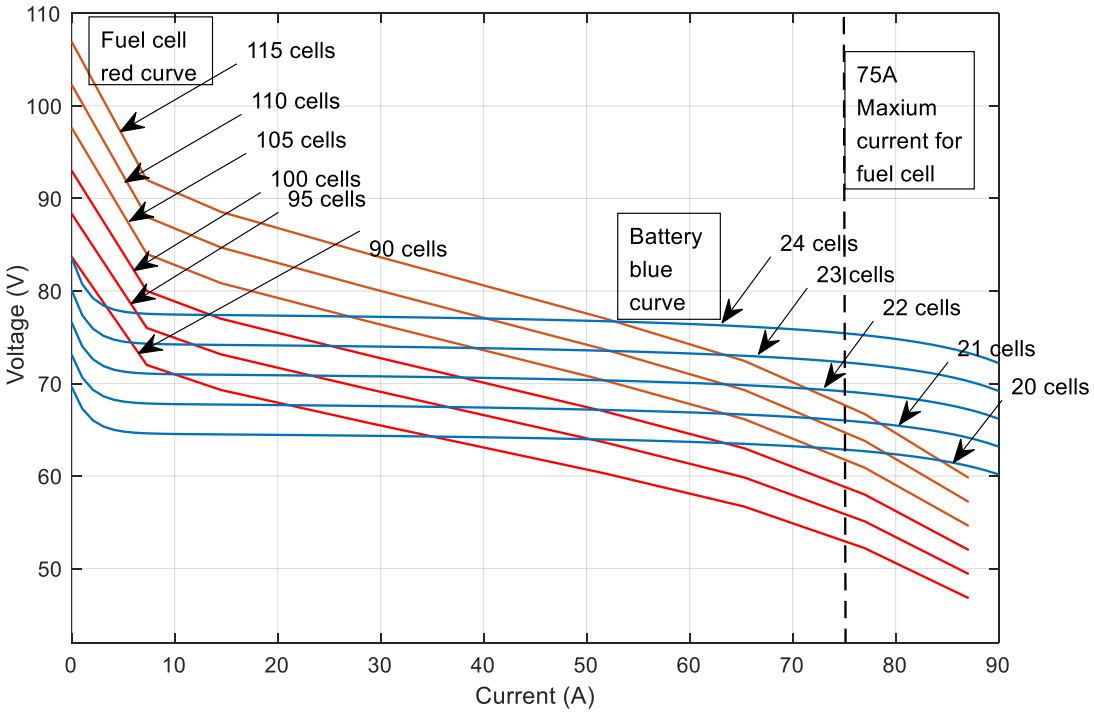

Figure 8-1 Number of fuel cells (red) and lithium battery cells (blue) in the passive hybrid system

As an example, if the 20-cell lithium battery is used in a passive hybrid system, according to rules 2a and 2b, 90 to 105 fuel cells can be selected for the system. Following the rule 2d, a 105-fuel-cell-stack will provide the best performance

for the system. Figure 8-2 shows the comparison for an FCEV passive hybrid system, under a UDC drive cycle, equipped with 100, 105 or 110 fuel cells. It can be seen that when the vehicle load increases, passive hybrid system fuel cell power responds the increased power demand. The 100-cell fuel cell and 105-cell fuel cell can work appropriately for the hybrid system. The 105-cell stack provides 7.7% more power to the system compared to the 100-cell stack. The 110-cell fuel cell stack, as a negative example, is not following the selection rule 2b. It can be seen that the stack is not able to supply a constant power to the system, with the stack power dropping sharply at 0s, 20s, 60s and 140s. Figure 8-3 shows the 110-cell fuel cell stack and 20-cell battery voltage in a passive hybrid system. The UDC drive cycle has a higher speed at 20s, 60s, and 140s periods, and the vehicle needs higher power when it starts. Therefore, during these periods the battery and fuel cell both supply power to the system. In the passive hybrid system, the fuel cell and battery are operating at the same voltage. The voltage at the peak power point for the 110-cell fuel cell stack is 63.8V when the battery voltage is lower than 63.8V. The fuel cell stack cannot exceed its limit to provide the same voltage to the system. As a result, the 105-cell fuel cell stack that satisfies the rules shows the best performance in this test.

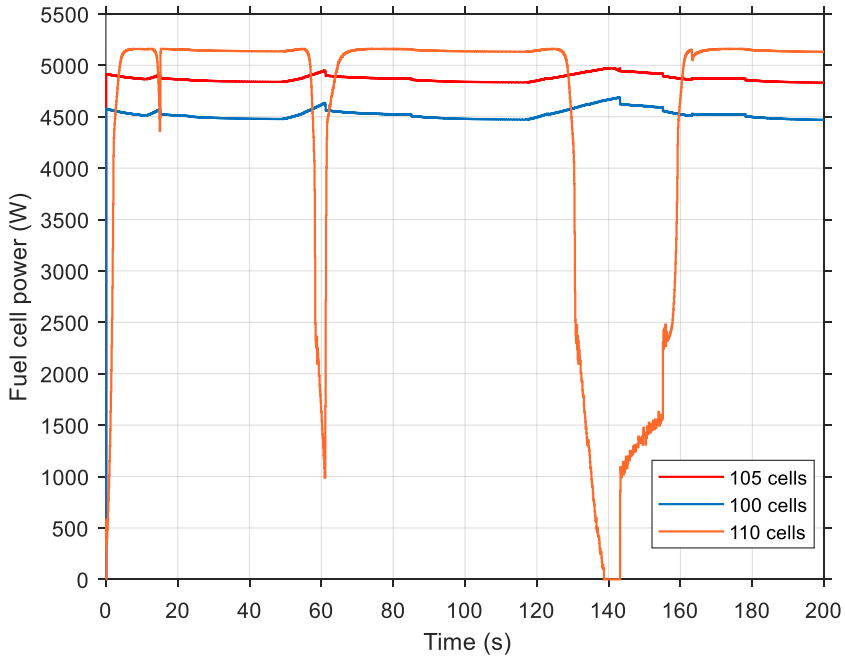

Figure 8-2 Comparison of 100-cell, 105-cell and 110-cell fuel cell stack with 20 cell lithium battery in the passive hybrid system

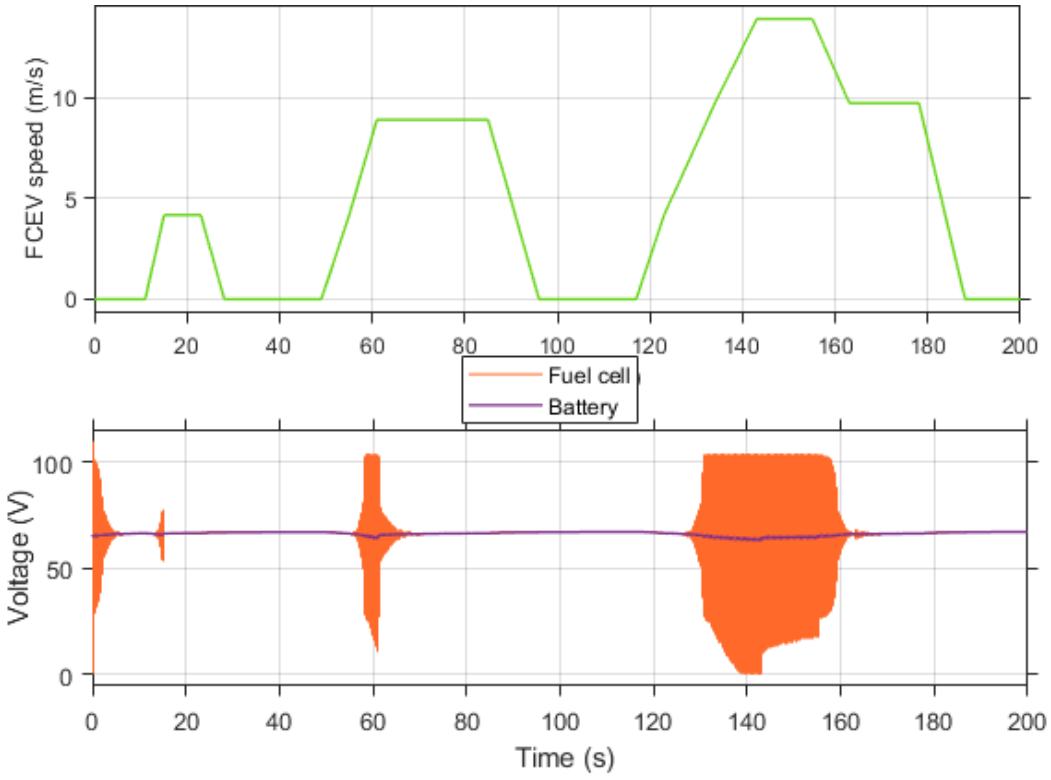

Figure 8-3 110-20 cells passive hybrid system voltage under UDC driving cycle

In previous chapters, the 100-cells PEMFC and 24-cell lithium battery are selected for the passive hybrid system. According to the selection guidelines, a 100-cell PEMFC could exhibit better performance when combined with a 20-cell lithium battery. Figure 8-4 shows the different numbers of lithium battery cells combined with a 100-cell PEMFC in the passive hybrid system. The test is under four UDC drive cycles with a battery at 70% SoC level. The average power for the 20-cell combination is 4498W, which is close to the maximum power of the stack. However, the average power of a 24-cell combinations is 1311W lower than the 20-cell combination. The standard deviation of the 20-cell combination and the 24-cell combination is 76.45 and 100.1, respectively. The PEMFC with the 20-cell combination is able to continually output the maximum fuel cell power, resulting in a smoother power curve than the 24-cell combination. Therefore, downsizing the fuel cell stack or the battery pack is possible for the passive hybrid system.

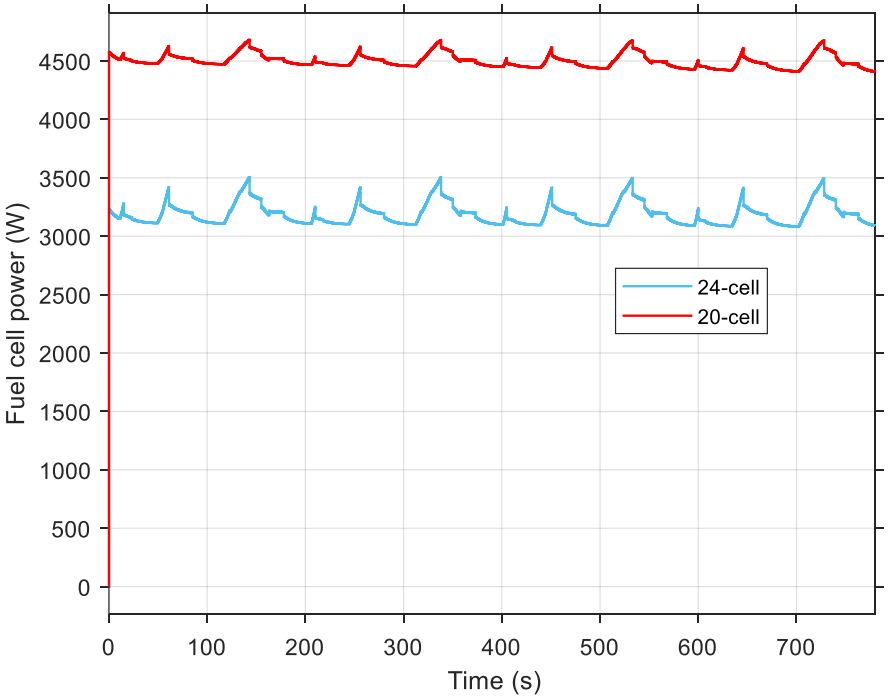

Figure 8-4 100-cell PEMFC combinate with 20-cell and 24-cell lithium battery in the passive hybrid system

A further simulation for selecting fuel cell stack and battery pack size was designed and conducted. A combination of 100-cell PEMFC and 24-cell lithium battery pack was replaced by the combination of 95-cell PEMFC and 20-cell lithium battery pack. Figure 8-5 shows the stack performance for a passive hybrid FCEV with different stack and battery pack sizes under the UDC drive cycles. Downsizing the passive hybrid system could increase performance by 22.05% and improve the stability of the stack by 16%. Downsizing has the additional advantage of reducing the weight of the vehicle by 8.32kg. However, the new combination cannot satisfy the peak load for the drive cycle and is only suitable for lighter vehicle or more gentle drive cycles. Thus, when the passive hybrid system is able to meet the power requirements for load cycles, an optimal combination of the stack and battery pack can significantly increase the passive hybrid FCEV efficiency as well as reduce the cost.

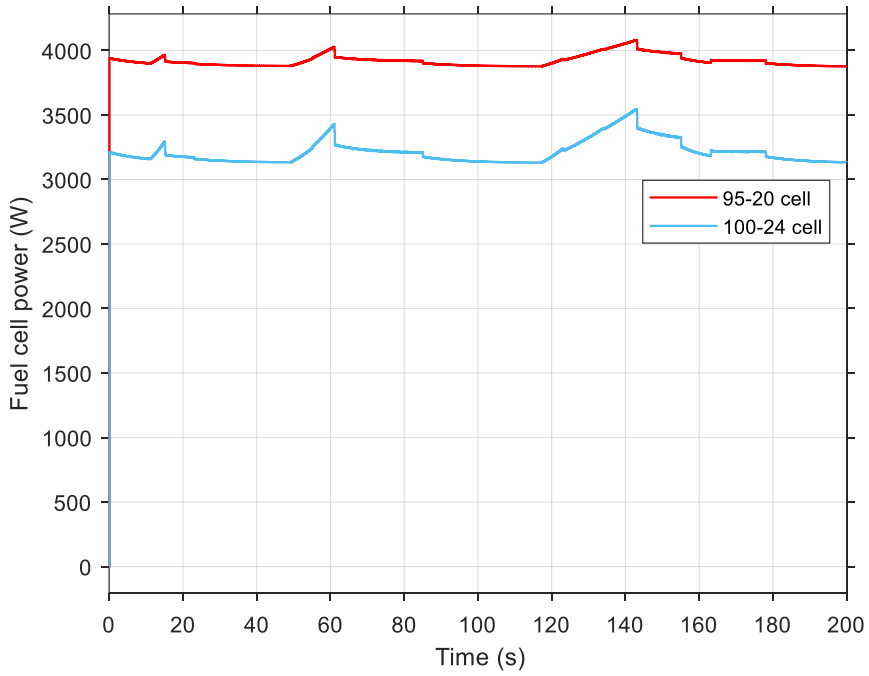

Figure 8-5 Comparison of 100-cell PEMFC combined with a 24-cell lithium battery, and a 95-cell PEMFC combined with 20-cell lithium battery in the passive hybrid system

8.4.2 Rules verification for lead-acid batteries and fuel cell selection

The same rules apply for fuel cell and lead-acid battery passive hybrid systems. Figure 8-6 shows the number of cells for a lead-acid battery and fuel cells for the passive hybrid H2EV.

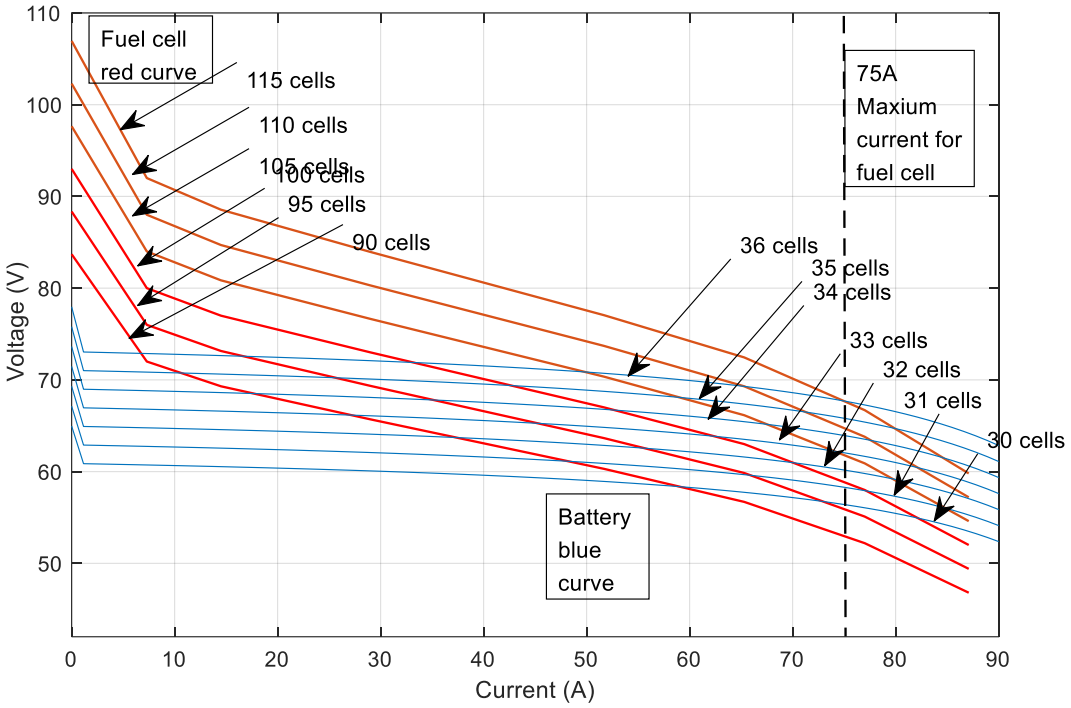

Figure 8-6 Number of fuel cells (red) and lead-acid battery cells (blue) in a passive hybrid system

For a 100-cells fuel cell, the peak power point for the stack is 58V. As the rules 2a and 2b recommend, 31 to 36 cells of a lead-acid battery are acceptable for the system. Within the rule 2d, a 31-cell lead-acid battery is assumed the perfect choice for the system. Figure 8-7 depicts the three combinations for the 100-cell fuel cell under UDC drive cycle at a battery 70% SoC level. In the 31-cell and 32-cell lead-acid battery systems, the fuel cell operates well. The

PEMFC of a 31-cell battery passive hybrid system provides more power (1.22%) compared to the PEMFC of the 32-cell battery passive hybrid system. Furthermore, the fluctuation of the power curve is reduced by 39.84% compared to the 36-cell battery passive hybrid system. As section 8.3 expected, the 30-cell lead-acid battery is below the lower limit of the passive hybrid system. Therefore, excessive low battery voltage caused fuel cell behaviour disorders in the 30-cell lead-acid battery passive hybrid system. The 31-cell lead-acid battery meets the assumptions that the rules expect. Hence, the selection rules are working correctly for a lead-acid battery.

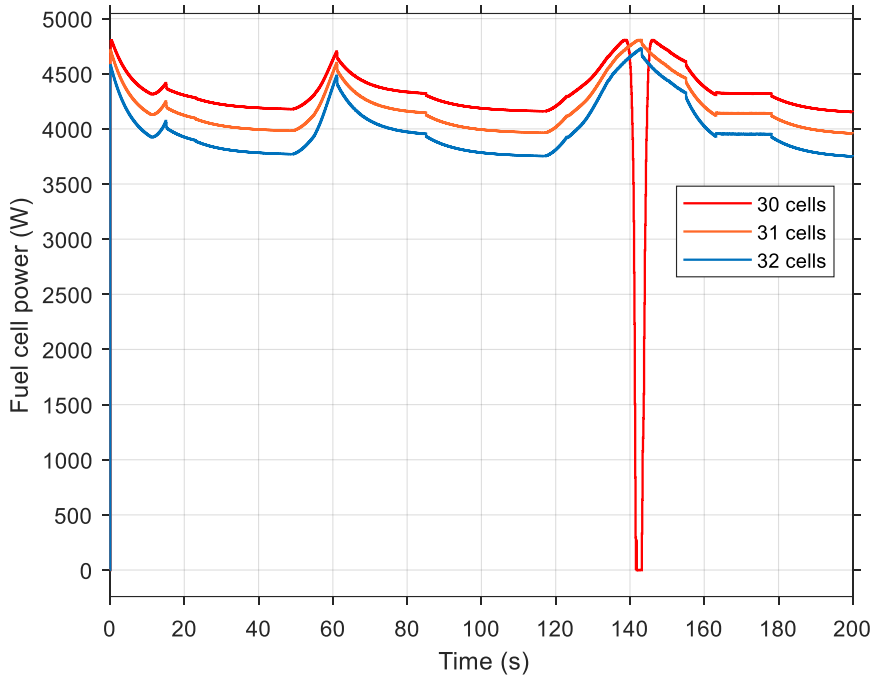

Figure 8-7 Comparison of 30-cell, 31-cell and 32-cell lead-acid batteries with a 100-cell fuel cell stack in the passive hybrid system

8.4.3 Rules verification for Ni-MH batteries and fuel cell selection

Figure 8-8 shows the characteristic voltage curves for Ni-MH batteries and fuel cell stacks. For example, a 110-cell fuel cell stack needs an appropriate Ni-MH battery pack. According to rules 2a and 2b, all battery packs from 60 to 72 cells can satisfy the requirement. Figure 8-9 shows that the combination of a 60-cell Ni-MH battery and a 110-cell fuel stack can supply more power to the system, meeting the requirement of rule 2d. For a 60-cell hybrid system, the performance increased by about 5.12% compared to a 64-cell hybrid system. Also, the stability of the fuel cell power curve increased by 23.63% and the power increased from 2932W to 4176W compared to the 72-cell system.

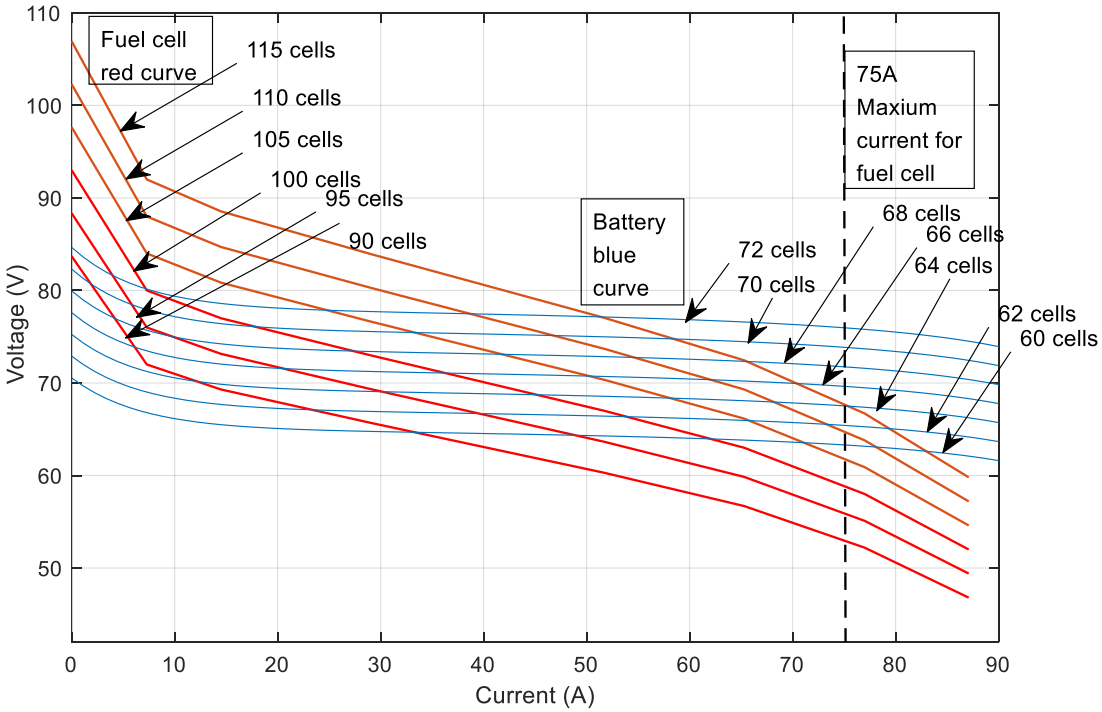

Figure 8-8 Number of fuel cells (red) and Ni-MH battery cells (blue) in passive hybrid system

Therefore, there is no need to increase the battery size to gain more energy from the fuel cell, resulting in saving space, weight and cost for the FCEV. The results demonstrate that the proposed rules lead to an appropriate combination of Ni-MH battery for a passive system.

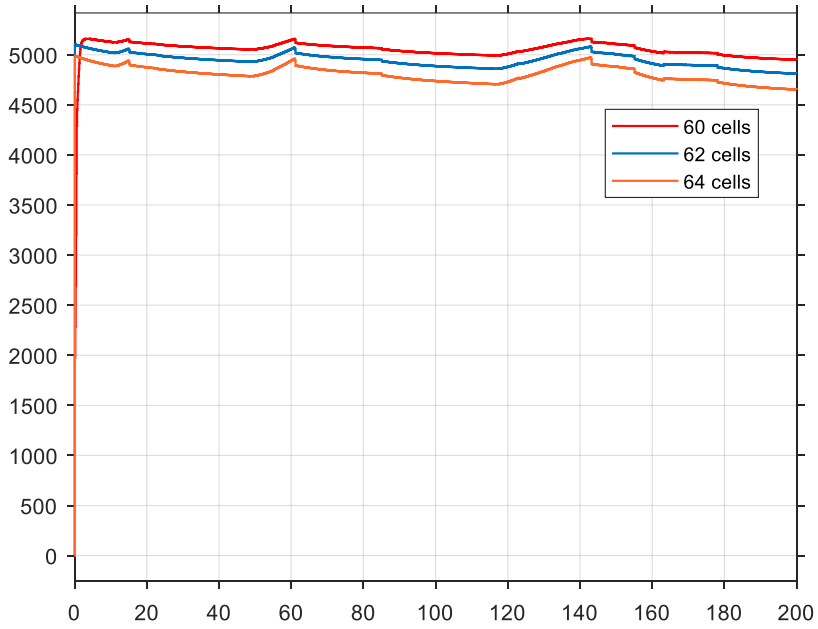

Figure 8-9 Comparison of 60-cell, 62-cell and 64-cell lead-acid batteries with a 110-cell fuel cell stack in the passive hybrid system

The selection rules have been validated by simulation results for the most commonly used batteries. Analysis of different batteries that are used in the passive hybrid system shows that fuel cell and battery sizing have a significant impact on fuel cell performance and safety. Downsizing the passive hybrid system is able to provide better performance than a larger system.

It becomes apparent that the optimal selection is dependent on the drive cycle and the energy management strategies. For urban drive cycles, the downsizing combination of a 95-cell PEMFC and a 20-cell lithium battery pack was selected for the Microcab H2EV. Further investigations on the third part of the methodology are discussed in the next section.

8.5 Evaluation of downsizing the passive hybrid system under urban drive cycles

According to the methodology in the first two sections, downsizing the passive hybrid system to a 95-cell PEMFC and a 20-cell lithium battery pack was selected to satisfy the power demand of urban drive cycles. Therefore, the proposed passive hybrid system will be tested under different target drive cycles to analyse its performance.

8.5.1 Worldwide Harmonised Light Vehicles Test Procedure

According to the Vehicle Certification Agency (2020), the NEDC is gradually being replaced by the new Worldwide Harmonised Light Vehicle Test Procedure (WLTP). The new driving cycle is aimed to provide a more realistic performance for vehicles. Due to the fact that Micro-cab is categorized as a low-powered FCEV, WLTP2 is suitable for this test. The WLTP2 driving cycle has three phases: the low phase of the first 3131m at an average speed of 51.4km/h, the medium phase distance is 4712m with a higher average speed by 44.1km/h and the high phase has the maximum speed of 85.2km/h to cover the remaining 6820m. Figure 8-10 shows the PEMFC performance under the WLTP2 drive cycle. It can be seen that the PEMFC is operating around the average power of 3951W. In the latest realistic driving cycle, the downsized passive hybrid system still provided a stable performance.

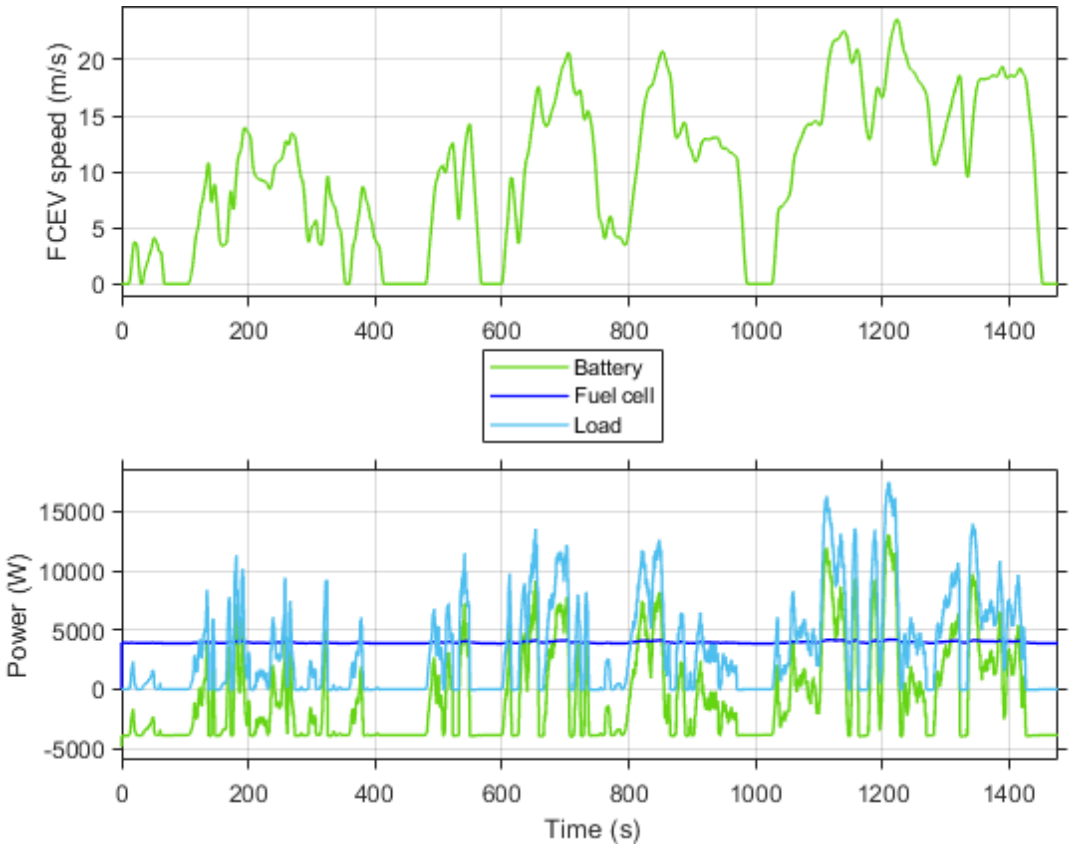

Figure 8-10 Passive hybrid system performance under the WLTP2 drive cycle

8.5.2 ARTEMIS urban European drive cycles

The ARTEMIS urban driving cycle represents urban driving conditions including urban dense, free-flow urban, congested stops, congested with low speed and flowing stable (André 2004). The drive cycle covers 4874m distance with 1.72 stops/km. This driving cycle is used to analyse the frequent stops effect on passive hybrid system performance. It can be seen in Figure 8-11, while the car is stopped frequently and various speeds are changed, the maximum and average speed is lower than the WLTP2 drive cycle, but maximum acceleration and deceleration speed is 2.861 m/s^2 and -3.139 m/s^2 which is much higher than the WLTP2 drive cycle. As a result, the peak load of the FCEV is 22.9% higher than the WLTP2 drive cycle. In this stricter condition, the fuel cell still has a stable output power of 3928W.

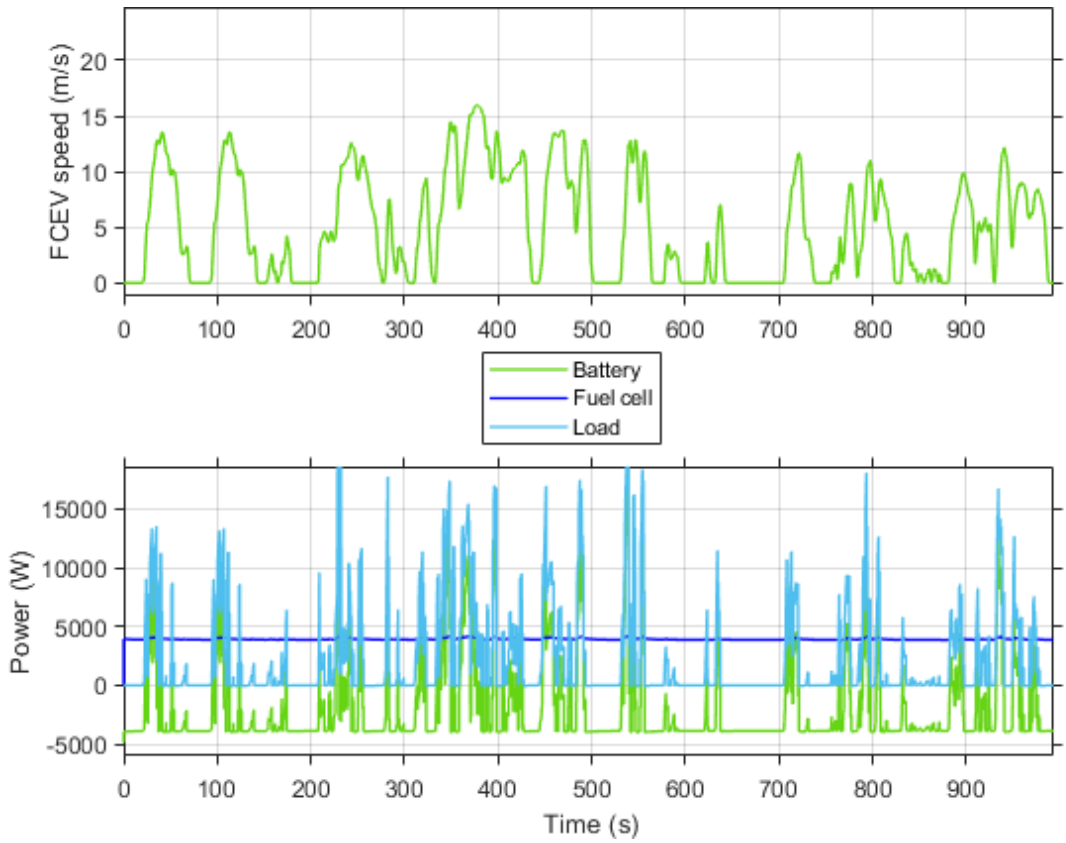

Figure 8-11 Passive hybrid system performance under ARTEMIS urban drive cycle

8.5.3 FTP-75 drive cycle

FTP-75 (Federal Test Procedure) is an American driving cycle for light-duty vehicles, it is also known as ADR 37 (Australian Design Rules) cycle in Australia (Crolla 2014). The overall driving cycle duration is 1877s and distance travelled 17.77km, with a more aggressive maximum speed of 91.25km/h. It consists of four phases: a cold start transient phase lasting 505s, a stabilized phase from 506s to 1372s, a hot soak phase to see what happens when the engine is turned off, and the hot start phase to cover the additional 505s after being stopped for 10 minutes. The long idling time of the drive cycle could simulate the passive hybrid FCEV performance during the idling situation. Figure 8-12 shows the passive hybrid system performance. The stack average power is 3935W during the 1877s travelled. In the idling condition the fuel cell provided an average 3844W power, which is slightly lower than the average power.

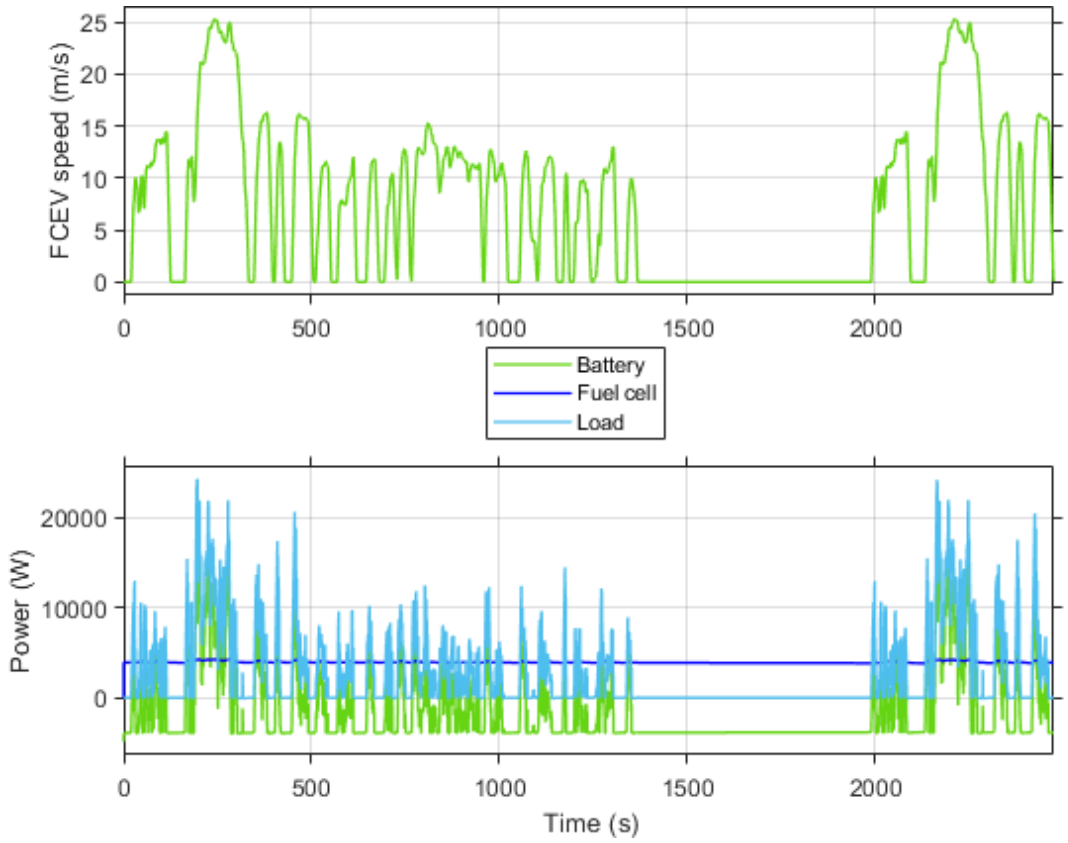

Figure 8-12 Passive hybrid system performance under the FTP-75 drive cycle

8.5.4 Japanese JC08 Cycle

As Europeans use WLTP to replace NEDC, the drive cycle in Japan also moves with the times. Jap 10-15 mode was used for testing the vehicle with a hot start and a maximum 70km/h speed. The new JC08 cycle consist of 300s of JC08 cold start and 900s of JC08 hot start with a top speed 81.6 km/h. The cycle represents typically congested urban traffic in Japan. Figure 8-13 shows passive hybrid system performance under the JC08 drive cycle. The stack provides a relatively stable power of around 3901W.

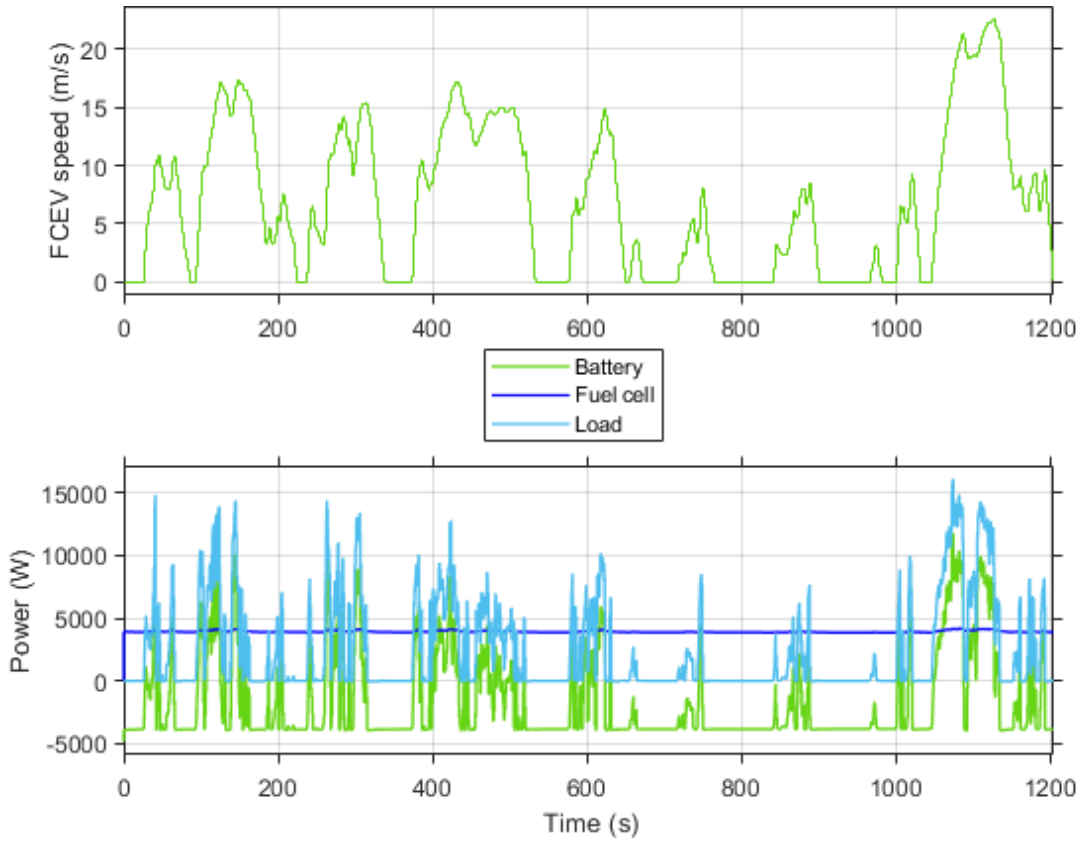

Figure 8-13 Passive hybrid system performance under JC08 drive cycle

8.6 Discussion and analysis

8.6.1 Drive cycle analysis

Table 8-1 Main parameters of urban drive cycles

	WLTP2	Artemis-urban	FTP-75	JC08	4*UDC
Total time (s)	1477	993	1877	1204	780
Total distance (m)	14664	4869.8	17769.4	8172	3976.4
Average speed (km/h)	35.7	17.65	34.08	24.4	18.35
Maximum speed (km/h)	85.2	57.70	91.25	81.6	50
Maximum acceleration (m/s2)	0.8	2.861	1.475	1.69	0.599
Maximum deceleration (m/s2)	-1.1	-3.139	-1.475	- 1.69	1.042
Stops/km	1.87	2.87	1.07	1.22	3.01
Idling time (s)	240	260	338+600	326	228
Average stack power (W)	3951	3928	3935	3901	3909
Average stack power at idling (W)	3862	3863	3844	3862	3864
Fuel cell power output fluctuation (standard deviation)	85.42	75.13	95.2	80.68	64.27
Vehicle load power usage (kJ)	4860.8	2183.6	6954.4	2870	1223.8
Peak load (W)	17463	21462	24265	16144	10420

Table 8-1 and Figure 8-14 show the fuel cell stack performance comparison between different drive cycles. It can be seen that fewer high load power supply from fuel cell stack would reduce the instability of the passive hybrid system. The downsized passive hybrid system has a lower hydrogen consumption of 7.3g/km compared to a 100-24 cell combination of 9.73g/km and provides more average power to the system. The 95-20 cell combination selected by the design methodology is more suitable for urban drive cycles. The results again proved the correctness of the selection methodology.

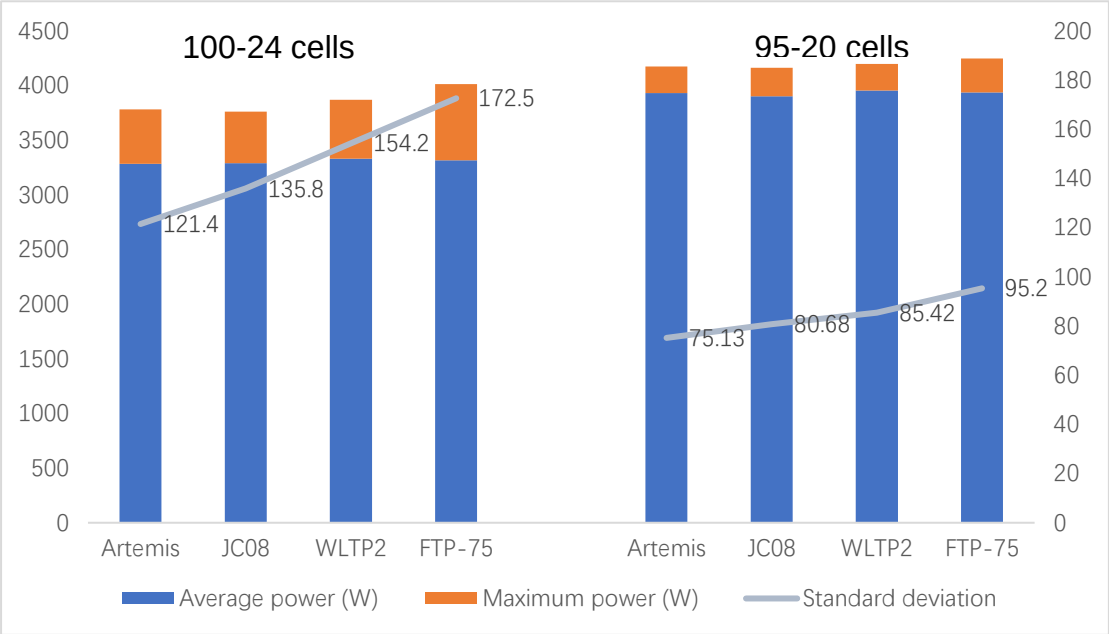

Figure 8-14 Fuel cell stack performance of two passive hybrid systems under different drive cycles

Table 8-1 also summarises the main parameters of urban drive cycles and allows analysis of the fuel cell curve. It is necessary to analyse the drive cycles to identify the effect for the passive hybrid system. It can be seen for the optimal passive hybrid system; the fuel cell stack average power is very close under four drive cycles. The main differences between different drive cycles are maximum power and stability.

In the case of the FTP-75 drive cycle, because of a long idling time and maximum speed of the driving cycle, the fluctuation of fuel cell power is most obvious. The same trend can be observed in the other drive cycles, when the maximum speed of the WLTP2 drive cycle is higher than the JC08 drive cycle, and the stack power stability is reduced by 5.32%. When maximum acceleration and deceleration speed, and stops are then considered, the Artemis-urban drive cycle required the most stops with the highest maximum acceleration and deceleration speed. It can be seen that the passive hybrid system works most stably under the Artemis-urban drive cycle. High transient power demand is satisfied by the lithium battery; therefore, the fuel cell stack can provide relatively stable power to the system. In the other drive cycles, the fuel cell stack needs to meet the higher load requirements due to the higher maximum speed. The results from the WLTP2 and JC08 drive cycles also show similar trends. By contrast, the JC08 drive cycle with lower maximum speed and higher maximum acceleration and deceleration resulted in a more stable power curve of the fuel cell stack. Thus, the parameter analysis of the drive cycles for the passive hybrid FCEV can be arranged Figure 8-15.

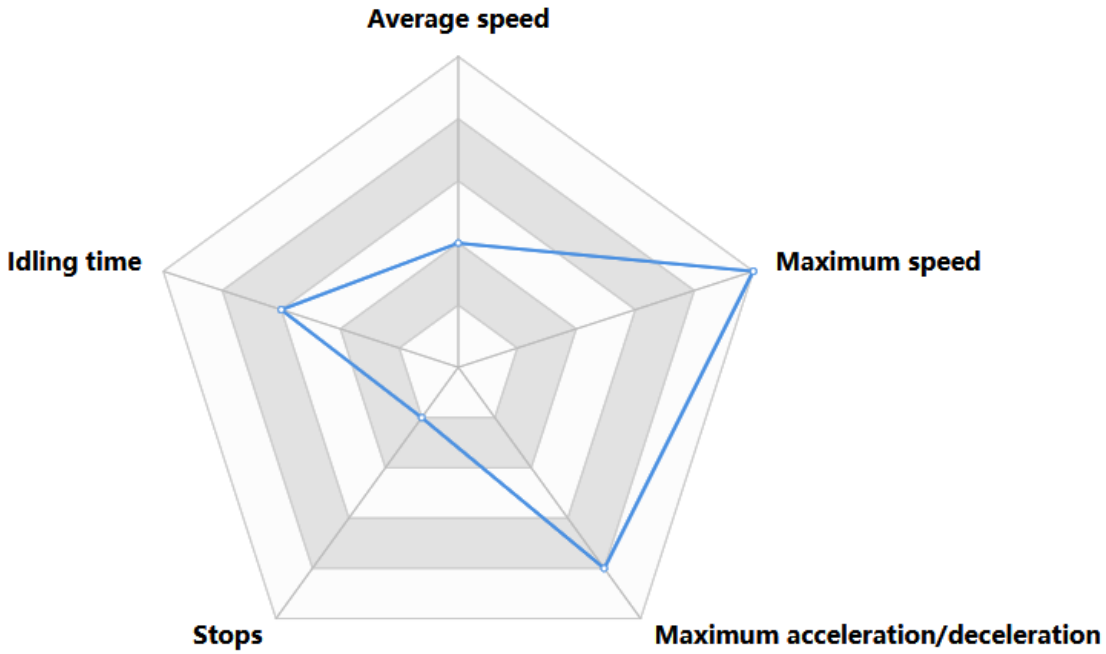

Figure 8-15 Sensitivity of passive hybrid system to drive cycles

8.6.2 Well-to-wheel analysis

Moreover, detailed carbon footprint analysis for the passive hybrid FCEV gives a clear picture of fuel economy compared with the other vehicle. Whilst the optimal hydrogen economy of the passive hybrid H2EV is available, it is possible to provide a life cycle GHG emission analysis of H2EV.

Natural gas reforming is the most common method for hydrogen production – the GHG emission is between 7399.26g to 10832.25g CO_2/kg H_2 without CCS technology, and for the GHG emission form wind turbines it significantly reduces to 970 g CO_2/kg H_2 (BEIS 2019). For compressed hydrogen 100km road transportation reports emission of about 926.90 g CO_2/kg H_2 (Ramsden et al 2013). For the Microcab H2EV, the hydrogen tank storage pressure is 350 bar, and the compression efficiency for hydrogen storage is 87% (Ryan et al. 2014). The average GHG emission of hydrogen production from natural gas reforming with 100km road transportation is 10042.66g CO_2/kg H_2 and GHG

emission from wind turbine with 100km road transport is 1896.90 g CO_2/kg H_2. Then the WTW GHG emissions of passive hybrid H2EV are calculated as 84.27 g CO_2/km (natural gas) and 15.92 g CO_2/km (wind turbine).

Therefore, the carbon footprint of the passive hybrid H2EV with different powertrains is shown in Figure 8-16, vehicle data from EERE (2016). As excepted, ICE and ICE hybrid vehicles emit more CO_2 than ZEVs. The FCEV and BEV emit similar CO_2 because current commercial FCEVs require a larger car body to house the complicated powertrain. The Microcab passive H2EV is a lightweight FCEV. With its simpler powertrain it emits lower CO_2, and has a higher energy efficiency. In addition, when considering the hydrogen production method, wind power produces a much lower carbon footprint than that of natural gas. Half of the CO_2 is produced by road transportation when wind turbines are the energy source used to produce hydrogen. It can be predicted that renewable energy will play a major part in hydrogen production in the future, resulting in less GHG emission for FCEVs.

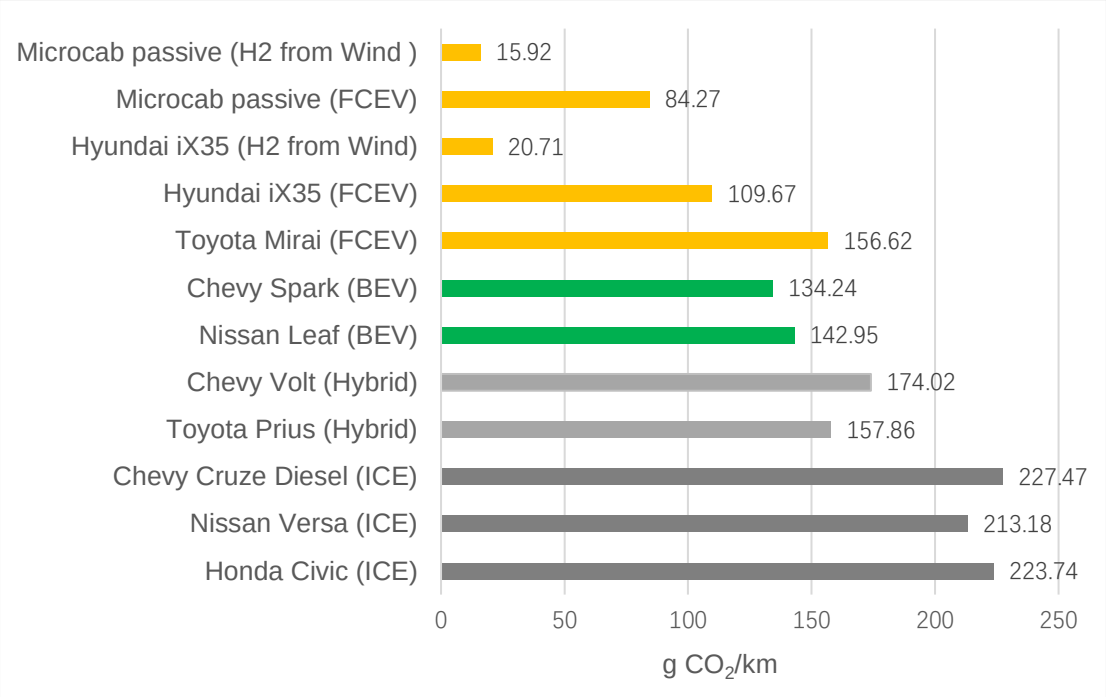

Figure 8-16 WTW emission for different vehicles

8.7 Conclusion

This chapter established the passive hybrid design methodology for the H2EV. With appropriate sizing of the fuel cell and batteries, the passive hybrid system offers some flexibility for saving space, weight and cost for the FCEV. At the same time, improving the FCEV drive range and system stability.

The results suggest that using the maximum power of the fuel cell stack reduces the robustness of the system. From the perspective of safety and risk concerns, the lowest operating voltage of the battery pack needs to be carefully considered for the passive hybrid system.

It was also found that the battery capacity is irrelevant to hybridization performance, and it is convenient to add additional battery cells in parallel to increase the operating time of the PMEFC. However, adding batteries increases FCEV weight.

From analysis of different drive cycles, it can be found that the stability of passive hybrid FCEVs is significantly influenced by the maximum speed of the drive cycle, and less affected by the stops, average speed, acceleration and deceleration. Drive cycles categorised as urban and rural drive cycles are most suitable for passive hybrid FCEVs. However, the effect of fuel cell degradation under aggressive rural and highway drive cycles needs to be carefully considered in future road tests.

Based on the selection methodology, an optimised passive hybrid is applicable for typical urban drive cycles with similar average output power and reduced hydrogen consumption. The WTW GHG emission results showed the Microcab passive hybrid H2EV as a lightweight passenger vehicle, has the lowest carbon

footprint which is more likely to realise the goal of ‘net-zero’ GHG in the UK by 2050.

Chapter 9: Conclusions and future works

This thesis aimed to investigate the suitability of passive hybrid FCEV powertrain for the Coventry University Microcab H2EV (Hydrogen Electric Vehicle). The work has resulted in a number of original contributions which are presented in the conclusions together with the findings from this work. The areas of further work identified are then presented.

9.1 Conclusions

The academic literature review has shown the state of art of ZEVs and related technologies. The review identified that the main BEV limitations were the range and raw material availability to manufacture large battery packs on the scale that is required. The main FCEV limitations were the limited hydrogen infrastructure and distribution network as well as the high purchase cost. Latest fuel cell and ESS technologies whilst improving, still require further developments. An alternative to the traditional BEV, which can enable an increase to the drive range and speed of charge is the FCEV. For example a FCEV can charge in 5-10 min whereas am EV needs more than 45 min. Having identified the purchase cost as a barrier to adoption of FCEVs, this work aims to reduce their costs and increase their overall powertrain efficiency through the development of passive hybridization. In particular, the Microcab H2EV can save £800 for DC-DC converter. The fuzzy controller, in addition to reducing hydrogen consumption, can extend fuel cell and battery life and therefore reduce future replacement cost of fuel cell stack and battery pack. The rules developed to select the components can reduce the size of passive hybrid system, whereas a reduction from 120 cells to 100cells can save £453 for the FCEV stack.

An original passive hybrid FCEV powertrain model has been developed that allowed the simulation of different FCEV architectures under urban, highway and user-defined drive cycles. The model was validated against experimental data for both active and passive hybrid systems. The good agreement between experimental data and simulation provided the confidence to apply this model to develop an original power management system and evaluate various battery and fuel cell combination for an urban FCEV. This model has been developed using the MATLAB®/Simulink® environment and is therefore well suited to be shared with the academic community.

Direct passive hybridization between fuel cell and lithium battery exhibits an extended drive range whilst keeping the fuel cell average power to a similar level than the active system. This is achieved by allowing the fuel cell power to respond to small changes in electrical load demand. The simulation results indicated that passive hybrid systems are able to provide a simpler system with longer drive range and lower cost.

As the process parameters of the PEMFC are analysed in the sensitivity test. Using the powertrain model, a fuzzy management strategy is designed for the passive hybrid to control the power flow between fuel cells and ESS by modulating the hydrogen pressure. With the fuzzy controller, the passive system can satisfy the load of FCEV while reducing the number of fuel cell start-stop times and extending the overall range.

The parameters of the PEMFC were analysed in the sensitivity test. It was found that the most significant control variables were the fuel cell pressure and the fuel flow rate. The air pressure and air flow rate were less significant in terms of enabling an efficient load output variation. To keep the control system as simple as possible, only the most significant variable was selected as the

control variable, namely the hydrogen pressure.

The aim of the controller is to enable the fuel cell to charge the battery if it is required and complement the battery to provide the required load when the battery is at maximum output power. The battery state of charge and fuel cell power output were used as input to the proposed fuzzy controller to calculate the most appropriate fuel cell pressure and consequently fuel cell output power. This controller was specifically developed for a passive hybrid system to control the power flow between fuel cells and ESS. The fuzzy controller was shown to be able to satisfy the load of the FCEV whilst, at the same time, reducing the number of fuel cell start-stop times and extending the overall range. The reduction in the need to stop and or start the fuel cell should result in significant gains in term of cell life cycle and is expected to compensate for the degradation associated with the higher fuel cell power fluctuation compared to the active hybrid system. The controller was able to extend the range by 27.28% with a about 27% charge speed increase for passive method compared to active method. The passive hybrid Microcab H2EV has 23.16% lower GHG emission than the Hyundai IX35 FCEV.

The current Microcab H2EV utilises a lithium-ion battery. Different battery technologies have been investigated to evaluate potential application areas depending on the size and usage of the vehicle. Considering the lifespan and cost of fuel cell stack, it was found the currently used lithium batteries are well suited to FCEV that operate in an urban environment as the inherent variability of power demands results in less fuel cell power fluctuation than NiMH batteries and lead-acid batteries.

A method for the selection of fuel cell and battery sizes for passive hybrid system was proposed. The application of the rules was demonstrated for

different battery technologies and PEMFC. It was shown that the sizing of battery and fuel cell has a significant impact on the passive system performance. Downsizing of fuel cell stack and battery is possible to exhibit better performance based on the vehicle usage of targeted drive cycles. It was found that the exploitation of the fuel cell stack power curve is a critical selection criteria that is often overlooked.

Analysis of latest urban cycles showed that the proposed passive hybrid system is ideal for urban driving with many stops. The WTW GHG emissions analysis of current vehicles suggests passive hybrid H2EV as a lightweight passenger vehicle which results in lower GHG emissions is more likely to meet 'net zero' target by 2050.

9.2 Future works

The work carried out in this thesis was mostly based on Microcab H2EV. Further modelling and experimental work are listed below:

9.2.1 Simulation work

1. The developed model could add automotive auxiliary systems such as heating and air conditioning system as well as various comfort loads.
2. More accurate models of the power electronic and system components could help design a cost-effective alternative to DCDC converters.
3. The degradation of the battery and the fuel cell model requires further work. The model only considers the operating condition of these devices at the beginning of life. Thus, further improvement and validation of battery and fuel cell life cycle should be done so that it can be included in the controller objectives.

4. Optimisation techniques could be used to evaluate the impact of a potentially large number of parameters affecting the efficient, effective, safe, reliable and robust operation of a passive hybrid system.
5. A simple by design fuzzy control strategy was developed with a manageable number of rules. Further work could include the development of more complex rules or control structure to be able to take into account the additional objectives associated with the optimal performance of the vehicle under different more of operation.
6. Passive hybrid system can be used for a range of vehicles. An identified application area is light-duty automotive applications such as electric mobility scooter. According to National Travel Survey, 56.46% people who have a disability for more than one year stated to have mobility difficulties. The ageing population is increasing the need for practical means of transportation to meet their increased intered in making trips compared to the younger population (Department for Transport 2019). Major cities in the UK have problems of traffic congestions. The use of mobility scooter in place of larger vehicle could help address some of the congestion problems. A market study carried out in (Barton et al. 2014) estimated the annual growth in sales of scooters at approximately 5-10% with the buyers most interested in their range. Currently, commercial electric mobility scooter mainly use lead- acid battery pack as ESS. Because of the limited space for the electric mobility scooter, the driving range is much worse than BEV. Passive hybrid system as a simple and high efficiency system could be integrated within electric mobility scooter.

9.2.2 Experimental work

1. The complete passive hybrid FCEV will be implemented and optimised based on Microcab H2EV.
2. The degradation of different batteries and fuel cell in a passive hybridization

system on FCEV under real drive cycles is worthy of further investigation.

3. Apply the strategy developed to other types of vehicles.

References

Aaron Brooker, Kristina Haraldsson, Terry Hendricks, Valerie Johnson, Kenneth Kelly, Bill Kramer, Tony Markel, Michael O'Keefe, Sam Sprik, Keith Wipke, M.Z. (2013) ADVISOR Advanced Vehicle Simulator [online] available from <http://adv-vehicle-sim.sourceforge.net/> [7 January 2019]

Al-Alawi, B.M. and Bradley, T.H. (2013) 'Total Cost of Ownership, Payback, and Consumer Preference Modeling of Plug-in Hybrid Electric Vehicles'. Applied Energy [online] 103, 488–506. available from < https://doi.org/10.1016/j.apenergy.2012.10.009> [7 August 2019]

André, M. (2004) 'The ARTEMIS European Driving Cycles for Measuring Car Pollutant Emissions'. Science of the Total Environment 334–335, 73–84

Anwar Sattar, David Greenwood, Martin Dowson and Puja Unadkat. (2020) Automotive Lithium ion Battery Recycling in the UK [online] available from < https://warwick.ac.uk/fac/sci/wmg/business/transportelec/22350m_wmg_battery_recycling_report_v7.pdf> [7 January 2021]

APH Community (2018) Is Your Commute Getting Slower? Average Speeds in the UK's Major Cities Revealed for 2017 [online] available from https://www.aph.com/community/holidays/commute-getting-slower-average-speeds-uks-major-cities-revealed-2017/

Apicella, M. (2017) A Multi-Disciplinary Approach to Fuel Cell Vehicle Modelling and Simulation – A Study to Investigate and Optimise Overall Electric Vehicle and Hydrogen Fuel Cell Electric Vehicle Efficiency.

Automotive Council UK. Product Roadmap 2017: Passenger Car. [online] available from https://www.automotivecouncil.co.uk/wp-content/uploads/sites/13/2017/09/Passenger-Car_.jpg [28 December 2017].

AVL (2019) AVL CRUISETM [online] available from <https://www.avl.com/cruise> [7 March 2019]

Azevedo, M. and Hoffman, K. (2018) Mckinsey-Lithium-and-Cobalt-A-Tale-of-Two-Commodities [online] available from <https://www.mckinsey.com/~/media/mckinsey/industries/metals and mining/our insights/lithium and cobalt a tale of two commodities/lithium-and-cobalt-a-tale-of-two-commodities.ashx> [7 August 2019]

Ballarld, Manual, P., and Guide, I. (2011) Putting Fuel Cells to Work FCgen ® -1020ACS Fuel Cell Stack FCvelocity ® -1020ACS Fuel Cell Stack Product Manual and Integration Guide. 5117480

Ballarld, Manual, P., and Guide, I. (2011) Putting Fuel Cells to Work FCgen ® -1020ACS Fuel Cell Stack FCvelocity ® -1020ACS Fuel Cell Stack Product Manual and Integration Guide. 5117480

Ballon, Santos M. Electrovaya (2011) ‘Tata Motors to make electric’ Indica. Cleantech Group. [Online]. Available from: <http://www.cleantech.com>.

Barlow, T., Latham, S., Mccrae, I., and Boulter, P. (2009) ‘A Reference Book of Driving Cycles for Use in the Measurement of Road Vehicle Emissions’. TRL Published Project Report [online] 280. available from http://www.trl.co.uk/online_store/reports_publications/trl_reports/cat_traffic_and_the_environment/report_a_reference_book_of_driving_cycles_for_use_in_t

he_measurement_of_road_vehicle_emissions.htm%5Cnhttps://www.gov.uk/government/uploads/system/uploads/a

Barnes, J.H., Chatterton, T.J., and Longhurst, J.W.S. (2019) 'Emissions vs Exposure: Increasing Injustice from Road Traffic-Related Air Pollution in the United Kingdom'. Transportation Research Part D: Transport and Environment [online] 73, 56–66. available from < https://doi.org/10.1016/j.trd.2019.05.012> [30 July 2019]

Barton, C., Holmes, J., and Jacobs, C. (2014) 'Mobiltiy Scooters: A Market Study'. Research Institue for Consumer Affairs [online] (May), 1–41. available from https://www.gov.uk/government/uploads/system/uploads/attachment_data/file/362989/Rica_Mobility_scooter_market_study_final.pdf

Bernard, J., Hofer, M., Hannesen, U., Toth, A., Tsukada, A., Büchi, F.N., and Dietrich, P. (2011) 'Fuel Cell/Battery Passive Hybrid Power Source for Electric Powertrains'. Journal of Power Sources [online] 196 (14), 5867–5872. available from < https://doi.org/10.1016/j.jpowsour.2011.03.015> [28 October 2019]

Bernard, J., Hofer, M., Hannesen, U., Toth, A., Tsukada, A., Büchi, F.N., and Dietrich, P. (2011) 'Fuel Cell/Battery Passive Hybrid Power Source for Electric Powertrains'. Journal of Power Sources [online] 196 (14), 5867–5872. available from < https://doi.org/10.1016/j.jpowsour.2011.03.015> [28 October 2019]

BLOOMBERG (2017) Toyota Targets 1,000-Km Driving Range with Fuel Cell Concept Car [online] available from <https://www.japantimes.co.jp/news/2017/10/18/business/corporate-business/toyota-targets-1000-km-driving-range-fuel-cell-concept-

car/#.XIopaEJKiUk> [7 August 2019]

BMW (2019) BMW I3 and I3s | New Vehicles | BMW UK [online] available from <https://www.bmw.co.uk/bmw-cars/bmw-i/2018-i3-and-i3s?gclid=Cj0KCQiArenfBRCoARIsAFc1FqforYlMbfaw-eV39IF4OF2A0fQ6X-dhPtKoXphBnmmUAunbUk9eF2QaAiNnEALw_wcB&gclsrc=aw.ds/> [7 January 2019]

Bolton, P. (2018) Energy Imports and Exports [online] available from <https://researchbriefings.parliament.uk/ResearchBriefing/Summary/SN04046> [4 August 2019]

Brennan, J.W. and Barder, T.E. (2016) Battery Electric Vehicles vs . Internal Combustion Engine Vehicles [online] available from <https://www.adlittle.de/sites/default/files/viewpoints/ADL_BEVs_vs_ICEVs_FINAL_November_292016.pdf> [7 August 2019]

Bridgewater A.V. (2004) 'Biomass fast pyrolysis' Thermal Sci, 8 (2) , pp. 21-49.

Bromaghim, G.; Gibeault, K.; Serfass, J.; Serfass, P.; Wagner, E. Hydrogen and Fuel Cells: The U.S. Market Report, 1st ed.; National Hydrogen Association: Washington, DC, USA, 2010.

Bubeck, S., Tomaschek, J., and Fahl, U. (2016) 'Perspectives of Electric Mobility: Total Cost of Ownership of Electric Vehicles in Germany'. Transport Policy [online] 50, 63–77. available from < https://doi.org/10.1016/j.tranpol.2016.05.012> [9 December 2018]

Bulletin, M. (2017) Commodities Comment The 2017 Battery Metal Story Might

Well Be Cobalt [online] available from <https://www.metalicity.com.au/sites/metalicity.com.au/files/files/MacquarieCommoditiesComment Feb 2017.pdf > [12 May 2019]

Bundesregierung (2016) Weitere Steuervorteile Für Elektroautos [online] available from <https://www.bundesregierung.de/breg-de/aktuelles/weitere-steuervorteile-fuer-elektroautos-454582> [7 February 2019]

Calzavara, Y., Joussot-Dubien, C., Boissonnet, G., and Sarrade, S. (2005) 'Evaluation of Biomass Gasification in Supercritical Water Process for Hydrogen Production'. Energy Conversion and Management 46 (4), 615-631

Carbon Capture& Storage Association (2019) What Is CCS? [online] available from <http://www.ccsassociation.org/what-is-ccs/> [16 August 2019]

Committee on the Medical Effects of Air Pollutants (2018) Associations of Long-Term Average Concentrations of Nitrogen Dioxide with Mortality - A Report by the Committee on the Medical Effects of Air Pollutants.

Copson, M. (2017) Hydrogen in Transport [online] available from <http://www.climate-change-solutions.co.uk/wp-content/uploads/2017/03/Mike-CopsonHFC2017.pdf/> [16 August 2019]

Crolla, D. (2014) Encyclopedia of Automotive Engineering. University of Leeds, UK.: John Wiley & Sons

Das D., Veziroglu T.N. (2001) ‘Hydrogen production by biological processes: A survey of literature’ International Journal of Hydrogen Energy, 26 (1) , pp. 13-28.

Das, H.S., Tan, C.W., and Yatim, A.H.M. (2017) 'Fuel Cell Hybrid Electric Vehicles: A Review on Power Conditioning Units and Topologies'. Renewable and Sustainable Energy Reviews [online] 76, 268–291. available from < https://doi.org/10.1016/j.rser.2017.03.056> [1 November 2018]

Department for Business, Energy & Industrial Strategy （BEIS） (2019) H2 Emission Potential Literature Review.

Department for Transport (2019) National Travel Survey: England 2018 [online] available from <https://assets.publishing.service.gov.uk/government/uploads/system/uploads/attachment_data/file/823068/national-travel-survey-2018.pdf> [6 August 2019]

Department for Transport (2020) Transport Use during the Coronavirus (COVID-19) Pandemic [online] available from https://www.gov.uk/government/statistics/transport-use-during-the-coronavirus-covid-19-pandemic

Department for Transport, Office for Low Emission Vehicles, and M.E.Q.M. (2019) New Requirements for Electric Charge points as Country Moves towards Net Zero [online] available from <https://www.gov.uk/government/news/new-requirements-for-electric-chargepoints-as-country-moves-towards-net-zero> [1 August 2019]

Department for Transport, Office for Low Emission Vehicles, and The Rt Hon John Hayes CBE MP (2017) £23 Million Boost for Hydrogen-Powered Vehicles and Infrastructure [online] available from <https://www.gov.uk/government/news/23-million-boost-for-hydrogen-powered-vehicles-and-infrastructure> [7 August 2019]

Department of Transport, D. (2018) The Road to Zero Nukes [online] available from <https://assets.publishing.service.gov.uk/government/uploads/system/uploads/attachment_data/file/723501/road-to-zero.PDF> [31 July 2019]

Dharmalingam, S., Kugarajah, V., and Sugumar, M. (2019) 'Membranes for Microbial Fuel Cells'. Microbial Electrochemical Technology [online] 143–194. available from < https://doi.org/10.1016/B978-0-444-64052-9.00007-8> [2 April 2020]

Dongxiao Wu, Jin Ren *, Huw Davies and Jinlei Shang (2019) Intelligent Hydrogen Fuel Cell Range Extender for Battery Electric Vehicles. World Electr. Veh. J. 2019, 10(2), 29; https://doi.org/10.3390/wevj10020029.

Elmer, T., Worall, M., Wu, S., and Riffat, S.B. (2015) 'Fuel Cell Technology for Domestic Built Environment Applications: State of-the-Art Review'. Renewable and Sustainable Energy Reviews [online] 42, 913–931. available from < https://doi.org/10.1016/j.rser.2014.10.080> [7 August 2019]

Energy efficiency & renewable energy (2016) : Life-Cycle Greenhouse Gas Emissions and Petroleum Use for Current Cars [online] available from < https://www.hydrogen.energy.gov/pdfs/16004_life-cycle_ghg_oil_use_cars.pdf> [16 August 2019]

Energy efficiency & renewable energy (2017) 'Hydrogen Production and Distribution' [Online]. Available from < http://www.afdc.energy.gov/fuels/hydrogen_production.html/> [12 July 2016]

Energy efficiency & renewable energy (2019) Hydrogen Production: Natural

Gas Reforming [online] available from <https://www.energy.gov/eere/fuelcells/hydrogen-production-natural-gas-reforming> [16 August 2019]

ERTRAC (2018) ERTRAC Roadmaps [online] available from <https://www.ertrac.org/index.php?page=ertrac-roadmap> [7 August 2019]

EUROPA, E.C. (2012) Driving and Parking Patterns of European Car Drivers – a Mobility Survey.

European Commission. Proposal for post-2020 CO2 targets for cars and vans.[online] available form: https://ec.europa.eu/clima/policies/transport/vehicles/proposal_en [22 March 2018].

Everett, T., Ishwaran, M., Ansaloni, G.P., Rubin, A., Price, R., Maguire, S., Dickens, R., Cotterill, A., Connolly, C., Dunn, H., Spencer, C., Harris, R., and Williams, S. (2010) Defra Evidence and Analysis Series Economic Growth and the Environment The Authors Are Grateful to Colleagues in Defra and in Other Government Departments for Their Advice and Support. Particular Thanks Go To [online] available from <https://assets.publishing.service.gov.uk/government/uploads/system/uploads/attachment_data/file/69195/pb13390-economic-growth-100305.pdf> [4 August 2019]

Fletcher, T. and Ebrahimi, K. (2020) ‘The Effect of Fuel Cell and Battery Size on Efficiency and Cell Lifetime for an L7e Fuel Cell Hybrid Vehicle’. Energies 13 (22), 5889

Frano Barbir. PEM Fuel Cells: Theory and Practice. Academic Press, 2005.

Fuel Cell & Hydrogen Energy (2020) Road Map to a US Hydrogen Economy [online] available from < https://researchbriefings.files.parliament.uk/documents/CDP-2020-0172/CDP-2020-0172.pdf/>

GasTerra (2019) Hydrogen and CCS: A Smart Combination [online] available from <https://www.gasterra.nl/en/news/hydrogen-and-ccs-a-smart-combination> [16 August 2019]

Gencoglu, M.T. and Ural, Z. (2009) 'Design of a PEM Fuel Cell System for Residential Application'. International Journal of Hydrogen Energy [online] 34 (12), 5242–5248. available from < https://doi.org/10.1016/j.ijhydene.2008.09.038> [7 August 2019]

Global Energy Metals (2019) Cobalt Demand [online] available from <https://www.globalenergymetals.com/Cobalt/Cobalt-demand/> [7 August 2019]

Goodwolfe. (2019) X2E 15Ah 40166 Cell [online] available from <https://s3-eu-central-1.amazonaws.com/centaur-wp/theengineer/prod/content/uploads/2012/10/15132200/GWEX2E15AhCellTechnicalSpecification.pdf> [5 September 2019]

Government of the United Kingdom (2019) 2018 UK greenhouse gas emissions, final figures Statistical Release: National Statistics [online] available from <https://assets.publishing.service.gov.uk/government/uploads/system/uploads/attachment_data/file/790626/2018-provisional-emissions-statistics-report.pdf>

[26 July 2019]

Green Car Congress (2020) Toyota introduces second-generation Mirai fuel cell electric vehicle as design and technology flagship [online] available from < https://www.greencarcongress.com/2020/12/20201217-mirai.html/>

Grosjean, C., Miranda, P.H., Perrin, M., and Poggi, P. (2012) 'Assessment of World Lithium Resources and Consequences of Their Geographic Distribution on the Expected Development of the Electric Vehicle Industry'. Renewable and Sustainable Energy Reviews [online] 16 (3), 1735–1744. available from < https://doi.org/10.1016/j.rser.2011.11.023> [24 November 2018]

Gu, X., Ieromonachou, P., Zhou, L., and Tseng, M.-L. (2018) 'Developing Pricing Strategy to Optimise Total Profits in an Electric Vehicle Battery Closed Loop Supply Chain'. Journal of Cleaner Production [online] 203, 376–385. available from < https://doi.org/10.1016/j.jclepro.2018.08.209> [25 November 2018]

H. Hemi, J. Ghouili, A. Cheriti A real time fuzzy logic power management strategy for a fuel cell vehicle Energy Convers Manag, 80 (2014), pp. 63-70

Hagman, J., Ritzén, S., Stier, J.J., and Susilo, Y. (2016) 'Total Cost of Ownership and Its Potential Implications for Battery Electric Vehicle Diffusion'. Research in Transportation Business & Management [online] 18, 11–17. available from < https://doi.org/10.1016/j.rtbm.2016.01.003> [7 August 2019]

HALL-GEISLER, K. (2015) How Can Lithium-Ion Batteries Improve Hybrids? [online] available from <How can lithium-ion batteries improve hybrids?> [7 August 2019]

Huang, B., Pan, Z., Su, X., and An, L. (2018) ‘Recycling of Lithium-Ion Batteries: Recent Advances and Perspectives’. Journal of Power Sources [online] 399, 274–286. available from < https://doi.org/10.1016/j.jpowsour.2018.07.116> [20 March 2019]

Hunt, J. (2018) Toyota Fuelling the Future [online] available from <http://www.climate-change-solutions.co.uk/wp-content/uploads/2017/03/JonHunttransportHFC2017.pdf> [23 April 2019]

Hutchinson, T., Burgess, S., and Herrmann, G. (2014) ‘Current Hybrid-Electric Powertrain Architectures: Applying Empirical Design Data to Life Cycle Assessment and Whole-Life Cost Analysis’. Applied Energy [online] 119, 314–329. available from < https://doi.org/10.1016/j.apenergy.2014.01.009> [7 August 2019]

IEA International Energy Agency (2018). Hydrogen Tracking Clean Energy Progress. [online] Available at: https://www.iea.org/tcep/energyintegration/hydrogen/ [Accessed 8 Nov. 2019].

InfoMine (2019) 5 Year Cobalt Prices and Price Charts [online] available from <http://www.infomine.com/investment/metal-prices/Cobalt/5-year/> [15 January 2019]

International Energy Agency (2018) CO2 Emissions Statistics [online] available from <https://www.iea.org/statistics/co2emissions/> [29 July 2019]

International Energy Agency (2018) Global EV Outlook 2018. Towards Cross-Model Electrification [online] available from <https://www.connaissancedesenergies.org/sites/default/files/pdf-

actualites/globalevoutlook2018.pdf> [7 August 2019]

International Energy Agency (2019) What Is Energy Security? [online] available from <https://www.iea.org/topics/energysecurity/whatisenergysecurity/> [5 August 2019]

J. Larminie, A. Dicks, Fuel cell systems Explained, Second edition. Chichester : John Wiley & Sons Ltd., 2003. ISBN 0-470-84857-X.

Jaguemont, J., Boulon, L., and Dubé, Y. (2016) 'A Comprehensive Review of Lithium-Ion Batteries Used in Hybrid and Electric Vehicles at Cold Temperatures'. Applied Energy [online] 164, 99–114. available from < https://doi.org/10.1016/j.apenergy.2015.11.034> [1 November 2018]

Jason Deign (2019) 10 Countries Moving Toward a Green Hydrogen Economy [online] available from < https://www.greentechmedia.com/articles/read/10-countries-moving-towards-a-green-hydrogen-economy/>

Jia Tongguo, Wang Yinshan, Li Zhiwei , 'The Research of Status of Hydrogen Energy Development ' (2011) School of Auto and Transport T ianjin University of Technology and Education, Tianjin 300222, China

Johnson, N.M. (2014) Alternative Fuels and Advanced Vehicle Technologies for Improved Environmental Performance [online] available from <https://www.sciencedirect.com/topics/materials-science/lead-acid-battery> [7 August 2019]

Kane, M. (2018) Plug-In Electric Car Sales More Than Doubled In Germany In 2017 [online] available from <https://insideevs.com/news/336138/plug-in-

electric-car-sales-more-than-doubled-in-germany-in-2017/> [10 February 2019]

Karl BA. Mikkelsen (2010) Design and Evaluation of Hybrid Energy Storage Systems for Electric Powertrains [online] available from <https://uwspace.uwaterloo.ca/bitstream/handle/10012/5568/mikkelsen_karl.pdf?sequence=1> [6 August 2019]

King, S. and Boxall, N.J. (2019) 'Lithium Battery Recycling in Australia: Defining the Status and Identifying Opportunities for the Development of a New Industry'. Journal of Cleaner Production [online] 215, 1279–1287. available from < https://doi.org/10.1016/j.jclepro.2019.01.178> [20 March 2019]

Kumar, D., Kuhar, S.B., and Kanchan, D.K. (2018) 'Room Temperature Sodium-Sulfur Batteries as Emerging Energy Source'. Journal of Energy Storage [online] 18, 133–148. available from < https://doi.org/10.1016/j.est.2018.04.021 > [7 August 2019]

Li, L., Dababneh, F., and Zhao, J. (2018) 'Cost-Effective Supply Chain for Electric Vehicle Battery Remanufacturing'. Applied Energy [online] 226, 277–286. available from < https://doi.org/10.1016/j.apenergy.2018.05.115> [25 November 2018]

Li, Q., Chen, W., Li, Y., Liu, S., and Huang, J. (2012) 'Energy Management Strategy for Fuel Cell/Battery/Ultracapacitor Hybrid Vehicle Based on Fuzzy Logic'. International Journal of Electrical Power & Energy Systems [online] 43 (1), 514–525. available from < https://doi.org/10.1016/j.ijepes.2012.06.026> [31 January 2020]

López González, E., Sáenz Cuesta, J., Vivas Fernandez, F.J., Isorna Llerena,

F., Ridao Carlini, M.A., Bordons, C., Hernandez, E., and Elfes, A. (2019) ‘Experimental Evaluation of a Passive Fuel Cell/Battery Hybrid Power System for an Unmanned Ground Vehicle’. International Journal of Hydrogen Energy [online] 44 (25), 12772–12782. available from < https://doi.org/10.1016/j.ijhydene.2018.10.107> [29 October 2019]

M.K. Nikoo, S. Saeidi, A. Lohi (2015) ‘A comparative thermodynamic analysis and experimental studies on hydrogen synthesis by supercritical water gasification of glucose’ Clean Technol. Environ. Policy, 17, p. 2267

MacAdam, C. C. "An Optimal Preview Control for Linear Systems". Journal of Dynamic Systems, Measurement, and Control. Vol. 102, Number 3, Sept. 1980.

MathWorks (2019) Disc Brake [online] available from https://uk.mathworks.com/help/vdynblks/ref/longitudinalwheel.html?searchHighlight=Longitudinal Wheel&s_tid=doc_srchtitle#d120e50735

MathWorks (2019) Powertrain BlocksetTM User''s Guide R 2019 a.

Meier K.J.S., Berger C., Kinkel H. (2014) ‘Increasing coccolith calcification during CO2 rise of the penultimate deglaciation (Termination II)’ Marine Micropaleontology, 112, pp. 1-12.

Mekhilef, S., Saidur, R., and Safari, A. (2012) ‘Comparative Study of Different Fuel Cell Technologies’. Renewable and Sustainable Energy Reviews [online] 16 (1), 981–989. available from < https://doi.org/10.1016/j.rser.2011.09.020> [7 August 2019]

Mohr, S.H., Mudd, G.M., and Giurco, D. (2012) ‘Lithium Resources and

Production: Critical Assessment and Global Projections'. Minerals 2 (1), 65–84

Moliner, R., Lázaro, M.J., and Suelves, I. (2016) 'Analysis of the Strategies for Bridging the Gap towards the Hydrogen Economy'. International Journal of Hydrogen Energy [online] 41 (43), 19500–19508. available from < https://doi.org/10.1016/j.ijhydene.2016.06.202> [16 August 2019]

National Grid Group (2017) Electric Dreams: The Future for EVs [online] available from <https://www.nationalgrid.com/group/case-studies/electric-dreams-future-evs> [7 August 2019]

National Statistics. (2019) Energy Consumption in the UK (ECUK) 1970 to 2018 [online] available from <https://assets.publishing.service.gov.uk/government/uploads/system/uploads/attachment_data/file/820843/Energy_Consumption_in_the_UK__ECUK__MASTER_COPY.pdf> [5 August 2019]

Nissan (2019) Nissan LEAF—Top Selling Electric Vehicule in Europe 2018 | Nissan [online] available from <https://www.nissan.co.uk/vehicles/new-vehicles/leaf.html/> [7 January 2019]

Noori, M., Gardner, S., and Tatari, O. (2015) 'Electric Vehicle Cost, Emissions, and Water Footprint in the United States: Development of a Regional Optimization Model'. Energy [online] 89, 610–625. available from < https://doi.org/10.1016/j.energy.2015.05.152> [7 August 2019]

Oliveira, L., Messagie, M., Rangaraju, S., Sanfelix, J., Hernandez Rivas, M., and Van Mierlo, J. (2015) 'Key Issues of Lithium-Ion Batteries – from Resource Depletion to Environmental Performance Indicators'. Journal of Cleaner

Production [online] 108, 354 – 362. available from < https://doi.org/10.1016/j.jclepro.2015.06.021> [24 November 2018]

Omar, N., Monem, M.A., Firouz, Y., Salminen, J., Smekens, J., Hegazy, O., Gaulous, H., Mulder, G., Van den Bossche, P., Coosemans, T., and Van Mierlo, J. (2014) 'Lithium Iron Phosphate Based Battery - Assessment of the Aging Parameters and Development of Cycle Life Model'. Applied Energy [online] 113, 1575–1585. available from http://dx.doi.org/10.1016/j.apenergy.2013.09.003

ONS (2013) 2011 Census Analysis - Comparing Rural and Urban Areas of England and Wales [online] available from <http://www.ons.gov.uk/ons/dcp171776_337939.pdf> [30 July 2019]

Ottocar (n.d.) Revealed! London's Top 5 Most Popular PCO Cars [online] available from <http://www.ottocar.co.uk/blog/londons-top-10-popular-pco-cars> [21 December 2018]

P. Kurzweil, J.G. (2017) Lead-Acid Batteries for Future Automobiles [online] available from <https://www.sciencedirect.com/topics/materials-science/lithium-ion-battery> [7 August 2019]

Palmer, K., Tate, J.E., Wadud, Z., and Nellthorp, J. (2018) 'Total Cost of Ownership and Market Share for Hybrid and Electric Vehicles in the UK, US and Japan'. Applied Energy [online] 209, 108–119. available from < https://doi.org/10.1016/j.apenergy.2017.10.089 > [9 November 2018]

Pandu K., Joseph S. (2012) 'Comparisons and limitations of biohydrogen production processes: A review' Int J Adv Eng Technol, 2 (1), pp. 342-356.

Parvini, Y., Siegel, J.B., Stefanopoulou, A.G., and Vahidi, A. (2016) ‘Supercapacitor Electrical and Thermal Modeling, Identification, and Validation for a Wide Range of Temperature and Power Applications’. IEEE Transactions on Industrial Electronics 63 (3), 1574–1585

Pei, P., Chang, Q., and Tang, T. (2008) 'A Quick Evaluating Method for Automotive Fuel Cell Lifetime'. International Journal of Hydrogen Energy [online] 33 (14), 3829–3836. available from < https://doi.org/10.1016/j.ijhydene.2008.04.048 > [12 December 2019]

Pei, P., Yuan, X., Chao, P., and Wang, X. (2010) 'Analysis on the PEM Fuel Cells after Accelerated Life Experiment'. International Journal of Hydrogen Energy [online] 35 (7), 3147–3151. available from < https://doi.org/10.1016/j.ijhydene.2009.09.103> [11 December 2019]

Pollet, B.G., Staffell, I., and Shang, J.L. (2012) ‘Current Status of Hybrid, Battery and Fuel Cell Electric Vehicles: From Electrochemistry to Market Prospects’. Electrochimica Acta [online] 84, 235–249. available from < https://doi.org/10.1016/j.electacta.2012.03.172> [6 August 2019]

Qadrdan, M., Jenkins, N., and Wu, J. (2018) 'Smart Grid and Energy Storage'. McEvoy's Handbook of Photovoltaics [online] 915–928. available from <https://doi.org/10.1016/B978-0-12-809921-6.00025-2> [11 December 2019]

Ramsden, T., Ruth, M., Diakov, V., Laffen, M., Timbario, T.A. (2013) ‘Hydrogen Pathways Updated Cost, Well-toWheels Energy Use, and Emissions for the Current Technology Status of Ten Hydrogen Production, Delivery and Distribution Scenarios’ available from < https://www.nrel.gov/docs/fy14osti/60528.pdf> [29 October 2019]

Ren, G., Ma, G., and Cong, N. (2015) ‘Review of Electrical Energy Storage System for Vehicular Applications’. Renewable and Sustainable Energy Reviews [online] 41, 225–236. available from < https://doi.org/10.1016/j.rser.2014.08.003> [1 November 2018]

Renau, J., Sánchez, F., Lozano, A., Barroso, J., and Barreras, F. (2017) ‘Analysis of the Performance of a Passive Hybrid Powerplant to Power a Lightweight Unmanned Aerial Vehicle for a High Altitude Mission’. Journal of Power Sources 356, 124–132

RENAULT (2019) 250 Miles (NEDC)* Driving Range. [online] available from <https://www.renault.co.uk/vehicles/new-vehicles/zoe-250/driving range.html/.html> [2 February 2019]

Roth, M. (2015) Lifetime Costs, Life Cycle Emissions, and Consumer Choice for Conventional, Hybrid, and Electric Vehicles. [online] available from <https://trid.trb.org/view/1339160> [10 February 2019]

Ryan, D., Shang, J., Quillivic, C., and Porter, B. (2014) ‘Performance and Energy Efficiency Testing of a Lightweight FCEV Hybrid Vehicle’. European Electric Vehicle Congress (EEVC) (December), 1–12

SAE Technology roadmap for energy saving and new energy vehicles; Beijing: China Machine Press: BEIJING, 2016; pp. 47–53.

Satyapal, S., Petrovic, J., Read, C., Thomas, G. and Ordaz, G. (2007) The US Department of Energy’s National Hydrogen Storage Project: Progress towards Meeting Hydrogen-Powered Vehicle Requirements. Catalysis Today, 120, 246-256.

Saw, L.H., Somasundaram, K., Ye, Y., and Tay, A.A.O. (2014) ‘Electro-Thermal Analysis of Lithium Iron Phosphate Battery for Electric Vehicles’. Journal of Power Sources 249, 231–238

Segard, J.B. and Founder, S. (2015) EP Tender [online] available from <https://tbb.innoenergy.com/wp-content/uploads/2015/11/EP-Tender.pdf> [6 August 2019]

Shang, J., Kendall, K., and Pollet, B.G. (2016) ‘Hybrid Hydrogen PEM Fuel Cell and Batteries without DC-DC Converter’. International Journal of Low-Carbon Technologies 11 (2), 205–210

Sharaf, O.Z. and Orhan, M.F. (2014) ‘An Overview of Fuel Cell Technology: Fundamentals and Applications’. Renewable and Sustainable Energy Reviews [online] 32, 810–853. available from < https://doi.org/10.1016/j.rser.2014.01.012> [7 August 2019]

Sheldon H D Lee, Daniel V Applegate. (2004) ‘Hydrogen from natural gas: part 1 aerothermal reforming in an integrated fuel processor {J}’. international Journal of Hydrogen Energy. 29

SMMT (2016) Ultra Low Emission Vehicles Guide 2016 [online] available from <http://www.smmt.co.uk/wp-content/uploads/sites/2/ULEV-report-Final-1.pdf> [2 August 2019]

Souleman, N.M., Tremblay, O., and Dessaint, L.A. (2009) ‘A Generic Fuel Cell Model for the Simulation of Fuel Cell Vehicles’. 5th IEEE Vehicle Power and Propulsion Conference, VPPC ’09 1722–1729

Spiegel, C. (2008) ‘Mathematical Modeling of Polymer Exchange Membrane Fuel Cells’. East

Staffell, I. (2011) ‘Results from the Microcab Fuel Cell Vehicle Demonstration at the University of Birmingham’. International Journal of Electric and Hybrid Vehicles 3 (1), 62–82

Stark, C., Thompson, M., Andrew, T., Beasley, G., Bellamy, O., Budden, P., Cole, C., Darke, J., Davies, E., Feliciano, D., and Gault, A. (2019) Net Zero the UK’s Contribution to Stopping Global Warming [online] available from <https://www.theccc.org.uk/wp-content/uploads/2019/05/Net-Zero-The-UKs-contribution-to-stopping-global-warming.pdf> [31 July 2019]

Suzanna Hinson and Alex Adcock (2020) UK Hydrogen Economy [online] available from < https://researchbriefings.files.parliament.uk/documents/CDP-2020-0172/CDP-2020-0172.pdf/>

Swain, B. (2017) ‘Recovery and Recycling of Lithium: A Review’. Separation and Purification Technology [online] 172, 388–403. available from < https://doi.org/10.1016/j.seppur.2016.08.031> [7 August 2019]

T. Shiga, Y. Hase, Y. Kato, M. Inoue, K.T.C. (2013) A Rechargeable Non-Aqueous Mg–O2 Battery [online] available from https://pubs.rsc.org/en/content/articlelanding/2013/cc/c3cc43477j#!divAbstract

Tesla UK (2019) TESLA Model S [online] available from <https://www.tesla.com/en_GB/models/ > [9 January 2019]

The Department of Energy and Climate Change (2012) ‘Big Drop’ in UK Petrol

Stations as Fuel Reserves Fall [online] available from <https://www.bbc.co.uk/news/business-20791871> [7 August 2019]

Tie, S.F. and Tan, C.W. (2013) 'A Review of Energy Sources and Energy Management System in Electric Vehicles'. Renewable and Sustainable Energy Reviews [online] 20, 82–102. available from < https://doi.org/10.1016/j.rser.2012.11.077> [1 November 2018]

Tremblay, O., L.A. Dessaint. (2009) 'Experimental Validation of a Battery Dynamic Model for EV Applications.' World Electric Vehicle Journal. Vol. 3,

UK Government. Department for Business Energy & Industrial Strategy (2017) 'The Clean Growth Strategy: Leading the Way to a Low Carbon Future'. UK Gov [online] 165. available from https://www.gov.uk/government/

United States Environmental Protection Agency (2019) Compare Fuel Cell Vehicles [online] available from <https://www.fueleconomy.gov/feg/fcv_sbs.shtml/> [7 August 2019]

Vehicle Certification Agency (2020) The Worldwide Harmonised Light Vehicle Test Procedure (WLTP) [online] available from https://www.vehicle-certification-agency.gov.uk/fcb/wltp.asp

Vikström, H., Davidsson, S., and Höök, M. (2013) 'Lithium Availability and Future Production Outlooks'. Applied Energy [online] 110, 252–266. available from < https://doi.org/10.1016/j.apenergy.2013.04.005> [7 August 2019]

Volkswagen UK (2019) Volkswagen Electric & Hybrid Car Technology [online] available from <https://www.volkswagen.co.uk/electric-hybrid/> [2 January

2019]

Wall, M. (2015) Hydrogen, Hydrogen Everywhere... [online] available from <https://www.bbc.co.uk/news/business-31926995> [16 August 2019]

Wang Wei Lan Yuxin Li Ming Zheng Lei Liu Shijie Cheng Wenhan (2007) ‘Fast pyrolysis of biomass waste for hydrogen-rich gas’ Department of Environmental Science and Engineering, Tsinghua University, Beijing 100084

Wang, C., He, H., Zhang, Y., and Mu, H. (2017) ‘A Comparative Study on the Applicability of Ultracapacitor Models for Electric Vehicles under Different Temperatures’. Applied Energy [online] 196, 268–278. available from < https://doi.org/10.1016/j.apenergy.2017.03.060> [7 August 2019]

Wang, X., Gaustad, G., Babbitt, C.W., Bailey, C., Ganter, M.J., and Landi, B.J. (2014) ‘Economic and Environmental Characterization of an Evolving Li-Ion Battery Waste Stream’. Journal of Environmental Management [online] 135, 126–134. available from < https://doi.org/10.1016/j.jenvman.2014.01.021 > [7 August 2019]

Westbrook, M. The Electric and Hybrid Electric Car; Institution of Electrical Engineers: London, UK, 2001; pp. 87–99.

Wikner, E. and Thiringer, T. (2018) 'Extending Battery Lifetime by Avoiding High SOC'. Applied Sciences (Switzerland) 8 (10)

Wipke, K.B. and Cuddy, M.R. (1996) Using an Advanced Vehicle Simulator (ADVISOR) to Guide Hybrid Vehicle Propulsion System Development.

World Health Organization (2018) 9 out of 10 People Worldwide Breathe Polluted Air, but More Countries Are Taking Action [online] available from <https://www.who.int/news-room/detail/02-05-2018-9-out-of-10-people-worldwide-breathe-polluted-air-but-more-countries-are-taking-action> [29 July 2017]

Wu, B., Parkes, M.A., Yufit, V., De Benedetti, L., Veismann, S., Wirsching, C., Vesper, F., Martinez-Botas, R.F., Marquis, A.J., Offer, G.J., and Brandon, N.P. (2014) 'Design and Testing of a 9.5 KWe Proton Exchange Membrane Fuel Cell–Supercapacitor Passive Hybrid System'. International Journal of Hydrogen Energy [online] 39 (15), 7885–7896. available from < https://doi.org/10.1016/j.ijhydene.2014.03.083> [29 October 2019]

Wu, G., Inderbitzin, A., and Bening, C. (2015) 'Total Cost of Ownership of Electric Vehicles Compared to Conventional Vehicles: A Probabilistic Analysis and Projection across Market Segments'. Energy Policy [online] 80, 196–214. available from < https://doi.org/10.1016/j.enpol.2015.02.004> [7 August 2019]

ZAP-MAP (2019) Charging Point Statistics 2019 [online] available from <https://www.zap-map.com/statistics/> [7 August 2019]

Zhang, T., Wang, P., Chen, H., and Pei, P. (2018) 'A Review of Automotive Proton Exchange Membrane Fuel Cell Degradation under Start-Stop Operating Condition'. Applied Energy [online] 223, 249–262. available from < https://doi.org/10.1016/j.apenergy.2018.04.049> [17 March 2020]

Zhang, X., Liu, L., Dai, Y., and Lu, T. (2018) 'Experimental Investigation on the Online Fuzzy Energy Management of Hybrid Fuel Cell/Battery Power System for UAVs'. International Journal of Hydrogen Energy [online] 43 (21), 10094–

10103. available from https://doi.org/10.1016/j.ijhydene.2018.04.075

Zhang, X., Wang, X.-G., Xie, Z., and Zhou, Z. (2016) ‘Recent Progress in Rechargeable Alkali Metal–Air Batteries’. Green Energy & Environment [online] 1 (1), 4–17. available from < https://doi.org/10.1016/j.gee.2016.04.004 > [7 August 2019]

Zhou, S. (2017) Modeling and Simulation Technology of Fuel Cell Vehicle. Beijing institute of technology press

Zhu, C., X. Li, L. Song, and L. Xiang. (2013) ‘Development of a theoretically based thermal model for lithium ion battery pack.’ Journal of Power Sources. Vol. 223, pp. 155–164.

Appendices

1.1 Review of energy storage sources for ZEV

BEVs use the battery as an energy source and are charged by electricity supplied from the power grid. The battery is an important component, allowing energy storage over long periods of time. Different battery technologies have different capacities and other characteristics (Das, 2017). There are six types of batteries could be used in ZEV applications: lead acid batteries, nickel batteries, ZEBRA batteries, lithium batteries, metal air batteries and sodium-sulphur battery (Tie et al. 2013; Westbrook 2001; Jaguemont et al. 2016; Ren et al. 2015; Das et al. 2017).

1.1.1 Lead-Acid battery

Lead acid batteries haave been developed for more than 150 years. Due to its affordability, the lead-acid battery is used for ICE vehicles. As shown in
Table 0-1, the production cost of the Lead-acid batteries is three times less expensive than for Nickel batteries. ICE vehicles use Lead-acid batteries with start/stop technology to reduce the cost and for the same reason some early models of electric cars also use this battery technology, such as the Toyota RAV4. Lifetime is a serious problem for Lead-acid batteries. Test results from the earliest modern EVs from General Motors show that after 1000 cycles of 80% discharge under normal temperature, the batteries had lost more than 30% of their original capacity (Johnson 2014). For now, lead-acid batteries are not the first choice for EV batteries, however they are still the most favoured by automakers for starting, lighting and ignition (SLI) functions.

Table 0-1 Summary of Lead Acid battery characteristics and applications (Tie et al. 2013; Westbrook 2001; Jaguemont et al. 2016; Ren et al. 2015; Das et al. 2017).

Energy storage source type	Lead–Acid	Advance lead acid	Valve regulated lead acid (VRLA)	Metal foil lead acid
Specific energy (Wh/kg)	35	45	50	30
Energy density (Wh/L)	100	-	-	-
Specific power (W/kg)	180	250	150+	900
Life cycle	1000	1500	700+	500+
Energy efficiency (%)	>80	-	-	-
Production cost (£/kWh)	48	160	120	-
Advantage	Low cost, widely used, widely recycled and can supply high current.			
Disadvantage	Short life cycle, not environmentally friendly both at the production and disposal stage.			
Application	Lead acid batteries are widely used on traditional ICE vehicles, lighting, uninterruptible power supplies, submarines and backup energy sources			

1.1.2 Nickel battery

Nickel–metal hydride (Ni-MH) batteries started to infiltrate the market of lead-acid batteries in the 1990's. According to Table 0-2, the specific energy, energy density and specific power of Nickel-metal hydride (Ni-MH) batteries improved by 171%, 120% and 66.7% respectively, compared to Lead-acid batteries. Moreover, the weight advantage of Ni-MH batteries has played a prominent role due to EVs requiring batteries with larger capacities. For example, compared to lead-acid, the Ni-MH battery packs and for the General Motors EV1 reduce the weight of the battery packs by 114kg (23.7%), increased the battery capacity by 56.1% and increased the specific energy by 93% (Johnson 2014).

Lifetime is another merit of Ni-MH batteries. According to consumer reports, the performance of the battery from a Prius after driving 215,000 miles is still as good as the internal combustion engine (Consumer Reports 2011). In the meantime, automakers are preferring to use environmentally friendly batteries. Therefore, EVs advocate the use of Nickel-based batteries to replace lead-acid batteries. Many EVs such as the Toyota Prius, Honda CR-Z and Ford Escape have used Ni-MH battery packs in the past decade (HALL, 2015)

Table 0-2 Summary of Nickel-based battery characteristics and applications (Tie et al. 2013; Westbrook 2001; Jaguemont et al. 2016; Ren et al. 2015; Das et al. 2017).

Energy storage source type	Nickel–iron (Ni-Fe)	Nickel–zinc (Ni-Zn)	Nickel–cadmium (Ni–Cd)	Nickel–metal hydride (Ni–MH)
Specific energy (Wh/kg)	50-60	75	50-80	70-95
Energy density (Wh/L)	60	140	50-150	180-220
Specific power (W/kg)	100-150	170-260	200	200-300
Life cycle	2000	300	2000	<3000
Energy efficiency (%)	75	76	75	70
Production cost (£/kWh)	120-160	80-160	200-240	160-200
Advantage	Stable, deep cycling, long life time	High specific energy High rate of charge and discharge made by low-cost benign materials.	works well under the bad conditions, High rate of charge and discharge, wide temperature range	environment-friendly, high specific energy, long cycle life, large temperature ranges
Disadvantage	High cost Low voltage, heavy weight, high maintenance cost, high self-discharge rate	Shorter life due to growth of zinc dendrites	High cost, memory effect, Cadmium is a high-cost heavy metal and not environmentally friendly	High cost, memory effect (a little better than Ni-Cd), high self-discharge
Application	Traction and Off-grid power system storage	Traction, Electric Bicycles	Two-way radios, toys, emergency medical devices, camera Emergency lighting and power tools	Low powered devices, vehicle battery, Medical instruments and equipment

1.1.3 Lithium battery

In the same way that Ni-MH batteries have replaced the lead-acid batteries, Ni-MH batteries are now gradually being replaced by lithium batteries. Table 0-3 indicates the characteristics and highlight the advantages of Lithium-ion batteries. Specific energy, energy density and specific power are more than double that of Ni-MH technology. Although the life cycle is only 2/3 of that of Ni-MH batteries, the electrical efficiency is 25% higher than Ni-MH batteries. The high performance of Lithium battery allows lightweight battery pack design and modest resource requirements. For example, due to the high capacity available, a single lithium battery is able to replace three Ni-MH battery packs (Kurzweil and Garche 2017). Many researchers and companies have realised the superiority of lithium batteries for clean power vehicles (Ballon, 2011).

Table 0-3 Summary of Lithium battery characteristics and applications (Tie et al. 2013; Westbrook 2001; Jaguemont et al. 2016; Ren et al. 2015; Das et al. 2017).

Energy storage source type	Lithium–iron sulphide (FeS)	Lithium–iron phosphate (LiFePO4)	Lithium-ion polymer (LiPo)	Lithium-ion	Lithium–titanate (LiTiO/NiMnO2)
Specific energy (Wh/kg)	50	120	130-225	118-250	80-100
Energy density (Wh/L)	-	220	200-250	200-400	-
Specific power (W/kg)	300	2000-4500	260-450	200-430	4000
Life cycle	1000+	>2000	>1200	2000	18000
Energy efficiency (%)	80	-	-	>95	-
Production cost (£/kWh)	88	280	120	120	1600
Advantage	Low cost, high specific energy	high voltage operation, long life cycle, environmentally friendly and heat resistance	long storage lifetime, low discharge rate	High specific energy, high voltage operation, no memory effect low discharge rate	Safety, long life cycle, faster to charge and low-temperature performance
Disadvantage	Lifetime, high operating temperature	Performance reduced when low temperature	safety problem	national degradation, overcharge and discharge will reduce the lifetime	High cost
Application	Research area	EVs and lighting	Radio-controlled equipment, smartphone and laptop	Portable devices, EVs and electric devices	Electric power-trains, UPS and solar-powered street lighting.

1.1.4 Sodium-nickel and Sodium-sulphur battery

In 1966, Ford Motor Company used a sodium–sulphur (Na-S) battery for their early model of EV. Although Na-S batteries have advantages including high energy density, high energy efficiency and good cycling flexibility, the battery can only operate at about 300 °C. However, the normal operating temperature for the other battery technologies is in the range –20°C to 60°C. Therefore, sodium–sulphur (Na-S) batteries are widely used in large energy storage stations to help balance the power distribution in the electricity grid. A fire accident in a Na-S battery factory belonging to NGK INSULATORS, LTD, indicated the potential safety problems of these batteries. According to Kumar's review, Na-S batteries operating at high temperatures can cause fire and explosion if the solid electrolyte works incorrectly (Kumar 2018). As well as Sodium–sulphur batteries, Sodium–nickel chloride batteries require very high operating temperatures. The energy loss in the standby state is the main problem for use in EVs.

In view of these disadvantages, room temperature Na-S batteries might become a possible solution for EVs. Unfortunately, the electrochemistry of this new battery is very complicated and requires long-term fundamental research and technical development (Kumar 2018). The most likely applications for Na-S batteries in the future are in transportation that is operating long-term. The characteristics and applications of Na-S batteries are depicted in Table 0-4.

Table 0-4 Summary of Sodium-nickel and Sodium-sulphur battery characteristics and characteristics and applications (Tie et al. 2013; Westbrook 2001; Jaguemont et al. 2016; Ren et al. 2015; Das et al. 2017).

Energy storage source type	Sodium–sulphur	Sodium–nickel chloride
Specific energy (Wh/kg)	150-240	90-120
Energy density (Wh/L)	-	160
Specific power (W/kg)	150-230	155
Life cycle	800+	1200+
Energy efficiency (%)	80	80
Production cost (£/kWh)	200-360	184-276
Advantage	High energy density, High energy efficiency, good cycling flexibility	High energy density, at least 10-year calendar life, low maintenance cost
Disadvantage	Operating in very high-temperature 300-350 °C	270°C operating temperature, 90 W energy loss at stand by stage
Application	Submarines and Energy storage power station	Electric vehicles and railway

1.1.5 Metal-air battery

In addition to lithium batteries, rechargeable metal-air batteries are one of the most promising energy sources for EVs. With many researchers' contributions over the past 10 years, the improvement in metal-air batteries has been significant. However, according to recent research in (Shiga et al. 2013), the life cycle of Aluminium-air and Magnesium-air batteries is not sufficient. Problems such as instability of electrolytes and slow kinetic processes of oxygen reduction reaction and oxygen evolution reaction are hindering the development of metal-air batteries (Zhang, 2016). The characteristics and applications of metal-air batteries are described in Table 0-5.

Table 0-5 Summary of metal-air batteries characteristics and applications (Tie et al. 2013; Westbrook 2001; Jaguemont et al. 2016; Ren et al. 2015; Das et al. 2017).

Energy storage source type	Aluminium-air	Zinc-air	Zinc-refillable	Lithium-air	Magnesium-air	sodium -air
Specific energy (Wh/kg)	250-500	1085	460	3463	2843	1105
Energy density (Wh/L)	-	1400	-	-		
Specific power (W/kg)	60	80-140	-	-		
Life cycle	-	200	-	-		
Energy efficiency (%)	80	-	-	>95		
Production cost ($/kWh)	110	350	150	150		
Advantage	Low cost, safety, high specific energy,	high specific energy and high energy density	long storage lifetime, low discharge rate	long storage life, less weight	low cost, lightweight and biocompatibility	low cost, lightweight and biocompatibility
Disadvantage	Lifetime, high operating temperature	low specific power, heavy, short cycle life	safety problem	Influenced by temperature	parasitic corrosion causes high self-discharge rate and low Coulombic efficiency	High cost of the setup, low cycle life, low high over potential
Application	Vehicles, emergency power sources	Watches, hearing aids and safety lamps of railway and road.	Radio controlled equipment, smart phone and laptop	Research area	Research area	Research area

1.1.6 Ultra-capacitor (UC)

The UC is considered as a possible choice for vehicle energy storage systems due to its high specific power, ultra-long lifetime, lower maintenance needs and wide operating temperature range (Parvini et al. 2016). Ren stated that UC hybrids with other battery technologies could be the right solution for electric vehicles. As a result, this technique has been widely accepted by researchers of automakers (Ren et al. 2015). The characteristics and applications of UCs are described in Table 0-6.

Table 0-6 Ultra-capacitor (UC) characteristics and applications (Tie et al. 2013; Wang et al. 2017)

Energy storage source type	Electric double-layer capacitor	Electrochemical pseudo capacitor	Hybrid capacitors
Specific energy (Wh/kg)	5-7	10-15	10-15
Energy density (Wh/L)	-	-	-
Specific power (W/kg)	1-2M	1-2M	1-2M
Life cycle	80%+10 years	40 years	15 years
Energy efficiency (%)	>95	>95	>95
Production cost ($/kWh)	-	-	-
Advantage	High specific power, long life cycle, not sensitive or influenced by temperature		
Disadvantage	Low specific energy density		
Application	Electric vehicles, smart meter, wind power stations, power grid and LED		

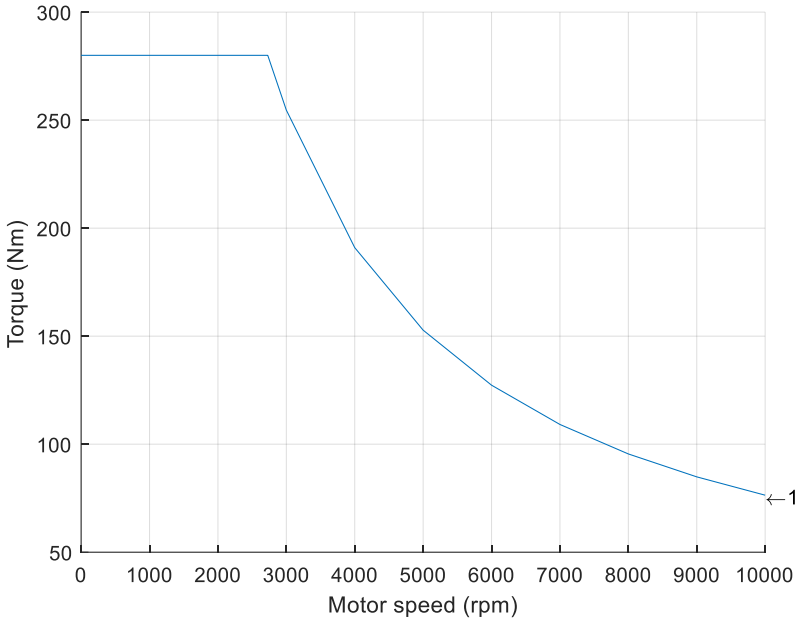

Appendix 1 Motor torque and speed curve map

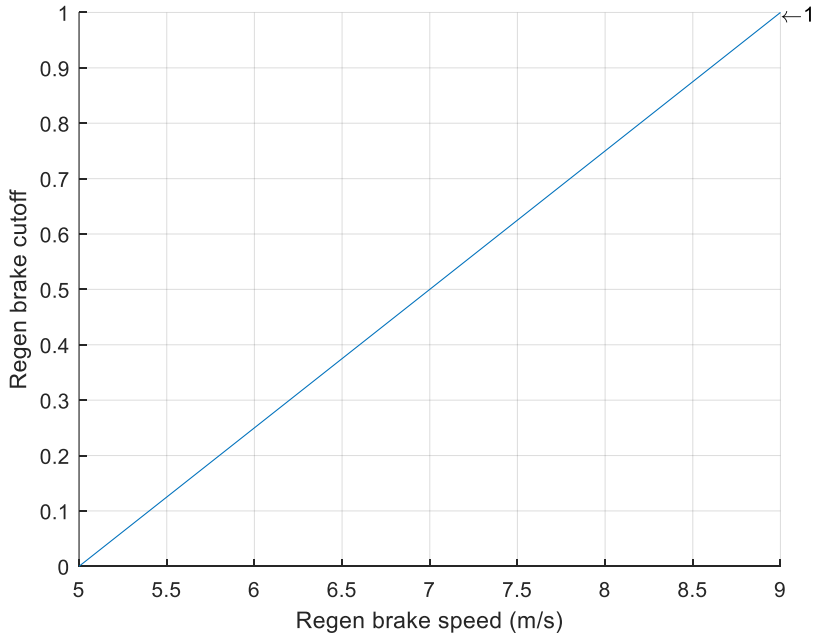

Appendix 2 Regenerative brake cut off point

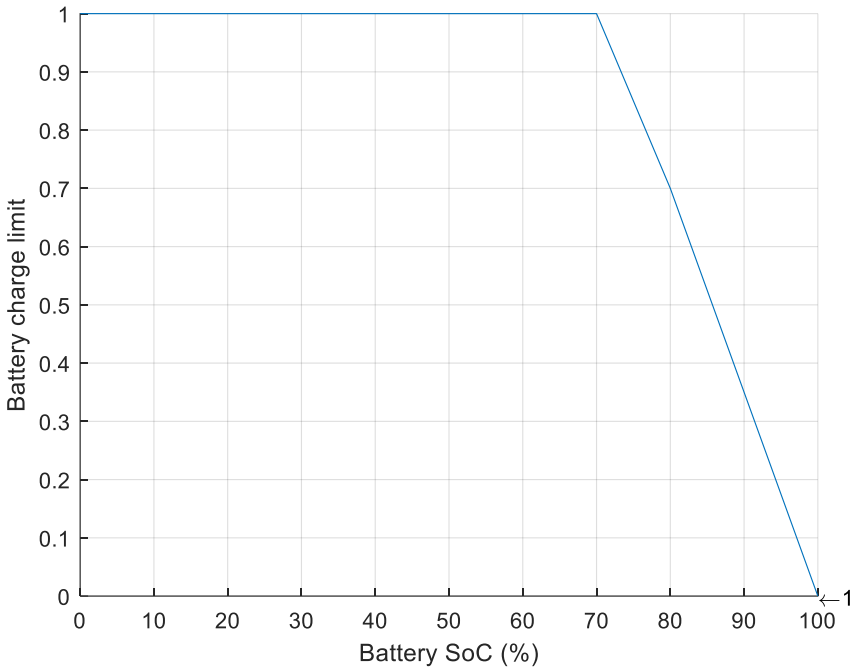

Appendix 3 Battery charge limit of regenerative brake

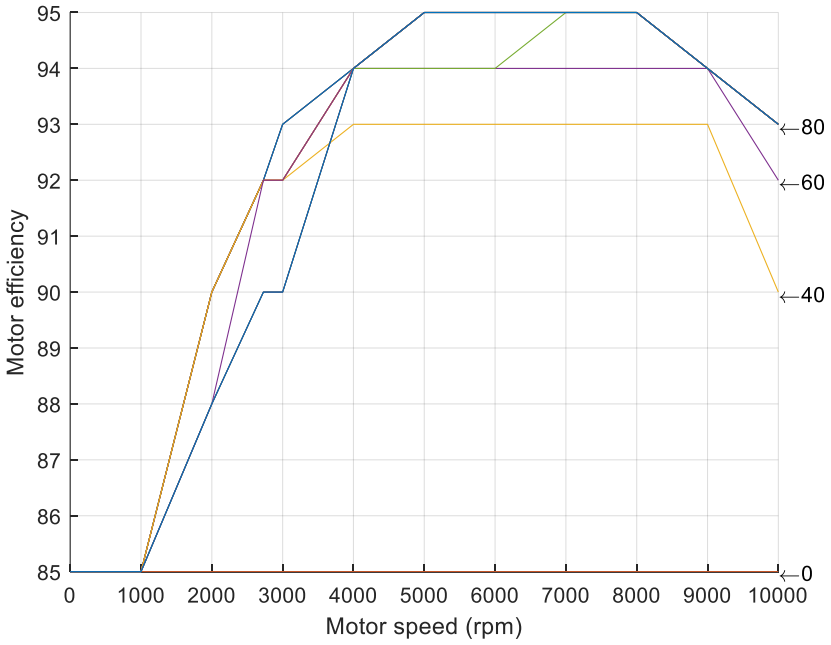

	0	20	40	60	80	100	120	140	160	180	200	220	240	260	280
0	85	85	85	85	85	85	85	85	85	85	85	85	85	85	85
1000	85	85	85	85	85	85	85	85	85	85	85	85	85	85	85
2000	85	85	90	90	90	90	90	90	90	90	88	88	88	88	88
2728.37...	85	85	92	92	92	92	92	92	92	92	92	90	90	90	90
3000	85	85	92	92	93	93	93	93	92	92	92	90	90	90	90
4000	85	85	93	94	94	94	94	94	94	94	94	94	94	94	94
5000	85	85	93	94	94	95	95	95	95	95	95	95	95	95	95
6000	85	85	93	94	94	95	95	95	95	95	95	95	95	95	95
7000	85	85	93	94	95	95	95	95	95	95	95	95	95	95	95
8000	85	85	93	94	95	95	95	95	95	95	95	95	95	95	95
9000	85	85	93	94	94	94	94	94	94	94	94	94	94	94	94
10000	85	85	90	92	93	93	93	93	93	93	93	93	93	93	93

Appendix 4 Motor efficiency map

The work has led to the following publications:

Conference Publication

Jin Ren, Olivier Haas, Jinlei Shang and Asim Mumtaz. ‘Modelling and simulation for Fuel Cell Passive Hybrid Electric Vehicle’ Fuel Cell & Hydrogen Technical Conference 2018. Gallery Suite, NEC Birmingham.

Journal articles

Dongxiao Wu, Jin Ren *, Huw Davies, Jinlei Shang and Olivier Haas (2019) Intelligent Hydrogen Fuel Cell Range Extender for Battery Electric Vehicles. World Electr. Veh. J. 2019, 10(2), 29; https://doi.org/10.3390/wevj10020029

Jin Ren, Olivier Haas, Jinlei Shang and Asim Mumtaz. ‘Evaluation of a hybrid FCEV based on a passive fuel cell/battery architecture FCEV’ submitted

Jin Ren, Olivier Haas, Jinlei Shang and Asim Mumtaz. ‘Direct passive hybrid system selection for fuel cell vehicle’ which is in preparation.